STUDIES IN INFRARED SPECTROSCOPY

Thesis by
Philip Ray Kennicott

In Partial Fulfillment of the Requirements
For the Degree of
Doctor of Philosophy

California Institute of Technology
Pasadena, California

1962

ACKNOWLEDGMENTS

I wish first to gratefully acknowledge the suggestions and patient help of my research advisor, Professor R. M. Badger. My studies were made possible by grants from the Alfred P. Sloan Foundation and the E. I. duPont de Nemours and Company Fund. Finally, I wish to express my appreciation to my wife for the typing of this thesis.

ABSTRACT

The modernization of a vacuum grating infrared spectrometer is described. Experiments using this spectrometer on N-methyl formamide in the vapor phase are described, and the results are interpreted in terms of the position, shape, and intensity change with temperature of the vibration bands of this substance. It is concluded that N-methyl formamide exists in two isomeric forms in the vapor phase. The less abundant form is the cis isomer which lies 1.4 kcal. above the trans isomer.

An echelle-type grating used with this spectrometer is shown to have an unusually wide and flat efficiency curve. This is ascribed to a scattering phenomenon in which both faces of a groove participate. Mathematical analyses based on both the Kirchhoff theory and on the Rayleigh theory are shown to predict the broad region of high efficiency for this grating.

An amplifier which is intended to be used with a novel double-beam ratio detection system is described.

TABLE OF CONTENTS

SECTION I

THE MODERNIZATION OF AN INFRARED SPECTROMETER

INTRODUCTION

This section of the thesis will deal with work involved in modernizing the vacuum grating spectrometer described by Badger, Zumwalt, and Giguere in 1948.[1] The many novel features of this instrument make it particularly well suited to infrared spectroscopy of a research nature as opposed to that of a routine nature for analytical purposes. The instrument employs a diffraction grating as the primary dispersive element instead of the more common prism. It has been designed for the use of a rather large grating (200 mm. x 150 mm.) allowing one to employ narrow slits for high resolution. It has been designed as a monochromator rather than as a spectrometer or spectrophotometer, allowing a great deal of flexibility in its use. With suitable accessories, it can provide a monochromatic source of radiation, measure the intensity of each wavelength of a given source, or compare the absorption or emission spectra of two substances. It has been designed to operate in a vacuum to allow freedom from interference of absorption bands due to water and carbon dioxide in the atmosphere.

The instrument has performed well in a large number of studies requiring high dispersion,[2] but progress in infrared techniques[3] has dictated that certain improvements be made. It was desired to make these improvements while retaining the above mentioned advantages of high dispersion, flexibility, and freedom from atmospheric interference.

To maintain the highest possible resolution, it is necessary to use the most sensitive detector available in order that the slit width may be reduced to the minimum consistent with a satisfactory signal-to-noise ratio.[4] In the shorter wavelength regions of the spectrum, photoconductors with relatively wide band-gaps such as PbS, PbSe, or PbTe will be used.[5] At longer wavelengths, one can change to other photoconductors with smaller band-gaps and operated at lower temperatures, or change to a thermal-type detector. Of the thermal detectors, (thermocouple, bolometer, and Golay detector[6]) the Golay detector is the most practical at this time in an application directed toward high resolution.

In any grating monochromator, means must be provided for separating the desired grating order from the other orders which are present. It is usually possible to accomplish this with filters if the orders are not too close to

each other and if individual scans do not cover too great a span in wavelength. With the conventional echelette grating used in the infrared, this is the case. With the grating described in Section III, however, a different situation is encountered. This grating can be described as one which has an effective blaze which covers nearly the entire range of grating angle. This means two things. First, at any grating angle several orders will be strong, and these may be quite close together in wavelength--much too close for separation by filters. Second, this unique feature of the grating gives one the capability of making long continuous scans without changing grating orders. Such a capability is desirable, for example, in survey work. In order to take advantage of this capability without stopping several times during the scan to change filters, a foreprism monochromator is needed. This must be of sufficiently high resolution to separate orders. It must also be coupled in some way with the grating drive so that it will be at the correct setting corresponding to the particular wavelength and grating order at which one is working.

In order to take advantage of the modern detectors now available, and to take advantage of the properties of the grating, the following changes were made in the spec-

trometer: A Golay detector was obtained, and provision was made for the use of other detectors when desired. A fore-prism monochromator was added. An extra range was added to allow the grating to be used at high grating angles. Finally several minor mechanical and optical changes had to be made in connection with these other changes. The various portions of the spectrometer will now be dealt with individually in more detail.

GRATING MONOCHROMATOR OPTICS

The main dispersive element in the instrument is a Littrow-mounted diffraction grating. The collimator is an off-axis paraboloid of 100 cm. focal length, roughly 230 x 180 mm. The mounting in this instrument is somewhat unusual in that the collimator paraboloid is cut and mounted so that its axis passes approximately through the center of the lower edge of the grating. The Newtonian mirrors thus are close to the center line of the optical system and near the lower edge of the grating (figure 1).

In the original instrument the entrance and exit slits were in the same vertical plane and used the same mechanical slit. A single Newtonian mirror was used. Although this arrangement had considerable optical advantage, it suffered

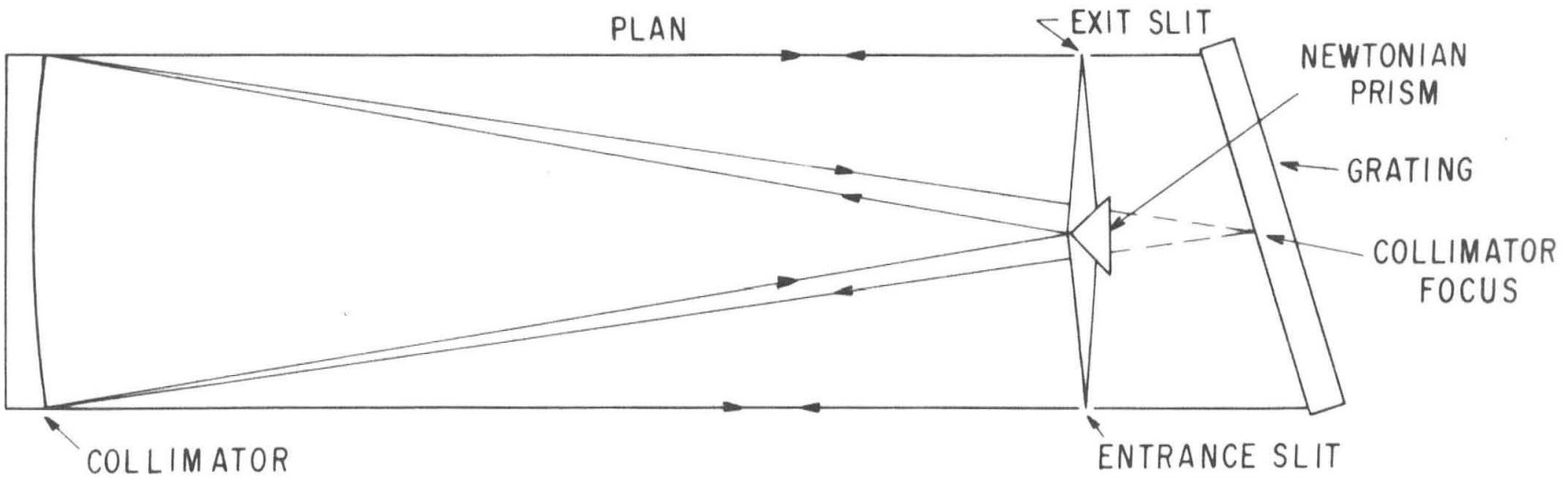

ELEVATION

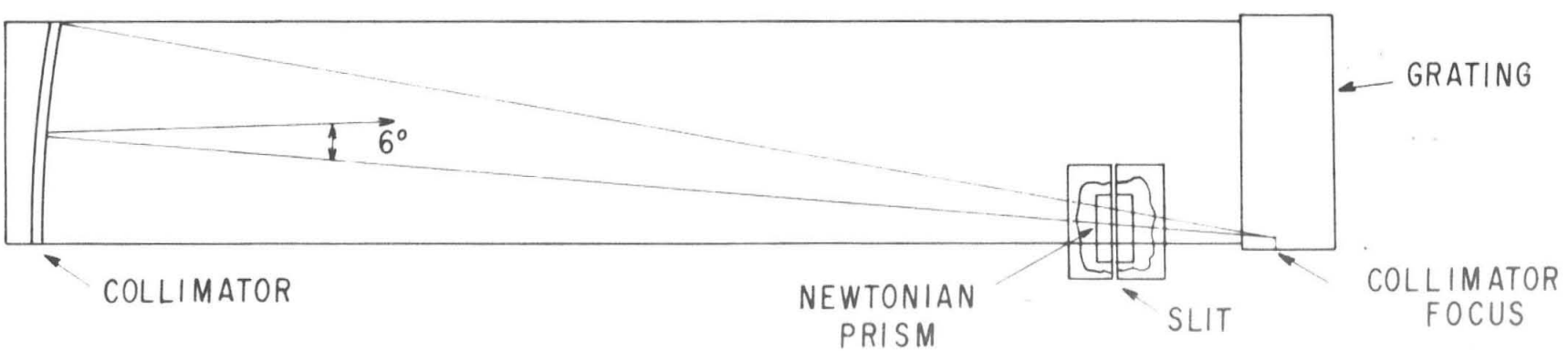

FIGURE I
MODIFIED GRATING MONOCHROMATOR

from the drawback that provision had to be made to prevent overlapping of incoming and outgoing beams. This presented some difficulty due to space limitations imposed by the vacuum housing of the instrument, but was accomplished by the use of two field lenses, one for each beam, located at the slit and so offset in the vertical direction that incoming and outgoing beams were separated by the prismatic effect.

The new space problems introduced by the addition of the foreprism monochromator and the various detectors to be used necessitated a more complete separation of incoming and outgoing beams. This was most easily accomplished by locating the entrance and exit slits on opposite sides of the spectrometer.

This change in the entrance slit position required a second Newtonian mirror. Space limitations precluded the installation of two separate Newtonians together with their associated adjusting mechanisms. Instead, a 90° prism was silvered and used for the two Newtonians. It is required that the two Newtonian mirrors be placed at an angle with respect to each other of approximately 90°. The paraboloid axis must bisect this angle. This is automatically fulfilled by the use of the prism with its right-angle edge on the axis and the plane opposite this edge perpendicular to the

axis. The prism is mounted on a table which can be tilted and rotated for making the necessary adjustments.

The exit optics are similar to the image reducer described by Greenler.[7] The exit slit is about one inch behind the larger mirror, rather than at its surface as in Greenler's system. This moves the real image formed by the smaller mirror farther behind its surface and thus reduces the demagnification. The optical diagram is shown in figure 2.

The more usual arrangement when using a Golay detector would employ a toroidal mirror. This produces a rather diffuse image, but this could be tolerated with the Golay. With a photoconductive detector, however, the sensitivity varies as 1/area, and there is an advantage in having the smallest image of the best quality possible. This system allows one to obtain a very high quality image with a demagnification of 1:8 while using inexpensive spherical mirrors. Greenler has shown that spherical aberration is eliminated (to the third order) and that coma is insignificant with this system.

The actual arrangement uses a 7" mirror from an arc motion picture projector lamp for M_1 and an aluminized ophthalmic lens for M_2. M_1 is mounted on the spectrometer carriage and is adjusted laterally by repositioning the

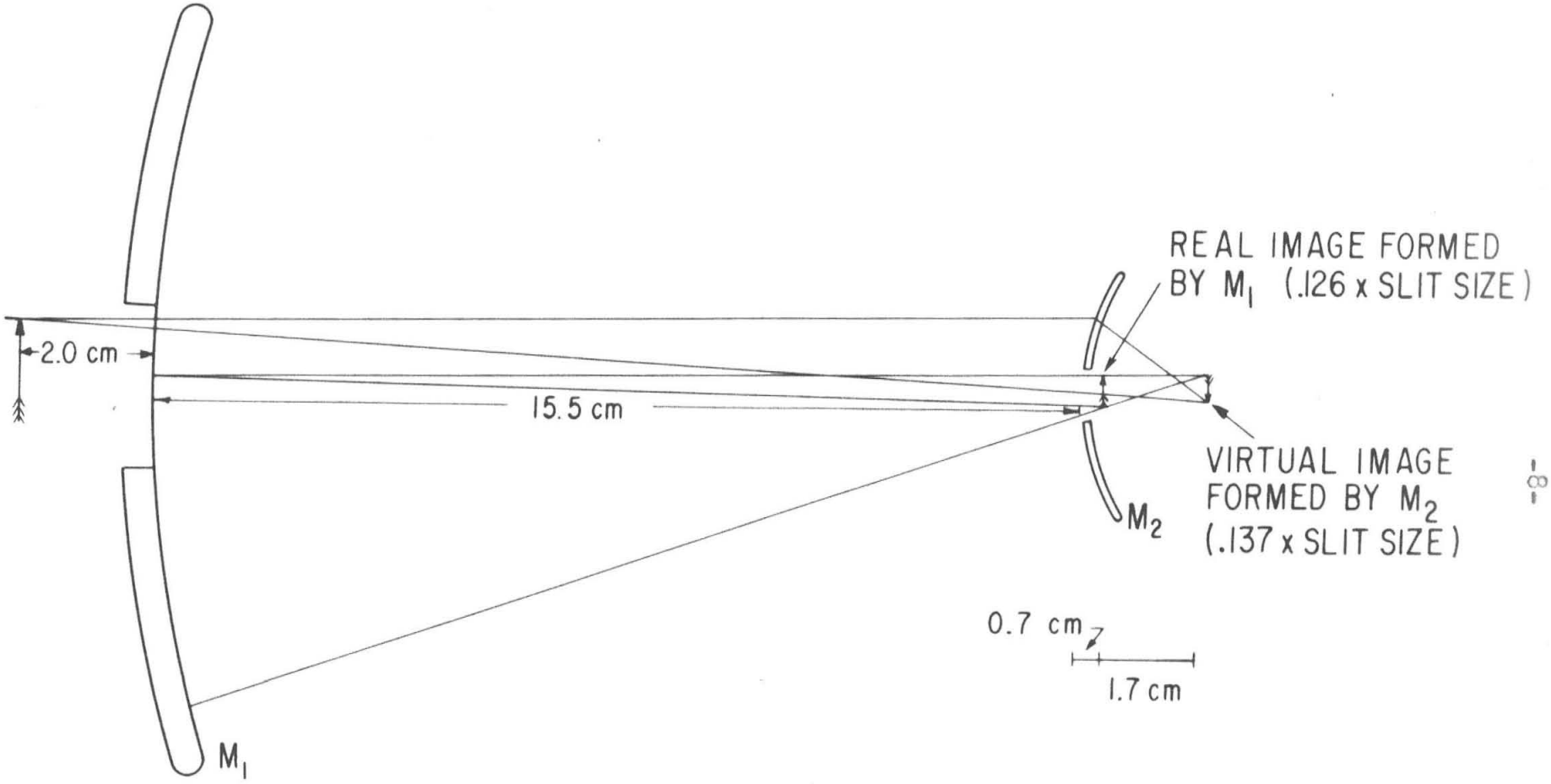

EXIT OPTICS

FIGURE 2

carriage. It can be rotated about the horizontal and vertical axes by adjusting screws. M_2 is attached to a short side arm welded to the casing (figure 3). This mirror constitutes part of the vacuum seal. A 7 mm. hole is drilled in the center and the potassium bromide exit window cemented over the hole. It has been found that the slight alteration of the focus of this mirror due to evacuating the casing is insignificant. The mirror mounting is provided with threads which screw into a plate and provide for adjustment of the focus. Upon reaching proper focus the threads are sealed with Glyptal varnish. The plate fits against the end of the side arm and can be moved about over its "O" ring seal to provide for adjustment in the vertical plane.

The Golay detector rests on a small bracket attached to this side arm. Its entrance window is placed in contact with the exit window. The position of the detector is adjusted horizontally by moving screws in slotted holes, and vertically by a set of shims.

In passing, it should be noted that certain difficulties have been noticed with this detector. There is wide variation in performance between apparently satisfactory detector heads. Also, the adjustment provided for focusing the grid inside the detector upon itself depends primarily on imperfections in machining for providing the necessary

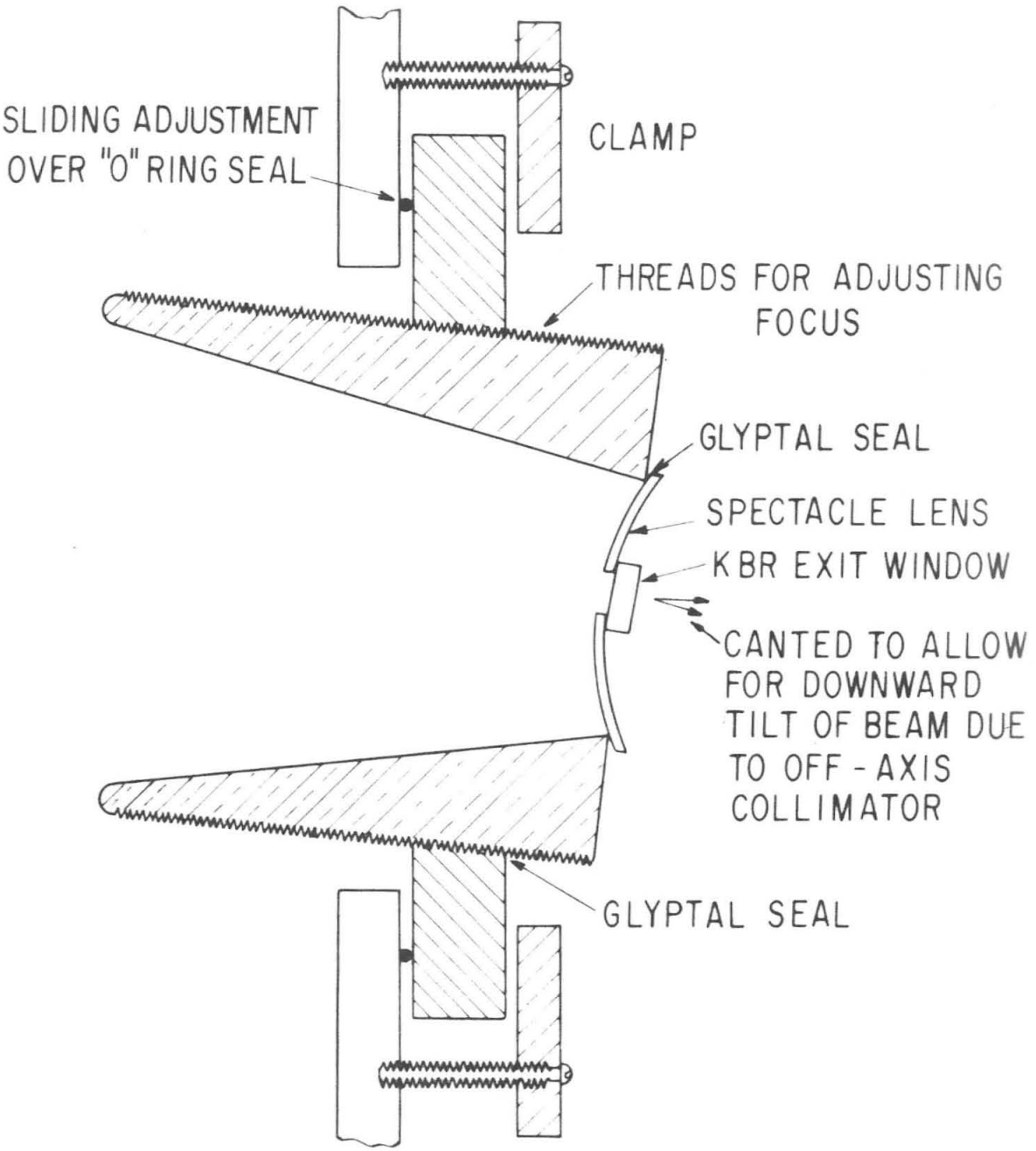

MOUNT FOR M_2

FIGURE 3

translation of the grid. This results in an extremely difficult adjustment to make--one best described as hit or miss. The manufacturers (Eppley Laboratories) have recently offered a mounting of improved design which unfortunately cannot be used with the detector heads supplied with the old mounting.

FOREPRISM OPTICS

The original design of the instrument provided for the future addition of a foreprism monochromator in a Wadsworth mounting in the sidetube containing the detector and entrance optics. This would create the problem of aligning two parts of the spectrometer on individual mountings. With the exercise of some ingenuity it was found possible to accommodate a foreprism monochromator with Littrow mounting on the same carriage as the grating monochromator. To accomplish this in the limited space available it was necessary to locate the prism monochromator on a level below the grating monochromator and to fold the optical path at one point. The optical arrangement is shown in figure 4. The collimator, M_2, is a 40 cm. spherical mirror. M_3 is a flat plate mirror installed to fold the optical path. The slit images are 11.5 cm. above the

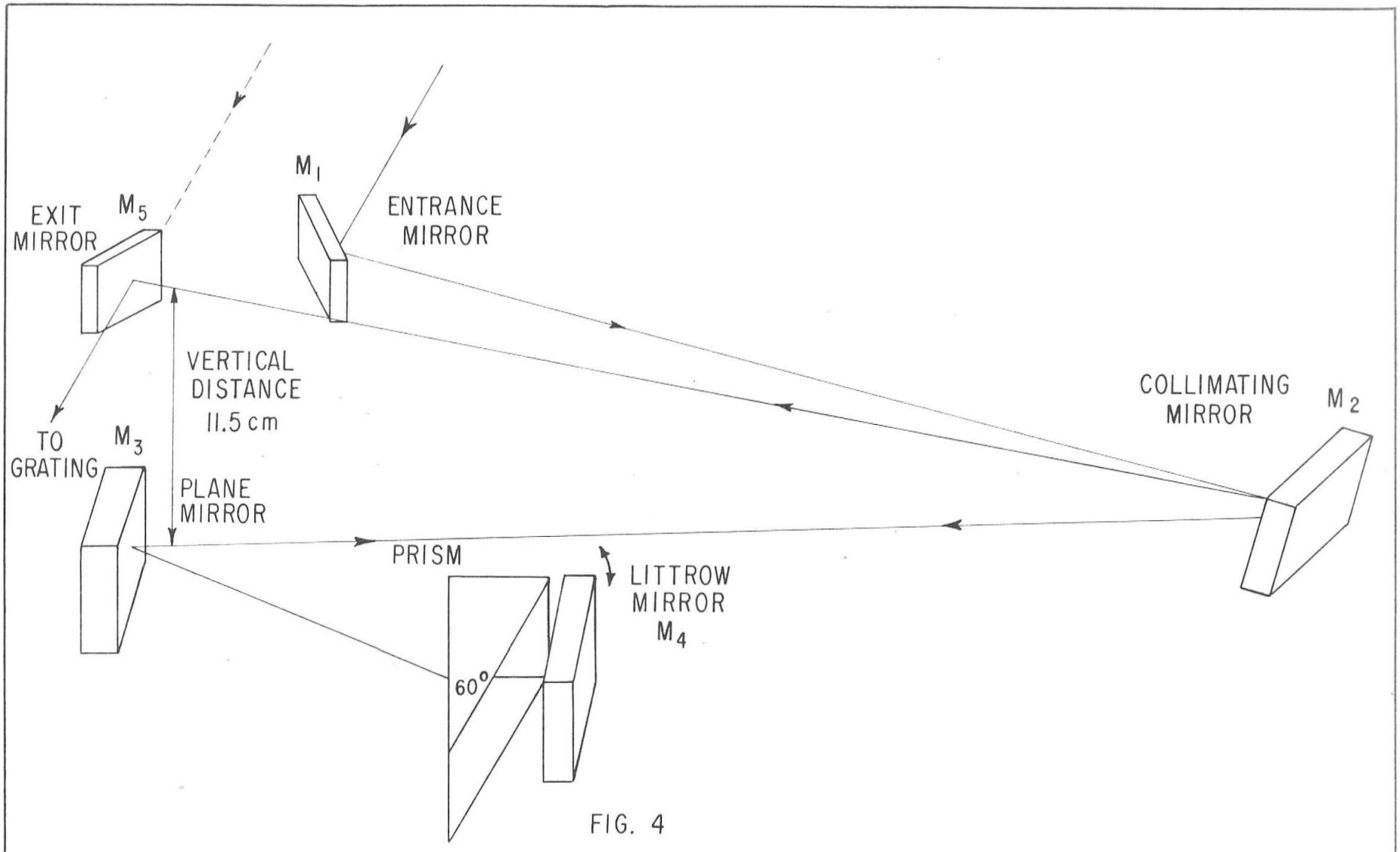

FIG. 4

FOREPRISM MONOCHROMETER OPTICS

horizontal plane containing the axis of the collimated beam. This is necessary to allow the prism monochromator to be placed below the grating monochromator, but has, as a consequence, a rotation of the slit images with respect to each other.

To study the aberrations introduced by using the collimator so far off-axis, a preliminary model of the monochromator was made and tested. It was decided that a resolution limit 0.1 micron at 3 microns would be required to properly isolate the grating orders. It was found that aberrations became serious if a much smaller resolution limit was attempted, but that for 0.1 micron, they would not be important. M_3 can be replaced by a correction plate if it should ever become necessary to improve the resolution. In practice, the potassium bromide prism can resolve the yellow doublet of the mercury spectrum at 5769-5790 Å.

Space limitations caused by the large concave mirror in the exit optics made it convenient to place the foreprism before the grating monochromator in the optical path. Space limitations caused by the narrow carriage on which it was wished to mount the foreprism dictated that it be designed so that its resolution would add to that of the grating. There will be occasions on which it is desirable to remove the foreprism from the optical path and substitute filters

to increase the energy available. Consequently, the intermediate and exit slits of the double monochromator were made so that they could function as a unit with the grating monochromator when the foreprism is not being used. Since only one of the two slits of a foreprism need be precisely made when the resolutions add, the entrance slit of the foreprism was designed to be a fixed slit. Several slits of various sizes are provided mounted on plates which can be rapidly substituted.

The above design considerations were made primarily on the basis of mechanical convenience, but they do have an important bearing on the performance of the instrument which is worthwhile to point out. If the intermediate slit were made the wide slit of the two foreprism slits, the wavelength which was passed by the instrument would depend on the coupling between the two monochromators as well as on their exact wavelength settings. With the slits arranged with the primary slit the wide one as is the case with this instrument, no such requirement exists on the coupling between the two monochromators. This is fortunate, since the wavelength calibration can then depend only upon the setting of the grating, and the grating mounting is by far the most precise element in the system.

In general, a potassium bromide prism is used because

of its wide wavelength range which corresponds closely to that of the echelle grating. In the event that its relatively low dispersion and high scattering should become objectionable at short wavelengths, prisms of sodium chloride or glass are available. Each prism is mounted on its individual table. The potassium bromide prism table is adjusted for height and tilt with adjusting screws in the optical bench. When these screws are set, screws in each of the other two prism tables are adjusted to conform to the potassium bromide table. In this way each table can be individually adjusted, while the more precise adjustments in the optical bench can be left set for the potassium bromide prism.

Ideally, each prism should be rotated about the vertical axis to produce minimum deviation at the midpoint of its wavelength range. It has been found more convenient to make this adjustment using the mercury green line. This can be done visually by observing the position of the green line and rotating the prism until the line is at its maximum deflection. The loss of resolution due to this is negligible.

MECHANICAL DETAILS

The grating drive incorporates a sine screw mechanism

to produce a movement of the grating table proportional to the sine of the movement of the drive shaft. This results in a scale which is linear in wavelength without the use of a cam (figure 5). The sine screw mechanism consists of a flat surface attached to a nut which travels on a very precisely-made screw. The flat is oriented on the nut so that the plane containing its surface passes through the axis of the grating table when the nut is in the zero position. This condition is necessary and sufficient for producing the sine function.

The mechanism worked well for an echelette grating where the angular range in which the grating is used is small, but, for the echelle-type grating to be described below, a longer range is required. A second range slightly overlapping the first and extending to larger grating angles was consequently added by making the following changes (figure 5): A second flat was attached to the sine-screw nut, facing the first, and making an angle of about 40° with it. The original ball follower was replaced by a barrel-shaped roller with its axis vertical. It could be caused to bear alternatively on either flat. The roller is connected to a pinion which meshes with a rack on either flat to insure that the roller actually rolls on the flat and does not slide. The clearances are such that the roller

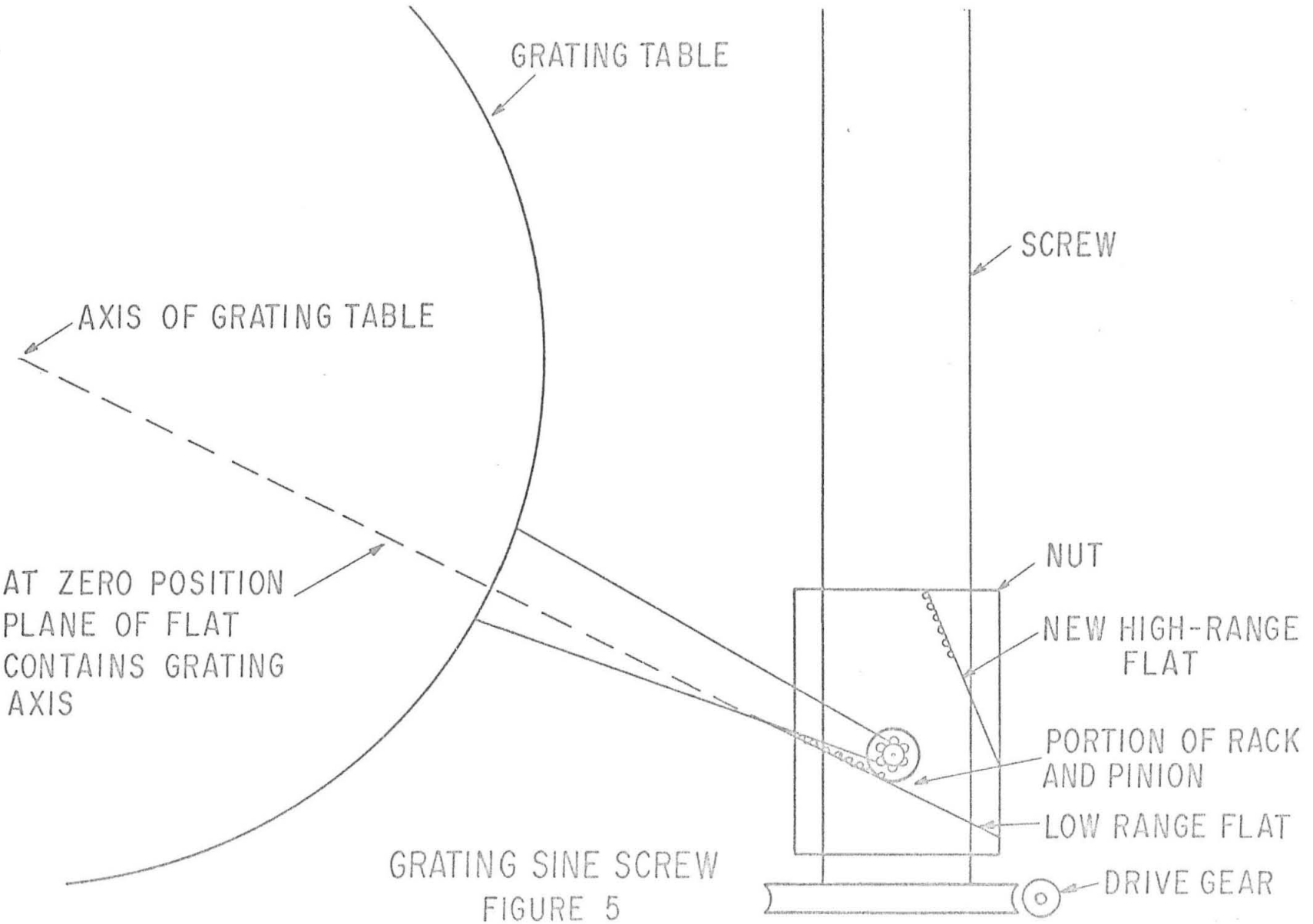

GRATING SINE SCREW
FIGURE 5

rests on the flat, and the rack and pinion mechanism merely turns the roller. With some care the rack and pinion can be engaged so that the same portion of the roller is used each time. This arrangement has the additional advantage that the rubbing of the ball on the flat is eliminated and calibration should not change on account of wear at this point.

To correspond to the angle which the two flats make with each other it was necessary to provide for two alternative locations of the grating and its holder on the grating table, differing by a rotation through this same angle. Since the grating holder is mounted in kinematic fashion with three feet resting in appropriate cavities in the face of the grating table, this was easily accomplished by providing the grating holder with three additional feet.

It was mentioned in the paper describing the original instrument that irregularities exist in the screw. To investigate these a Rayleigh interferometer was set up on the grating table as shown in figure 6. As the table rotates, the path lengths through the two plates change relative to one another, causing the fringes to move across the field of the microscope. The plates ideally should have beveled edges so they can be placed close together at the apex. This type of plate was not available and the rectan-

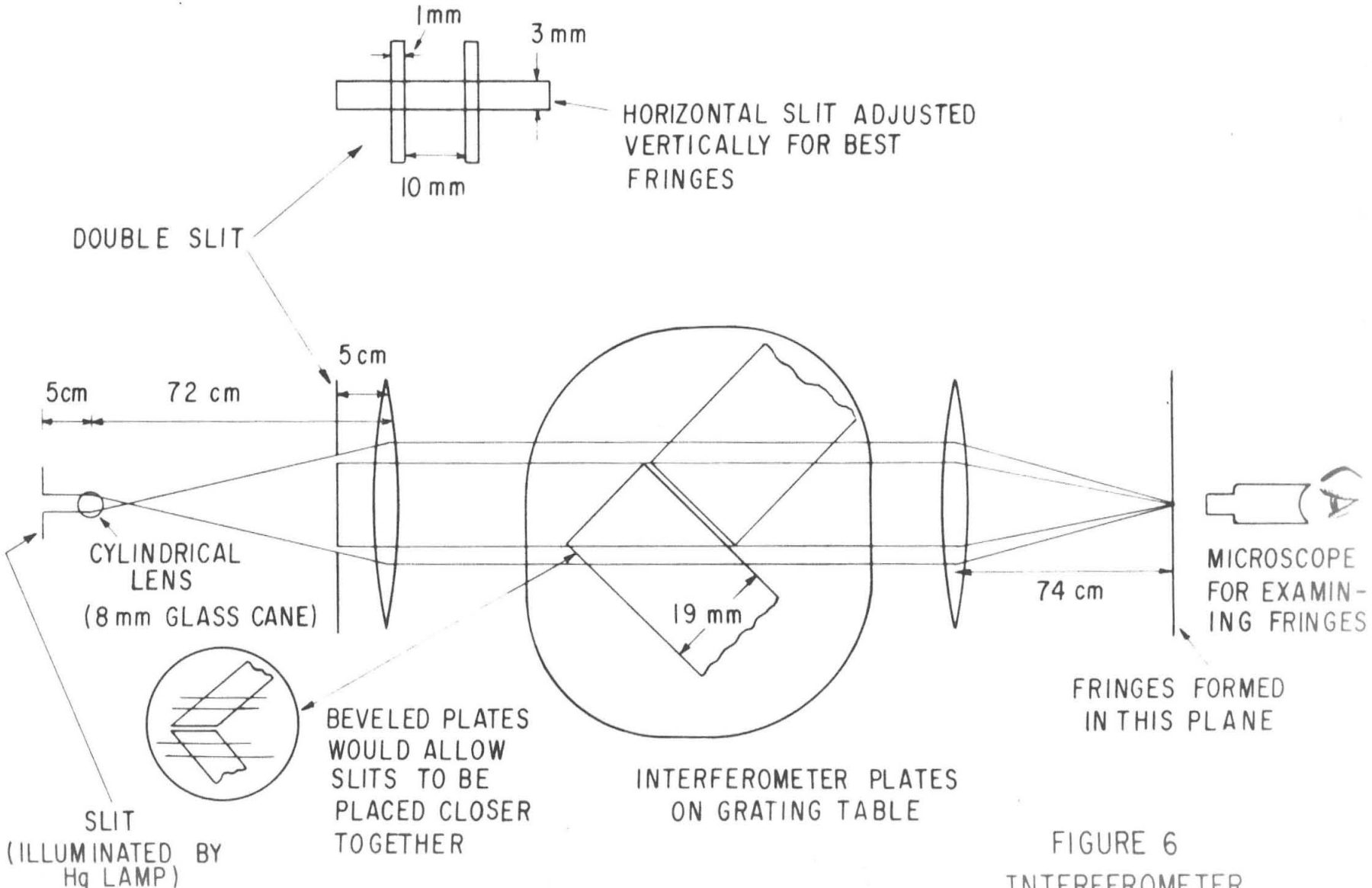

FIGURE 6
INTERFEROMETER

gular plates used made it difficult to obtain consistent fringes. One would observe several well-defined fringes followed by a region in which the fringes were either very poorly defined or missing altogether. This condition could be alleviated to some extent by very careful adjustment of the slits with respect to the flats. Because of the poor quality of the fringes, the results obtained should be regarded as indications rather than precise measurements.

It was assumed that, for small differences in table position, the number of fringes passing the field of the microscope was proportional to the angle of rotation of the table. A typical set of results is shown in figure 7. The Veeder-Root counter which gives the position of the grating drive was observed, and the number of counts corresponding to ten fringes passing through the field of the observation microscope was recorded. This was repeated until about two turns of the drive screw had been completed. The number of counts for each observation was averaged for the full two turns of the screw, and the deviation of each observation from this average was computed. These deviations are plotted as the ordinate in figure 7. The abscissa is the rotation of the screw.

The data in figure 7 are the average of several experiments made on the same portion of the screw (about two revo-

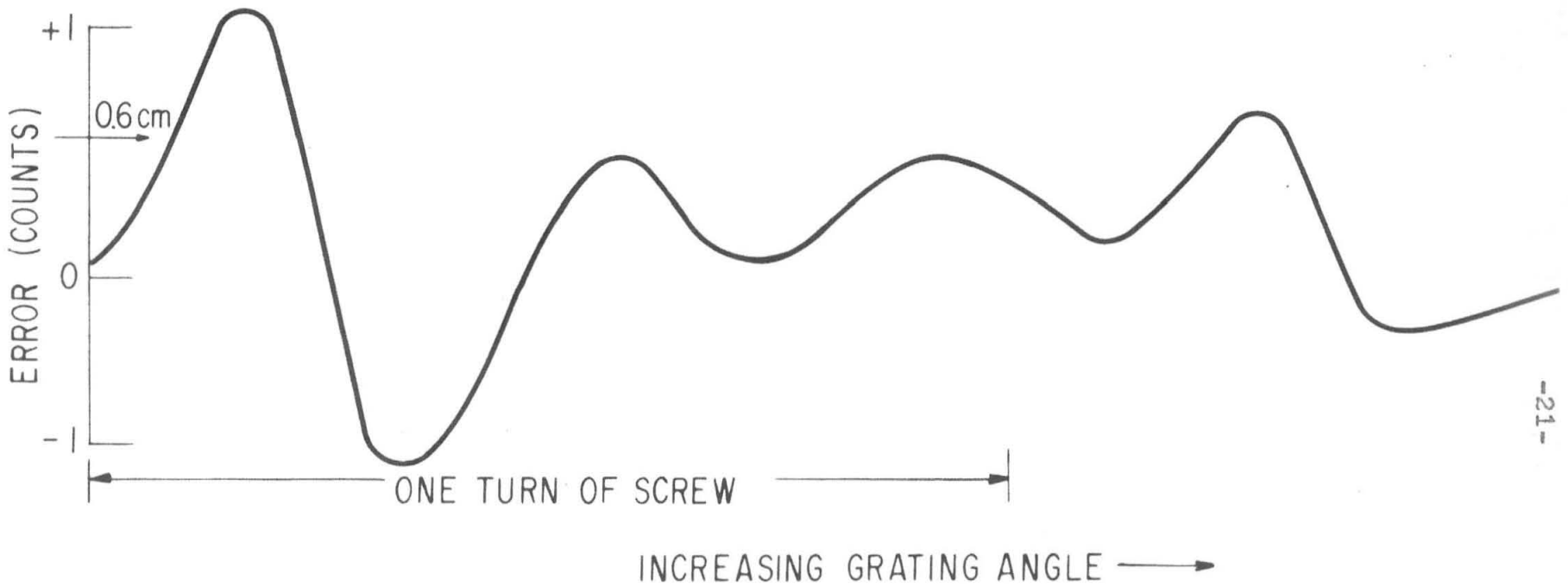

INTERFEROMETER RESULTS

FIGURE 7

lutions). The deviations between separate experiments were small enough to assure one that the errors observed were characteristic of the screw and not due to statistical fluctuations. The most obvious feature in figure 7 is the complex form of the curve. It is certainly not periodic in any integral number of revolutions as might be expected if the irregularities were due to some defect in the lathe on which the screw was cut. One can make an estimate of 0.06 counts for an average error. This corresponds to an error of $\delta\lambda/\lambda = 3 \times 10^{-4}$ which is satisfactory for routine measurements. For more precise measurements an interferometer might be incorporated in the grating monochromator to produce calibration fringes on the recorder tracing. Attempts to eliminate this error by calibration with known spectral lines are apt to be frustrated by the small period of the error in comparison with the spacing of suitable calibration lines.

The grating drive shaft passes through an "O" ring seal in the vacuum casing to a gearbox. The grating drive motor is mounted, together with its reduction gear, on vibrationless mounts on top of the vacuum casing, and is connected to the gearbox through universal joints. At the highest drive speed, no effect is discernible in the output of the spectrometer due to vibration from the drive

motor. The motor is a 3-phase synchronous motor running at 1800 rpm. Reduction ratios of 2^n are available where n is 1,2,...,8. Using the highest speed, the spectrum can be scanned at the rate of 0.5 μ/min. At the lowest speed the drive scans one micron in 8 hr. 32 min.

An interlock system is provided to prevent overrunning the mechanical limits of the grating screw. This is activated by two microswitches mounted at either end of the screw. A manual override is provided to return the nut past the actuation point of the switch when reversing direction.

A pipper system is provided for keeping track of the grating position on the recorder chart. A switch is momentarily closed on each revolution of the grating drive shaft. A second switch is arranged to either open or close on each tenth revolution. These two switches are connected in series with a battery and potentiometer. When both switches are closed the potentiometer adds a small negative signal to the output of the detector amplifier. Thus, a series of negative pips appear on the recorder tracing. Depending on the connection of the second switch, either a pip appears for each revolution except the tenth or for each tenth revolution.

The redesigned slit mechanism for the intermediate and exit slits is shown in figure 8. The slits are mounted on

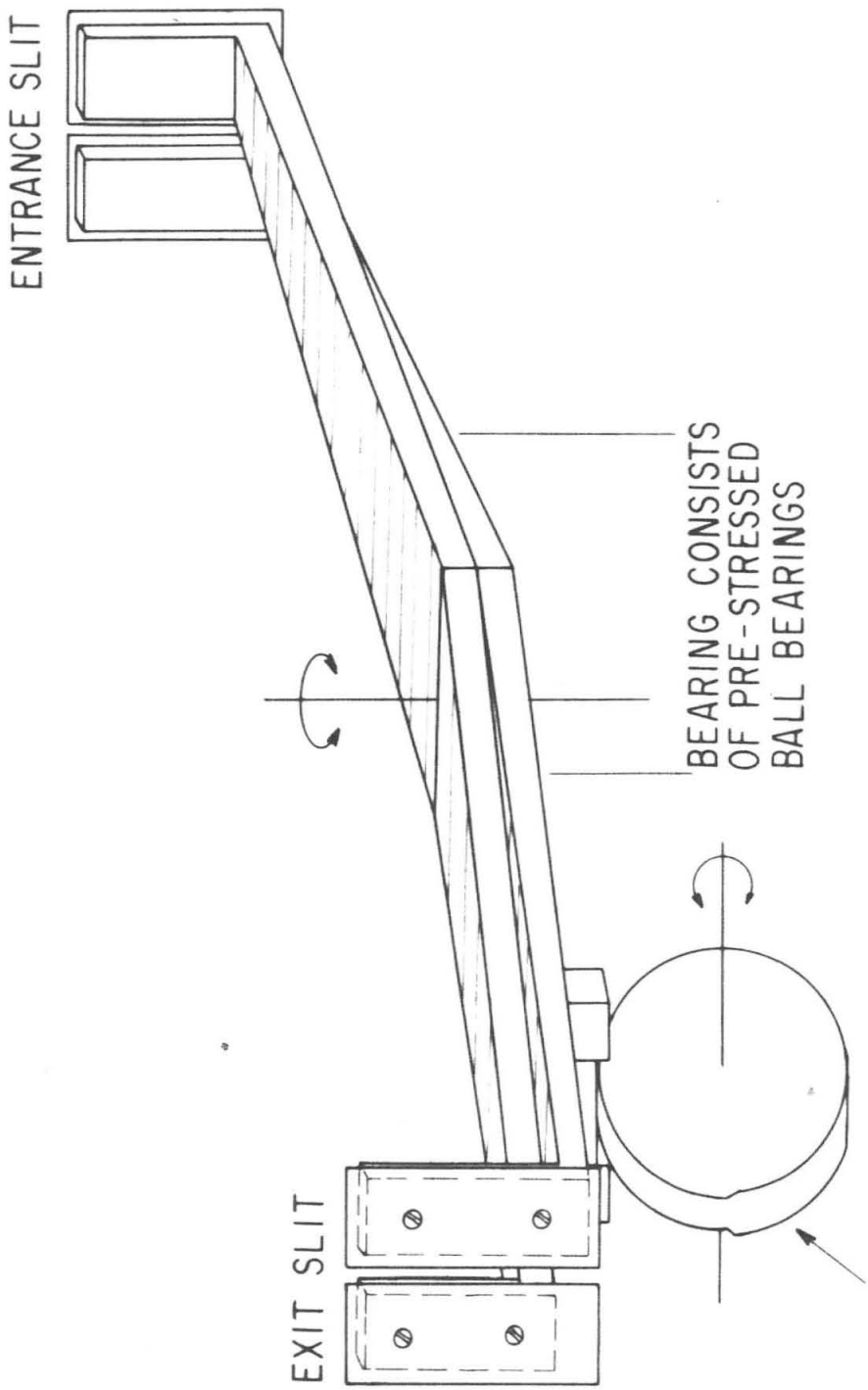
ENTRANCE SLIT
BEARING CONSISTS OF PRE-STRESSED BALL BEARINGS
EXIT SLIT
CAM FOR ACTUATING SLITS

FIGURE 8

the ends of two bars pivoted to form a scissors mechanism. The scissors are operated by a cam acting on followers at one end of the arms. The development of this cam is an isosceles triangle which is wrapped around the circumference of a wheel and thus moves each arm equally. The individual jaws are attached to their supports by screws passing through enlarged holes to allow for adjustment.

The drive shafts for the slit mechanism and for the foreprism Littrow mirror pass through "O" ring seals in the vacuum casing to the gear box. The gear box contains the mechanical and electrical components of the electric cam systems which synchronize the foreprism and slit drives with the grating drive.

An electric cam performs electrically exactly the same function as a mechanical cam--imparting a motion in a slave mechanism which is some mathematical function of the movement in a master mechanism. Mechanical cams are difficult and expensive to build and, once finished, cannot be easily readjusted. An electric cam can be built easily from standard components, and is easily adjusted. In addition, the function generated can conveniently be shifted or multiplied by a constant factor. This can only be accomplished mechanically by complicated linkages.

A simplified diagram of an electric cam is shown in

figure 9. The amplifier is connected so that any signal appearing between the two movable contacts of the potentiometers will be amplified and applied to the motor in proper phase to drive the slave potentiometer to decrease the signal. The motor will run until the input to the amplifier is below some threshold depending on the gain of the amplifier, and then stop.

Without the loading network this would operate as a normal follow-up, the slave drive reproducing the master drive movement. With the loading network, however, the voltage above ground on the movable arm of the slave potentiometer can be made to closely approximate any continuous monotonic function of the movement of the arm. The only requirement is a sufficient number of legs in the loading network. Since the amplifier and motor still tend to keep the voltages on the two movable arms equal, the slave drive will move an amount which is a function of the master drive movement. This function depends on the setting of the loading network, and can be varied at will. By placing varying resistances between a potentiometer and ground a constant factor can be added to the drive function. By changing the total voltage across the loading network and slave potentiometer, a small portion of the slave can be made to correspond to the entire length of the master,

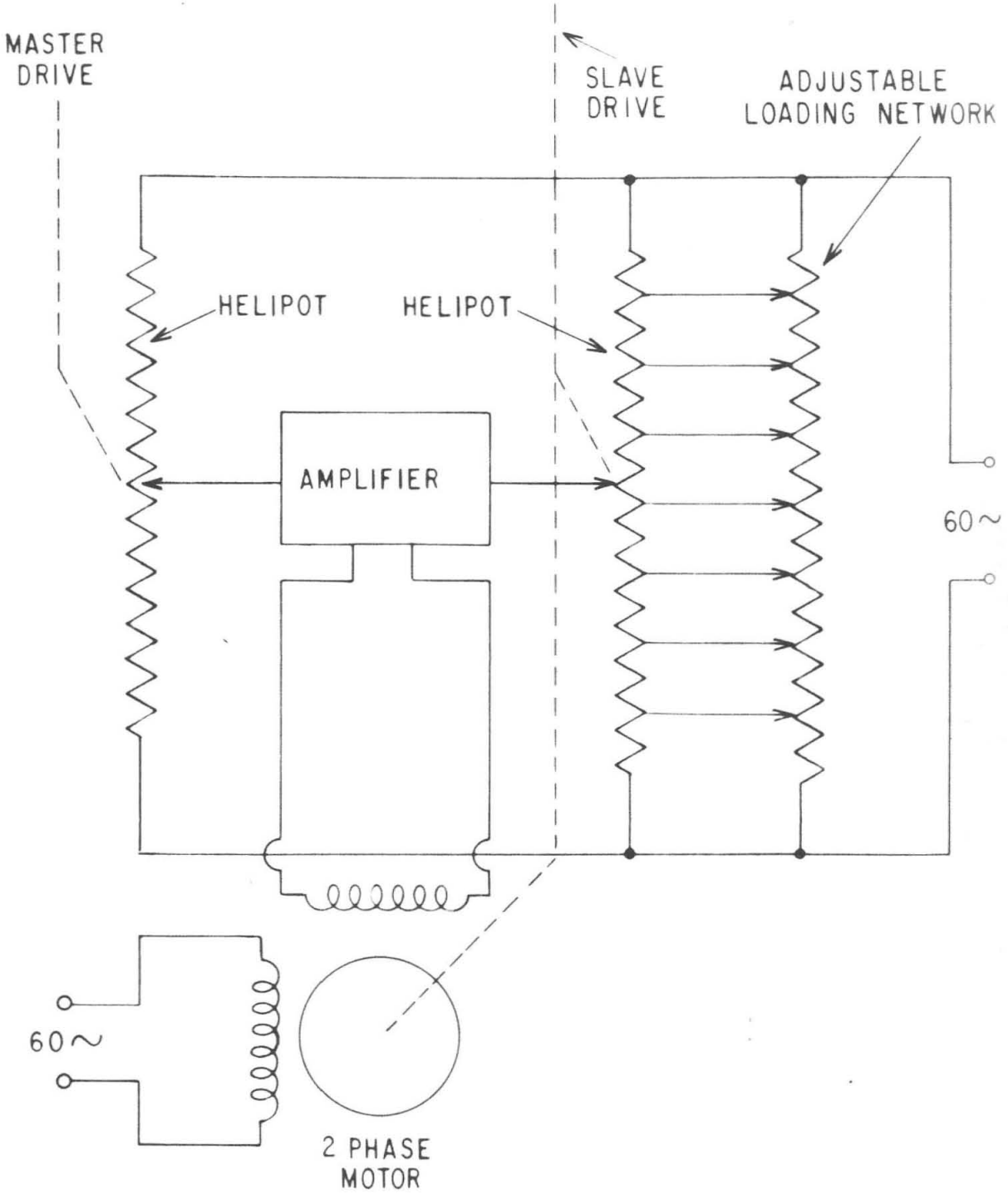

FIGURE 9
ELECTRIC CAM

and thus the drive function can be multiplied by a constant factor.

The circuit diagram for the slit cam is shown in figure 10. As can be seen, the function is linear. The absolute slit opening is controlled by the two variable resistors in the slit potentiometer circuit. The rate of opening is controlled by the switches in the master potentiometer circuit. This, of course, is only a very rough approximation to the required function, but has been found adequate.

The prism cam (figure 11) has a drive function corresponding to the prism dispersion. It is provided with a six-position switch for adjusting the relative voltages on the two potentiometers. At present, four positions are used--three for the lower range of grating travel in first, second, and third grating orders, and one for the high range in first order.

The loading network consists of a series of potentiometers connected to two busses by fixed resistors. The taps of the network are taken from the variable arms of the potentiometers. The total resistances in the slave potentiometer and the loading network are chosen so that approximately 170 times as much current flows in the loading network as in the potentiometer. This has the effect of making

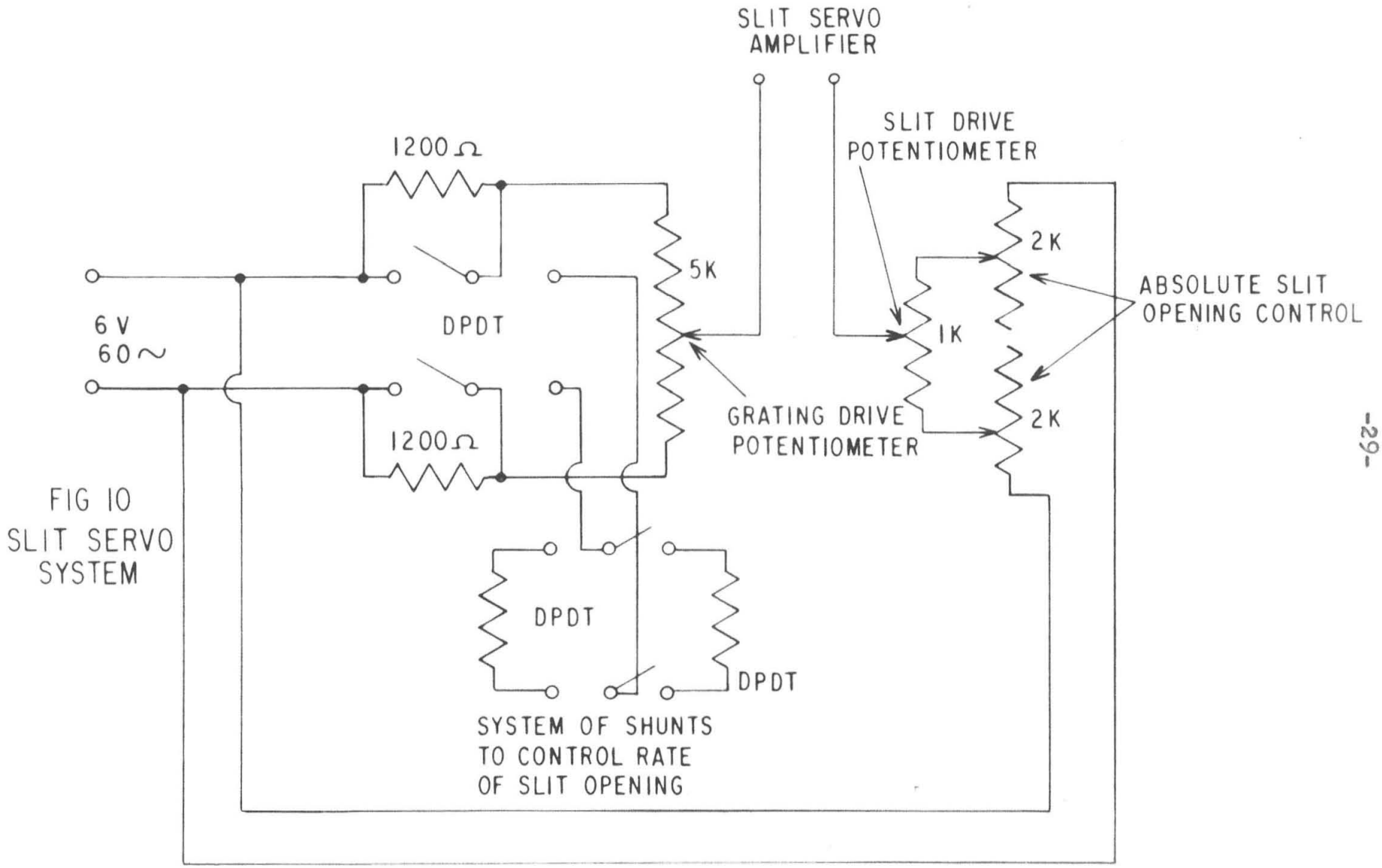

FIG 10
SLIT SERVO
SYSTEM

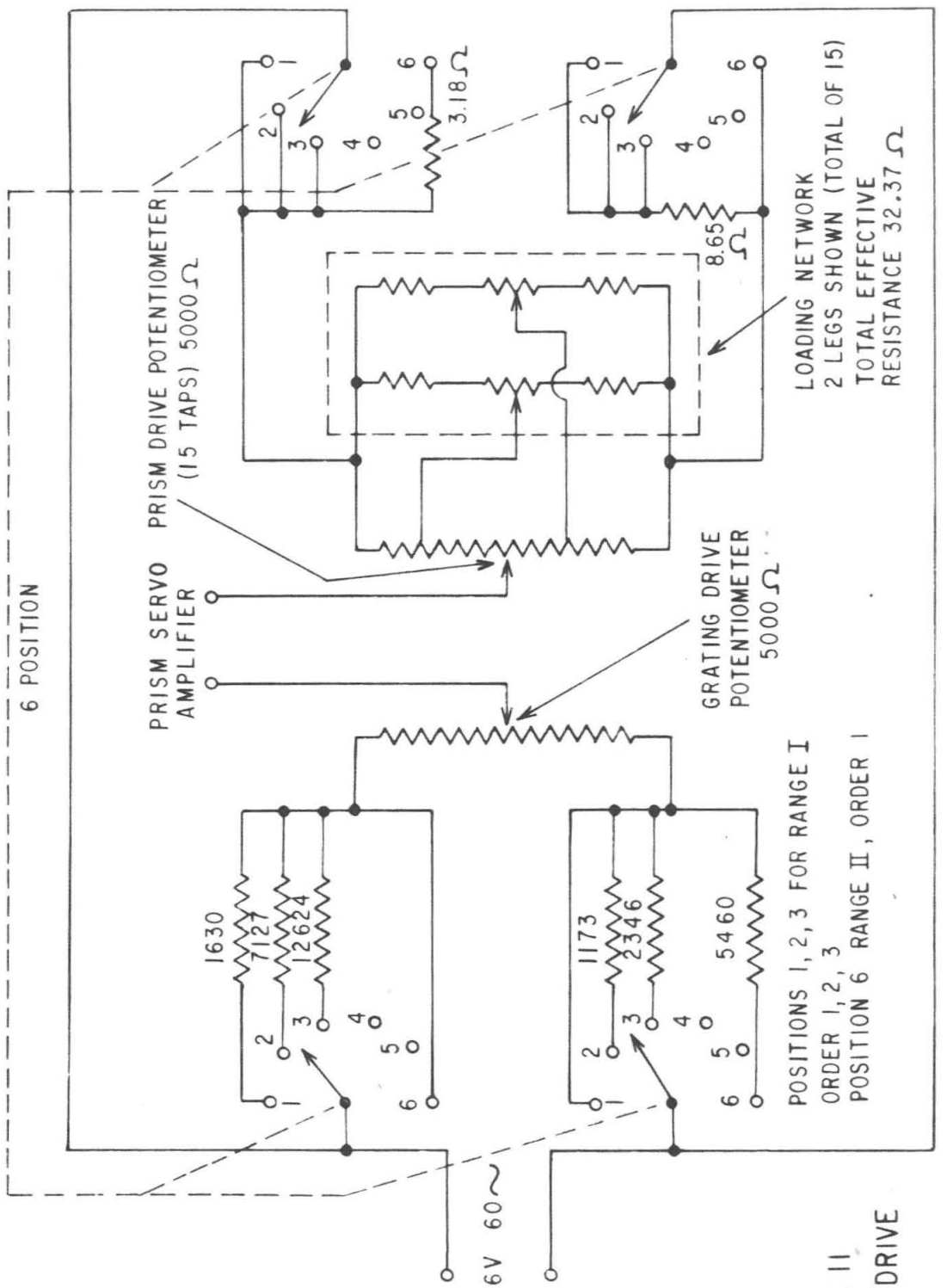

FIGURE 11
PRISM DRIVE

the individual adjustments of the loading network more independent. It also serves to protect the potentiometer from high currents.

The two servo amplifiers are practically identical to the Brown potentiometer recorder amplifier. A copy of the Brown circuit was made from standard components with one exception. It was found that any standard input transformer gave far too much pickup from stray fields in the laboratory. When Brown input transformers were substituted, the circuit worked well.

The input circuit is slightly different from the Brown circuit. When the cam circuits are operated on alternating current there is no need for the chopper common to potentiometer recorders. This was omitted from the prism amplifier. In the case of the slit system, it may be desirable to operate it from a DC source. For example, there is available in the detector system to be described in Section IV a DC voltage proportional to the total intensity falling on the detector. It would be convenient to subtract this voltage from a fixed voltage and apply this difference to the slit servo amplifier. This would have the effect of maintaining the intensity in the system constant. To provide for such applications, the slit amplifier was built to accommodate a synchronous chopper when desired. For

operation on alternating current, the chopper is removed and a shorting plug which makes the necessary circuit changes substituted in the socket. A second plug on which is mounted an on-off and a reversing switch can be substituted to provide for manual operation.

ADJUSTMENT PROCEDURE

In setting up the instrument, the grating monochromator was aligned first. The collimator was adjusted as well as possible visually about the transverse axis (the horizontal axis perpendicular to the long dimension of the carriage). Next, a plumb bob was suspended over the center of the grating table and its image observed in the collimator. The final adjustment of the collimator about its vertical axis was made by causing the plumb bob and its image to coincide when viewed from approximately one meter behind the grating table.

A flat was then installed on the grating table and the table set at zero. The flat was carefully adjusted to lie in a vertical plane with the aid of a spirit level. The image of a mercury lamp was focused on the exit slit. The collimator was then given a final adjustment about the transverse axis to illuminate the grating. It was noted at this

point that the beams going away from and toward the collimator coincided in the vertical direction and that the illuminated portions of the Newtonian mirrors had the same elevation. These two observations were taken as final evidence for the correct adjustment of the collimator mirror.

The Newtonian prism was given its final adjustment about the longitudinal axis by demanding that the illuminated portion of the entrance slit correspond in a vertical direction with the illuminated portion of the exit slit as measured with a scale. Finally, a second lamp was focused on the entrance slit, and the Newtonian prism was adjusted about the vertical axis to produce a symmetrical pattern on the collimator.

With the grating monochromator properly adjusted, the mirrors of the foreprism were adjusted. M_5 was installed, and the grating exit slit illuminated. A card was then used to follow the light path through the monochromator. The mirrors were adjusted until a spectrum was obtained at the entrance pupil of the foreprism.

The collimator was adjusted to bring the spectrum to a focus at the point calculated for the primary slit. With this preliminary adjustment made, the image of the flat replacing the grating was observed visually at the entrance pupil. The various mirrors of the foreprism monochromator

were adjusted until this image was not cut off by any object in the foreprism. Finally, the first Newtonian, M_1, was adjusted to place the entrance beam in a horizontal plane and perpendicular to the carriage of the instrument. With the instrument in the casing, the entrance slit was installed and adjusted to conform to the spectrum.

The above adjustments must all be made with the exit optics removed in order to illuminate the exit slit. With the entrance slit adjusted and the exit optics in place, a beam through the foreprism can be obtained for lining up exterior optics by removing the grating and focusing the image of a mercury lamp on the intermediate slit with the grating collimator. The prism Littrow mirror is then adjusted to place the green line on the entrance slit.

The grating monochromator was calibrated with the wide-range grating described below. A light from a mercury lamp was focused on the intermediate slit and the grating scanned throughout its range. The lines listed in Table I[8] were used for the calibration. They could be observed, except where overlapped by other lines, in all orders of the grating range. From the spacing of the lines on the tracing and the grating constant, the grating angle could be expressed as a function of grating driveshaft rotation. The function was linear within experimental error in the

TABLE I--SPECTROMETER WAVELENGTH CALIBRATION

WAVELENGTH (MICRONS)	NUMBER OF ORDERS OBSERVED	COUNTS PER MICRON[a]
0.54607 (green)	31	119.2
0.57696; 0.57906 (yellow doublet)	25	119.2
1.140	16	118.9
1.287	15	119.1
1.357	12	119.0
1.367	12	119.0
1.395	12	119.0
1.530	11	119.0
1.694	10	201.6
1.711	10	203.3

a. Number of counts on grating drive counter which correspond to one micron in the first order of the echelle grating.

lower range, but required a small second order term in the higher range.

ENTRANCE OPTICS

The exterior optics were intended to be as flexible as possible to accommodate different experimental set-ups. Basically it is only necessary to illuminate the entrance slit with radiation modulated at the amplifier frequency. The two set-ups used by the author in the study of N-methyl formamide are shown in figures 12 and 13. The first uses an absorption cell consisting of a steel tube 4" in diameter and 36" long. A bulkhead in one end supports the windows which are NaCl. A shroud extends beyond the windows to protect them from drafts, to confine the nitrogen used to flush away atmospheric moisture and CO_2, and to support the 45^{o} mirror. The chopper and source were mounted at the end of a short 7/8" tube soldered in the side of the shroud. A plate on the opposite end supports a 40 cm. concave mirror and provides a clean-out port. The entire cell, including the shroud, is heated by a resistance winding insulated with asbestos paper. The mirror end of the cell is given additional heat by a 1000 ml. heating mantle to prevent condensation on the mirror. The window portion is wound

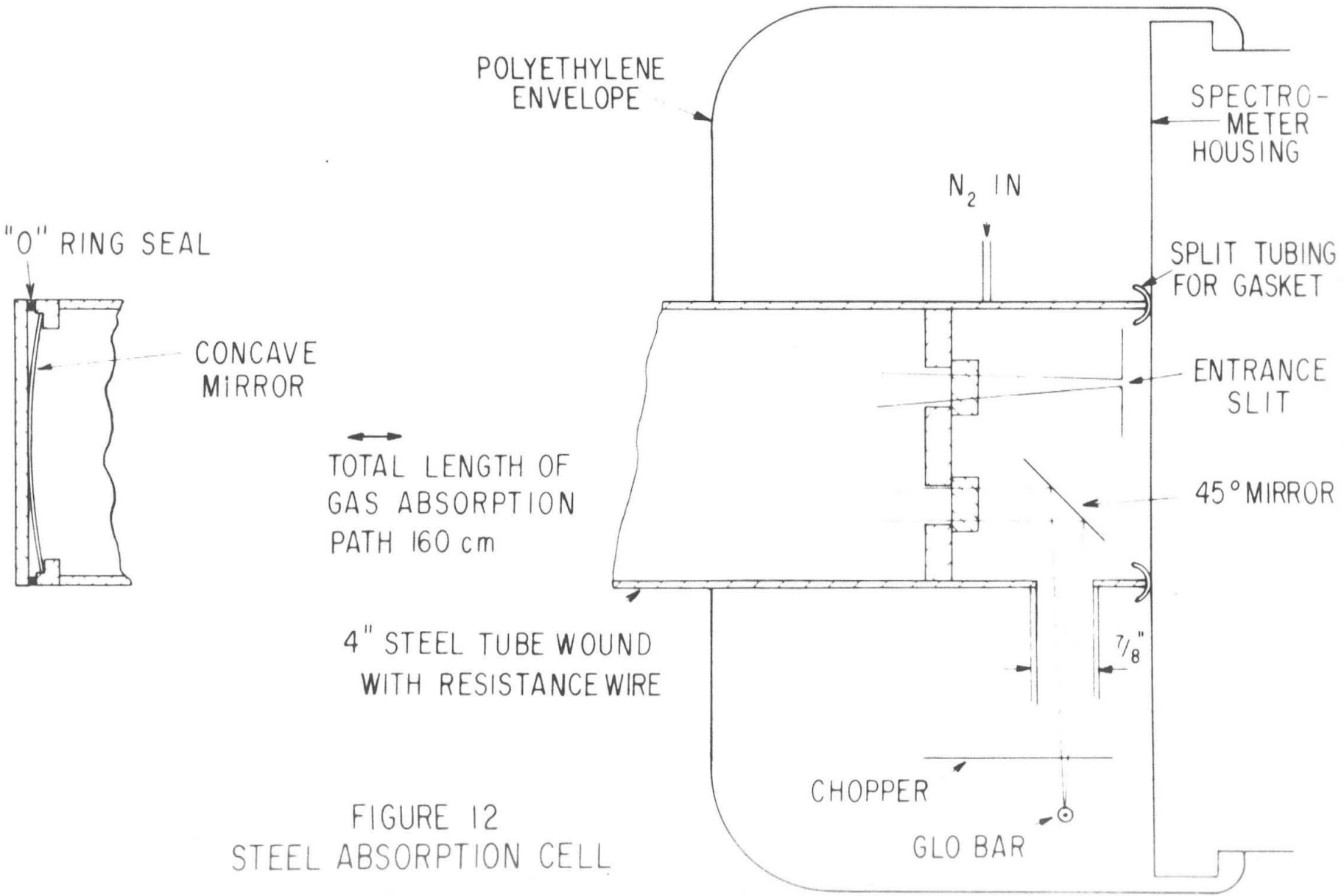

FIGURE 12
STEEL ABSORPTION CELL

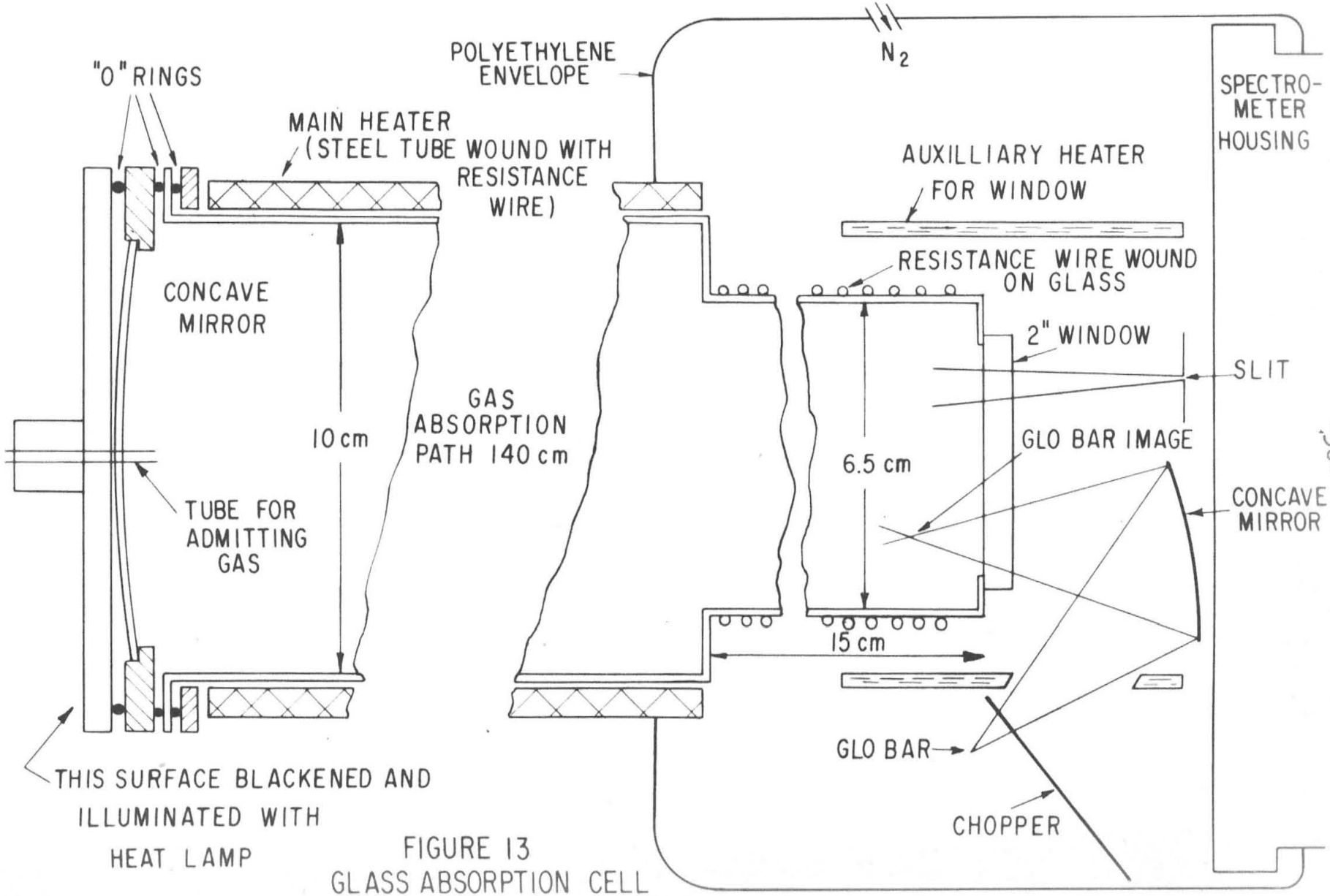

FIGURE 13
GLASS ABSORPTION CELL

more closely than the main portion to prevent condensation on the windows.

The second set-up was built when more precise temperature and pressure control became important. A glass tube was used with a single potassium bromide window on the end. This fitted into a steel tube wound with a resistance wire for a furnace. An auxiliary tube heated and protected the window, and a heat lamp heated the mirror. The mirror was held by a brass fitting clamped to a flange on the end of the glass tube. Contact with the glass was made by "O" rings to allow for differences in expansion. Gases were admitted and removed through a glass tube passing through a seal in the end plate and through a hole in the center of the concave mirror.

The source, chopper, and exterior part of the optical path of both set-ups were enclosed by a polyethylene film, the interior of which was flushed with nitrogen. With the steel tube, passing dry nitrogen first through the shroud and then out through the 7/8" tube to the interior of the polyethylene enclosure practically removed the effects of atmospheric absorption bands. The strongest water line in the 7μ band gave 95% transmission as opposed to 5% without flushing. Because of poorer nitrogen flow, the glass cell did not give this performance.

CONCLUSION

The instrument with its modifications is shown in figures 14 and 15. It is believed that the task of bringing the instrument up to date while retaining its advantages of high resolution, flexibility, and freedom from atmospheric interference has been accomplished.

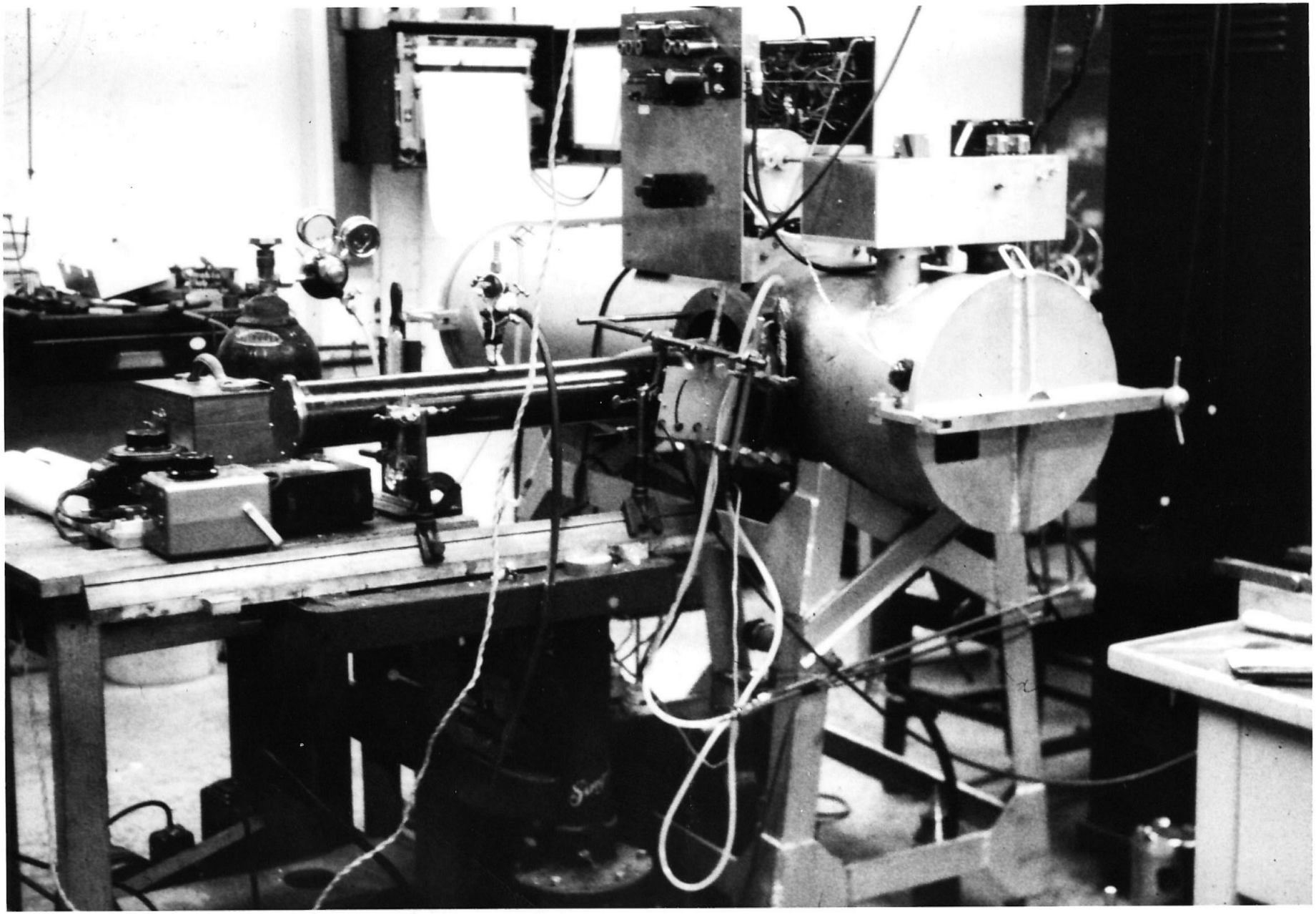

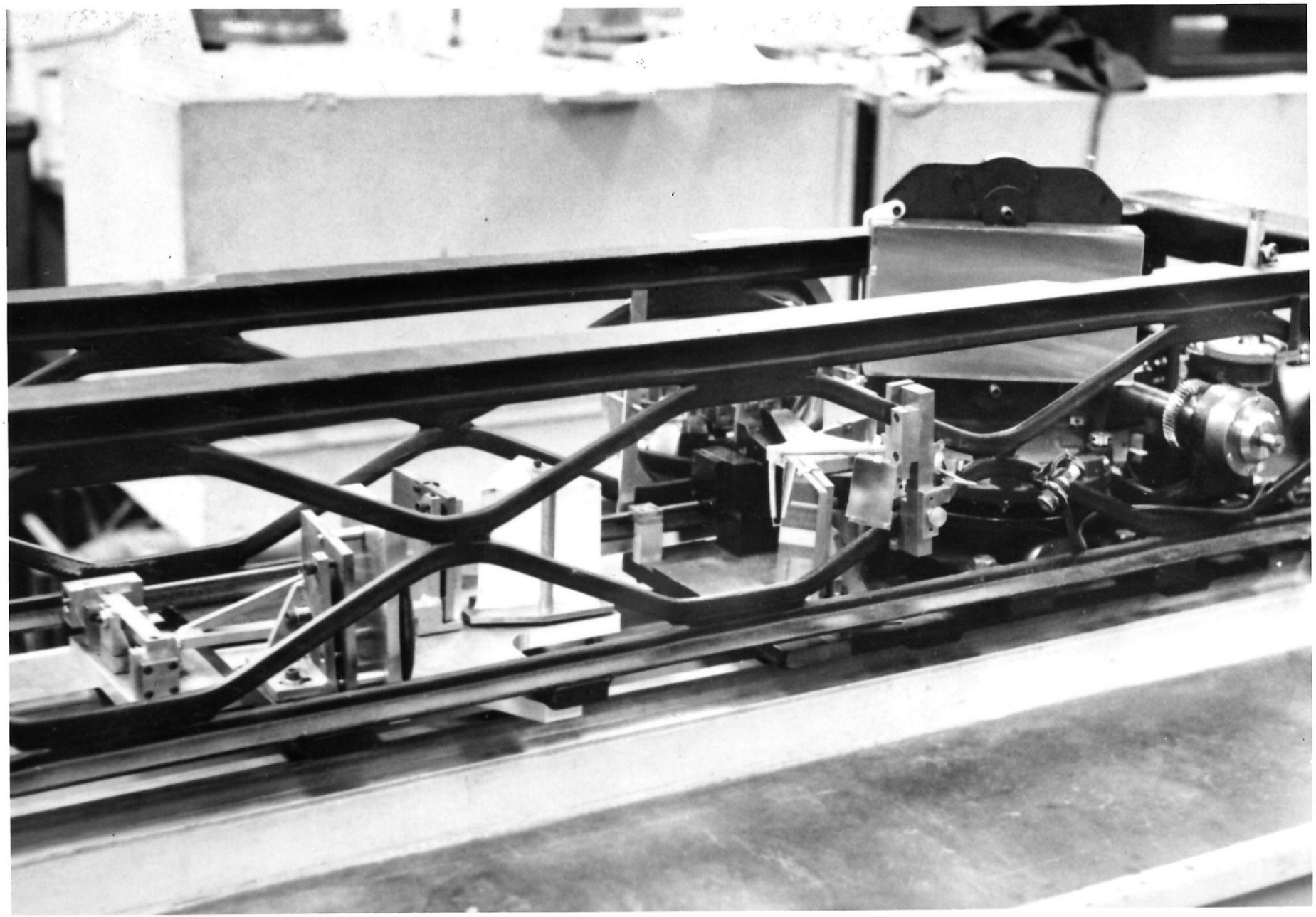

SECTION II

A STUDY OF N-METHYL FORMAMIDE VAPOR IN THE INFRARED

INTRODUCTION

This section of the thesis will present a study of N-methyl formamide in the vapor phase. The purpose of the study is to elucidate certain features in the structure and infrared spectrum of molecules in the vapor phase which contain the N-substituted amide group. It is important to do this for two reasons: In the first place, the identification and characterization of the amide group in a molecule by chemical means is difficult. On the other hand, it has been shown[9] that the infrared spectrum due to this group in a molecule is one of the most stable and reproducible in the condensed phases. In the vapor phase of the N-substituted amides, one might expect the spectrum to be quite different, but it is not clear exactly what the difference will be. Thus, an understanding of the infrared spectrum of a molecule containing the N-substituted amide group in the vapor phase is important from an analytical standpoint.

Of even greater importance is the understanding of the structure of the N-substituted amide group in terms of its biological significance. A protein molecule consists of amino acids linked together through peptide linkages. The

simplest molecules containing the peptide linkage are the N-substituted amides. Certain features of the infrared spectrum have been shown to be common to the condensed phases of the N-substituted amides, the polypeptides, and the proteins. The presence of these features in simple molecules greatly facilitates the understanding of the same features in the more complicated molecules. For this reason, there has been a great deal of effort devoted to the study of the condensed phases of the N-substituted amides.[10-13] While the understanding of the condensed phases may be said to be quite far advanced, this is by no means true of the vapor phase.

It certainly is not to be argued that the structure of the N-substituted amide group in the vapor phase has a direct biological significance. One very definite benefit can be expected, however, from a thorough study in the vapor phase of a small molecule containing the group. As will be brought out below, the basis for the present understanding of the structure of the amide group in the liquid phase and in solution is not nearly as well established as some authors seem to believe. Many of the previous experiments, which were intended to establish certain features of the structure, were based on faulty reasoning and need to be re-examined. It is hoped that information obtained from

this study, and from other studies which it may suggest, will facilitate this re-examination, and thus contribute to the understanding of biological problems which involve the structure of the peptide linkage.

This study, then, is directed toward obtaining a better understanding of the infrared spectrum and structure of the N-substituted amide group in the vapor phase. This understanding will be helpful in extending the usefulness of infrared techniques to the qualitative and quantitative analysis of molecules containing the amide group in the vapor phase, and in improving the understanding of the condensed phases of molecules containing the peptide linkage.

The discussion will begin with a review of the current understanding of the amide group, with particular emphasis on the N-substituted amide group, in each of the three phases. Experiments will then be described which were performed with the vacuum grating spectrometer described in Section I. Finally, a discussion of the results of these experiments in terms of the position, envelope, and behavior with changes of temperature of the various bands will lead to the conclusion that the N-methyl formamide molecule exists in two isomeric forms in the vapor phase.

THE AMIDE GROUP

The isolated amide group is commonly represented in elementary texts as having the structure shown in figure 16A. On the basis of this structure, barring steric hindrance, one would expect the molecule to be pyramidal about the nitrogen atom in a manner similiar to ammonia. One would expect the carbon-nitrogen distance to be approximately 1.47 Å on the basis of X-ray data from crystals of other compounds containing a carbon-nitrogen single bond.[14] The most reliable data with which to check these predictions come from X-ray studies of crystalline compounds containing the amide group. Corey[15] reviewed this field in 1948. The carbon-nitrogen distance in the amide linkage in a crystal is found to be much closer to 1.30 Å. The configuration of the atoms about the nitrogen atom is planar, or nearly so, rather than pyramidal. The literature which has appeared since Corey's review does not make any essential change in this picture, although, in a study of formamide, Ladell and Post[16] found a deviation from planarity of around ten degrees.

The above discrepancy between the predictions based on figure 16A and the observations on crystalline compounds were reconciled by Pauling[17] with the suggestion that a

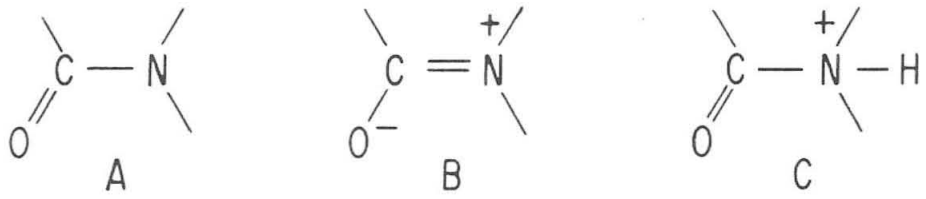

FIGURE 16

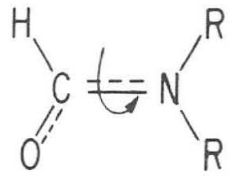

FIGURE 17

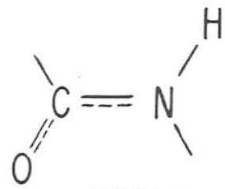

TRANS
FIGURE 18

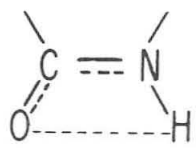

CIS
FIGURE 19

second form of the group, shown in figure 16B, makes an appreciable resonance contribution to the structure. A contribution of the structure shown in figure 16B would have the effect of making the molecule more planar about the nitrogen atom and of shortening the carbon-nitrogen bond distance. This contribution would also have the effect of greatly hindering rotation about the carbon-nitrogen bond. (Figure 17). If the two groups attached to the nitrogen atom (R in figure 17) are different, this hindered rotation will result in two geometrical isomers of the molecule being possible. In the N-substituted amides, it is customary to refer to the two isomers as cis and trans according to whether the N-H and the C-O bonds are in roughly the same, or in opposite directions, respectively. (Figures 18 and 19).

The X-ray data referred to above show that in the crystalline state, molecules having the N-substituted amide group all exist in the trans configuration. The molecules are linked together in long chains through hydrogen bonds between the carbonyl oxygen of one molecule and the amide hydrogen of the next.

If the structure of the linkage is understood in the crystal, and if suitable force constants can be obtained, it should be possible, in principle, to calculate the

normal modes of the linkage. With information regarding the dipole moment as a function of bond distance, the change in dipole moment due to the molecular vibration in a given normal mode could then be calculated. This information could be correlated with infrared polarization data on actual crystals, in order to obtain the orientation of certain bonds in the crystal. This would be particularly useful in determining the positions of hydrogen atoms, which cannot be located in the crystal with the use of X-rays. A great deal of work has been done along these lines.(18-20)

Because of the lack of suitable data on which to base the calculations outlined above, most of this work has been done using an empirical approach. Directions of change in dipole moment are measured experimentally for simple structures which have been determined accurately, and then an attempt is made to transfer this data to other more complicated structures.

The problem is complicated by the fact that the normal modes of the peptide linkage are by no means the simple ones one would expect from a consideration of the positions of the bands in an infrared spectrum of a molecule containing the linkage. For example, there is a band near 1500 $cm.^{-1}$ which one would ordinarily assign to the carbon-nitrogen stretch. It is observed, however, that the direction of the

transition moment is not along the carbon-nitrogen bond, but is inclined at some angle to it in molecules containing this linkage. In addition, if the nitrogen atom is deuterated, the band shifts markedly in frequency,[21] indicating a contribution of the hydrogen bend to the normal mode of the band.[22]

Two studies have been reported which attempt a quantitative discussion of the normal modes of the amide linkage. A Japanese group[23,24,25] attempted to calculate the normal modes and their frequencies by transferring force constant data from other molecules. Some objections can be made to this work, and these are discussed in detail below. The best data on the normal modes seem to be those obtained by Badger[26] with the aid of a mechanical model. The force constants of springs linking steel spheres representing the atoms of the linkage were altered so as to produce a set of modes whose frequencies bore the same relations to each other as the frequencies observed in the infrared spectra of molecules containing the linkage.

It is hoped that this study will improve the understanding of the normal modes. With a detailed knowledge of the normal modes and of the electronic structure of the molecule, it should be possible to make theoretical predictions regarding the direction of change in dipole

moment for the various infrared bands, and thus to make more useful the polarized infrared studies on proteins.

In the liquid phase, the existence of hindered rotation about the C-N bond has been established by nuclear magnetic resonance studies. The difference in energy levels between the two possible spin states of a hydrogen atom in a magnetic field is of the order of radio frequencies. If hydrogen atoms are placed in a suitable magnetic field, it is found that energy will be absorbed at the frequency corresponding to the transition from one spin state to the other. This frequency is accurately known for a free hydrogen atom, but, in general, is different in a molecule. One effect which changes the frequency in a molecule is the shielding by the remainder of the molecule of the field seen by the proton. This results in a shift of the frequency of resonance in a given field which is known as the chemical shift. This shift can be shown to be proportional to the applied magnetic field.[27]

Consider a di-methyl amide. The six methyl hydrogens will all show the same resonance except for the effect of the carbonyl oxygen atom on the three which are close to the oxygen atom. If the three hydrogen atoms are near the oxygen atom for an appreciable period of time, the effect will be a small splitting of the methyl hydrogen peak. If

there is rapid exchange of the hydrogens, as, for example, due to free rotation about the C-N bond, each of the six hydrogen atoms will see the same average field and there will be no splitting. Phillips[28] and Gutowsky and Holm[29] have studied di-methyl formamide and have observed the field-dependent splitting. Phillips calculated from the magnitude of the splitting that the exchange rate for the two methyl groups could be no greater than 38 $sec.^{-1}$.

It has been shown[30,31] that molecules containing the unsubstituted amide linkage exist in solution as dimers. These dimers contain eight-membered rings formed by two hydrogen bonds rather than long chains formed by many hydrogen bonds. This does not seem to be the case with molecules containing the N-substituted linkage. Huisgen and Walz[32,33] have done the most significant work on this point. They report a study of lactams containing various numbers of atoms in the ring. A lactam is a molecule containing the amide linkage in which the group attached to the carbonyl carbon is also attached to the nitrogen, thus forming a ring. If the ring is small enough, the molecule must have the cis configuration about the carbon-nitrogen bond. In solutions of lactams, these workers observed a marked change in the behavior of dielectric constant with dilution and a change in the infrared spectrum as the length

of the ring reached nine atoms. These changes were interpreted as resulting from the conversion from the cis form in the small ring compounds to the trans form in the large ring compounds. The reason for this conversion seems to be the preference of the compound to exist in the trans form when free to do so.

A similar preference for the trans form seems to exist in all N-substituted amides in the liquid and in not-to-dilute solution. The best evidence for this preference is the similarity in behavior of these compounds to the large ring lactams observed by Huisgen and Walz. There are many other works in the literature, of more or less merit, which support this contension.

Leader and Gormley[34] studied the dielectric constant of liquid amides. They found a large difference between the dielectric constant for molecules which they believed to have the cis form and molecules which they believed to have the trans form. The latter included the N-substituted amides. Their work with N-methyl formamide is open to some criticism. They noted that samples of this compound had abnormally high conductivities which they attributed to the presence of methyl ammonium formate. Using a resin column, they converted the methyl ammonium formate to formic acid. On the basis of an observation on acetic acid in formamide

solution, they believed this would have no effect on the dielectric constant of the N-methyl formamide.

Mizushima and co-workers[23] report a study of N-methyl acetamide using several different methods. They compared the position of the absorption in the ultraviolet of N-methyl acetamide to the position of the similar absorption of acetone. Their argument was that, if only the structure of figure 16A made an appreciable contribution to the structure of the molecule, the position of the ultraviolet absorption due to the carbon-oxygen double bond should coincide with a similar absorption in the spectrum of acetone. Experimental observation showed the absorption to be shifted toward shorter wavelengths in N-methyl acetamide. This would indicate that the form of the linkage in figure 16B contributes to the structure of the molecule, and thus implies hindered rotation about the carbon-nitrogen bond in the liquid. Only in highly acidic solutions, in which only the presence of the form shown in figure 16C was postulated, did the ultraviolet absorption coincide with that of acetone.

These workers measured the dipole moment of N-methyl acetamide and found it to coincide with the value which they calculated for the trans form of the molecule, but not with the value calculated for the cis form. This

portion of the work is highly questionable. In the first place, the measurement of the dipole moment involves the extrapolation of the data to infinite dilution. This extrapolation is an extremely difficult one to make because of its nonlinearity. In the published work no comment is made on how, or with what accuracy the extrapolation is made. Further, it is stated that a "simple vector calculation" was used to obtain the calculated values of the dipole moments. No details were given of this calculation. In particular, it is not explained how the partial double bond character of the carbon-nitrogen bond is taken into consideration. The dipole moment of such a bond is certainly not tabulated in lists of bond moments[35] which are usually used for such calculations. Finally, it is stated that the contribution of the solvent to the dipole moment is one Debye. No very good reason is given for this estimate, and one can only notice that it is exactly one Debye which is needed to make the value of the uncorrected dipole moment correspond to the observed value.

The Japanese group studied the infrared and Raman spectra of N-methyl acetamide. These were compared to normal coordinate calculations made for both the cis and trans form, and it was shown that the correspondence between observed and calculated frequencies was closer for

the trans form than for the cis form. The normal co-ordinate calculation was done assuming the methyl and the NH groups to be point masses. This approximation can scarcely be justified in view of the contribution of the NH bend to several of the amide modes.

A pair of papers published later, one by Miyazawa, Shimanouchi, and Mizushima[24] on the trans from of N-methyl acetamide, and one by Miyazawa[25] on the cis form, attempts to correct this objection to the normal co-ordinate calculations. In these papers, the problem is treated as a six-body problem, only the methyl group being treated as a point mass. It seems likely that even this is too great an approximation. The question is whether the methyl frequencies mix with the frequencies of the remainder of the molecule. While one does not like to state flatly that the stretching frequencies of the methyl group will, or will not, mix with the frequencies of the remainder of the molecule, it seems probable that the methyl deformation frequencies will definitely mix with the skeletal modes of the amide linkage. This fact in itself would open this work to serious criticism.

The calculations themselves could have been improved. In constructing the potential function for the molecule, three force constants were considered: the stretching force

constant between two atoms, the bending force constant which tends to maintain the angle between two adjacent bonds constant, and a repulsive force constant which acts between atoms at the far ends of pairs of adjacent bonds. As is usual in these problems, the values for these force constants were taken from other molecules for which normal co-ordinate calculations have been made, and which bear some resemblance to the structure of N-methyl acetamide. In some cases the resemblance was faint indeed. For example, the bending and repulsive force constants for the group C-N-C' (i.e., the angle between the bonds from the nitrogen atom to the carbonyl and the methyl carbons) and for N-C-C" are taken from the propane molecule and the acetate ion, respectively, neither of which has a nitrogen atom.

A normal co-ordinate calculation was first made for di-formylhydrazine which can be regarded as two formamide molecules joined together by a bond connecting the two nitrogen atoms. This is a simpler problem because of the higher symmetry of this molecule, and the results could have been useful in choosing values of the force constants for the calculation of the normal modes of N-methyl acetamide. To be useful, the force constants used in the calculation for the di-formylhydrazine problem should have been

corrected to bring the observed and calculated values for the normal modes of this molecule into closer agreement. It was evidently felt that this was not necessary, for the comment was made that the force constants were transferred without corrections, despite the fact that some of the deviations between calculated and observed frequencies were nearly 100 $cm.^{-1}$

The question of the structure of the di-formylhydrazine molecule also arises. The statement was made that this molecule has the trans structure and is planar. The evidence for this statement came from X-ray data obtained from crystals. The environment in the liquid phase, and also possibly the structure, could be quite different.

It cannot be said that the structure of the N-substituted amide group in the liquid phase or in solution has been definitely established, although in view of the work of Huisgen and Walz, it is highly probable that the molecule exists primarily in the trans configuration. From a consideration of the evidence for the two resonance forms of the molecule, it is probable that the amide group is nearly planar. Nevertheless, these statements must be regarded as only probable.

While there may be some justification for saying that the liquid phase and the solutions of the amides should

resemble the crystalline phase, which is fairly well characterized, nothing at all can be said on this basis about the structure in the vapor phase. Here the effects of intermolecular hydrogen bonding which are so important in the crystal and in the liquid are completely absent, and each molecule acts independently. A consideration of the cis structure in figure 19 suggests that the intramolecular hydrogen bond might stabilize this structure enough to permit its existence in the vapor. Such a situation has been observed for ortho-chloro phenol.[36,37]

The work in the literature devoted to obtaining a better understanding of the amide group in the vapor phase is disappointing. One exception to this is the paper by Costain and Dowling[38] on a microwave study of gaseous formamide. By obtaining the rotational constants for the molecule with ten different combinations of isotopes they are able to determine quite accurately the internuclear distances and bond angles. The C-N bond is found to be somewhat shortened due to partial double bond character. A deviation from planarity about the nitrogen atom of around ten degrees is observed. It is interesting to compare these results to those of Ladell and Post on crystalline formamide.

In a study of the N-substituted amides in the vapor phase, the logical molecule to choose is N-methyl formamide,

because of its relatively low molecular weight and high vapor pressure. Most of the studies reported in the literature have dealt with this molecule. Evans[39] studied N-methyl formamide in connection with his graduate work at the University of Wales. Rubalcava,[40] in his PhD thesis submitted to the California Institute, reports a study of N-methyl formamide in the vapor phase. Some vibrational assignments were given by him. DeGraaf and Sutherland[41] and DeGraaf[42] report studies in the vapor phase, but neither of these works is particularly useful except as a background for more extensive work. Jones[43] has made the most serious attempt to reach an understanding of the structure in the vapor. This work will be discussed at greater length below, but here it may be said that he erroneously assigned the cis structure to the molecule largely on the basis of a faulty interpretation of the envelopes of various bands.

The structure of the N-substituted amides is best understood in the case of molecules in crystalline form for which X-ray data exists. A number of papers have been published supporting the trans planar structure in the liquid and in solution. With the important exception of the two papers by Huisgen and Walz, none of these can be said to establish a structure for the group. In the vapor phase,

the work by Costain and Dowling is important in outlining the problem for the N-substituted amides, but cannot answer the question of the structure of the N-substituted group directly.

In view of this situation, it was thought that a study of an N-substituted amide in the vapor phase might be a useful first study for the spectrometer described in Section I. An important reason for the choice of this instrument lies in Jones' work. He based his hypothesis of the cis structure on a study of the envelopes of those bands in which he was able to distinguish P, Q, and R branches with his prism instrument. With the grating spectrometer, the band envelopes could be studied with higher resolution, thus increasing the chances of resolving their structure. In addition, those bands lying in regions of atmospheric interference could also be studied with greater facility. N-methyl formamide was selected for this study because of its relatively high vapor pressure for an amide, and its low molecular weight which increases the likelihood that the structure of the various bands could be resolved.

EXPERIMENTAL

Eastman N-methyl formamide was used as obtained. The only evidence of impurities was the appearance of extra water absorption upon allowing the vapor to stand for more than one hour at temperatures above 100° C. Presumably this was accompanied by other decomposition products, but these were not found.

The two absorption cells used are described in Section I. Thermocouples were embedded in the windings of each absorption cell to measure the temperature of the gas on the inside. In several of the runs with the steel absorption cell, the pressure in equilibrium at a given temperature was determined as follows: The rate of flow of air into the system through a small leak in the packing of valve B (refer to figure 20) could be balanced against the rate of removal of air from the system by the vacuum pump. This allowed one to maintain the manometer at any desired pressure. The cell was completely evacuated, the liquid introduced, and the pressure allowed to come to equilibrium with valve A closed. The leak was adjusted to maintain the manometer at the approximate pressure of the vapor inside the cell, and valve A was opened momentarily. The procedure was repeated, and the pressure on the outside of the cell

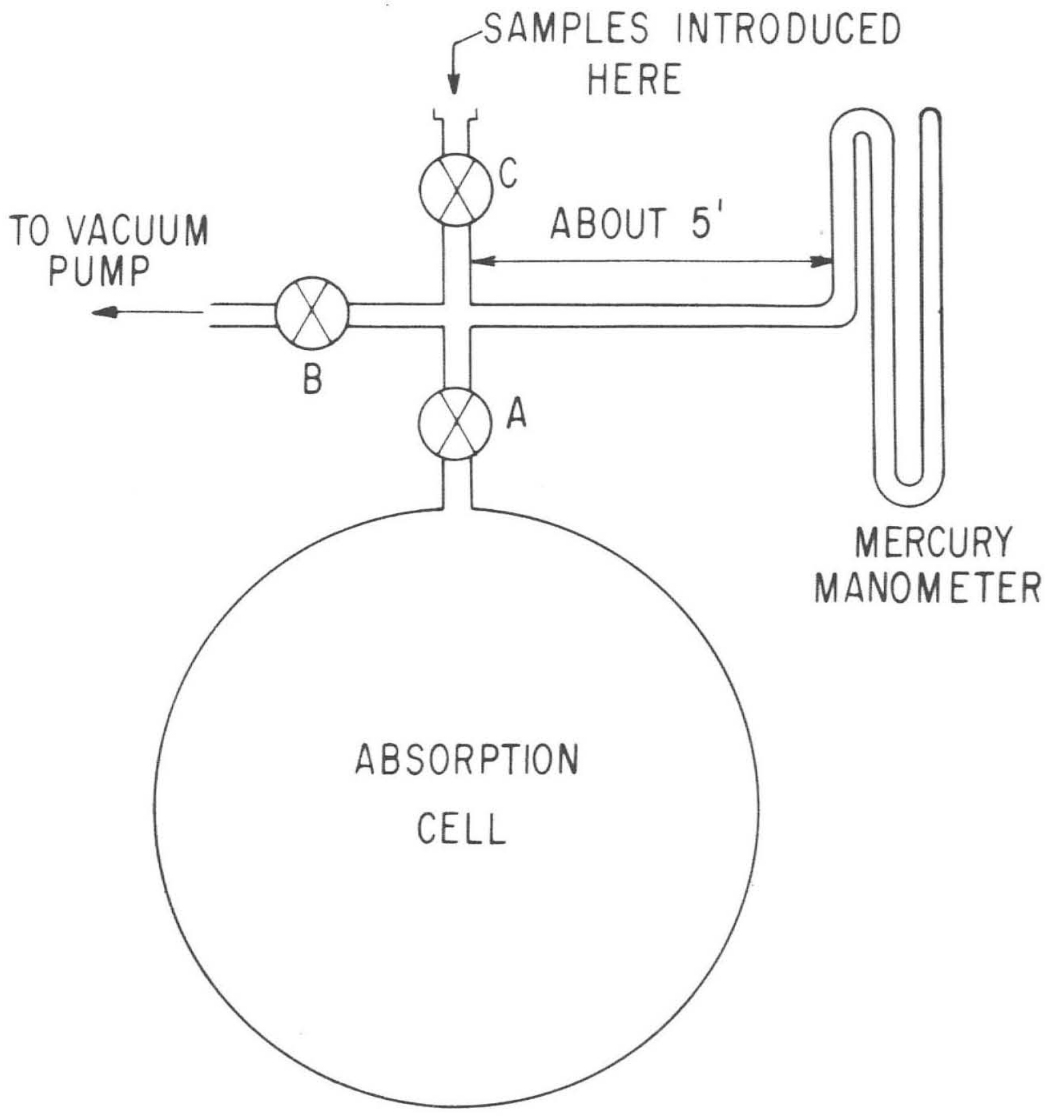

STEEL ABSORPTION CELL-GAS HANDLING EQUIPMENT

FIGURE 20

was adjusted with valve B until no change was observed on the manometer upon opening valve A. The final manometer reading was taken as the vapor pressure at the given temperature. It is estimated that the pressures are accurate to within 5 mm. of mercury at temperatures below 90° C.

The data obtained in this way were used along with the one datum of D'Alelio and Reid[44] to construct a Cox chart[45] from which the pressures at other temperatures could be read. The Cox chart is shown in figure 21.

Since the automatic prism and slit drives on the grating spectrometer had not been installed at the time this work was done, it was inconvenient to make long survey scans on the grating instrument. The glass cell was used on the Beckman IR7 spectrometer to make a rapid survey of the spectrum to assure that there were no bands present which had not previously been reported. The optical system used is shown in figure 22. Due to maladjustments in the optics, extra reflections, and scattering from the cell window, the energy in the sample beam was less than 10% of that in the reference beam. Accordingly, a screen with transmission of 10% was placed in the reference beam. With this screen, the energy in the two beams with the cell empty could be balanced, and the scale caused to read directly in absorption or transmission. This was, however, done at the

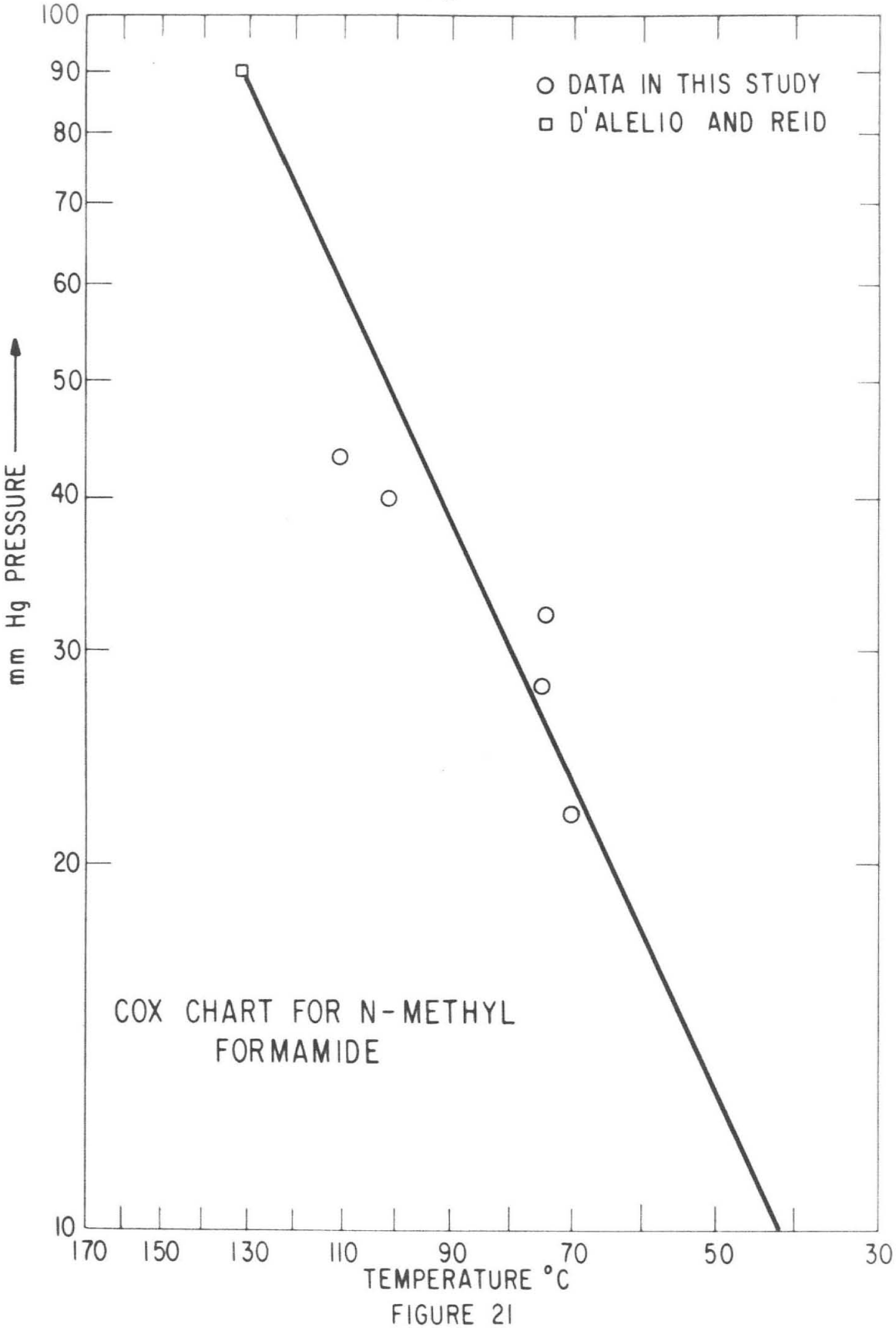
100
90
80
70
60
50
40
30
20
10
mm Hg PRESSURE
O DATA IN THIS STUDY
□ D'ALELIO AND REID
COX CHART FOR N-METHYL FORMAMIDE
170
150
130
110
90
70
50
30
TEMPERATURE °C

FIGURE 21

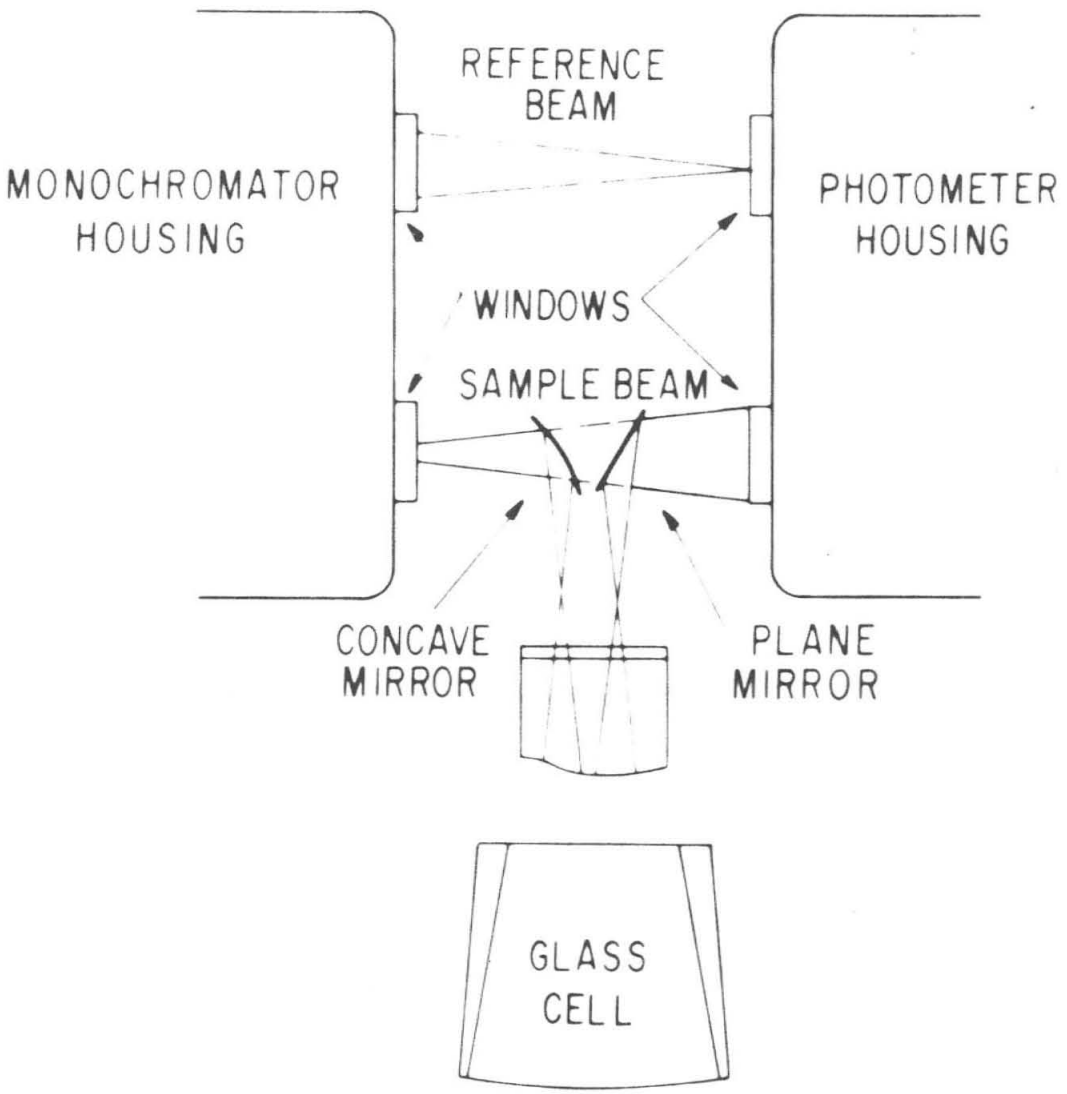

BECKMAN IR7 OPTICS

FIGURE 22

expense of introducing a great deal of noise. A 30 second time constant was used and the spectrum was run at the lowest possible speed.

The difference in path length through the atmosphere resulted in the superposition of the carbon dioxide and water spectra on the N-methyl formamide spectrum. This, of course, could have been avoided by using an identical cell in the reference beam. It was not felt, however, that the added trouble was justified for obtaining a survey spectrum. The desired result was obtained with this arrangement, namely, that there were no unreported bands in the specimen of N-methyl formamide being used.

The work on the grating spectrometer was done with the two absorption cells described in Section I. In a typical run, the foreprism was set at approximately the center of the desired region of the spectrum, and the grating was adjusted to the grating angle calculated from the reported position of the band to be studied. The prism was scanned across the region of the band to assure that overlapping grating orders were not present. Finally the prism was adjusted to give maximum intensity. The slit was adjusted to give the desired resolution, and the gain and time constant on the Golay amplifier were adjusted to give the desired gain and signal-to-noise ratio.

The polyethylene envelope was thoroughly flushed with dry tank nitrogen and a small stream set to give a positive pressure within the envelope. The cell was evacuated and the background measured by scanning the grating across the region of the band with the prism fixed.

About 2 ml. of liquid N-methyl formamide were then added to the cell and flushed inside with a small amount of nitrogen. The cell was slowly heated and spectra run continuously. Usually about ten spectra were run as the cell heated from 25° to 150° C. The temperature reported for each spectrum was that observed upon passing the center of the band.

Upon reaching 150° C, if a temperature effect was to be studied, the grating was set on the middle of the band. The gas was pumped from the cell until the absorption had fallen slightly below the level recorded earlier for the lower of the two temperatures at which it was desired to study the band. The cell was allowed to come to equilibrium, and the procedure was repeated. Due to the excess liquid usually present at the beginning, this procedure had to be repeated at least three times to assure that finally only vapor was present. When the intensity had remained constant for at least 30 minutes, the high temperature scan was run three times, and the cell was allowed to cool down to the

selected lower temperature. The spectrum at this temperature was run three times, and the cell was pumped out and flushed thoroughly with nitrogen. Finally, the background spectrum was repeated.

In a successful run, the two backgrounds agreed to within 3%. In all but four bands, which are discussed below, the scan at high and low temperature agreed to within 3%.

In a few instances, it was desired to scan a longer region than the pass-band of the foreprism would allow. In these cases, a program of prism settings was determined which allowed the foreprism to be maintained in synchronization with the grating. The program was followed by making the adjustments manually during each scan. Care was taken to insure that the spacing between individual adjustments was such that the effect of each adjustment was not noticeable on the recorder tracing.

Of the two cells, the steel one was built and used first. It proved to be more convenient in regions of atmospheric absorption due to the shroud around the exterior optical path. This made flushing with dry nitrogen much more efficient. It soon became evident, however, that it would not be convenient to do temperature effect studies in this cell because of its large thermal mass and several

small leaks. The glass cell was designed and built to overcome these difficulties, but it proved difficult to flush the exterior completely with nitrogen in order to remove atmospheric moisture.

Because of the error-curve shape of the foreprism pass-band and occasional Wood anomalies, the background often made it difficult to determine the shape of weak bands. With each band, the background and spectrum were plotted point-by-point on semi-logarithmic paper. The distance between the two curves was taken off by dividers and plotted at closely-spaced wavelength intervals. This results in a plot of logarithmic absorption rather than percent transmission. In some of the spectra this absorption plot was used, and in some, when the shape was especially clear, a tracing of the recorder chart itself was used.

RESULTS AND DISCUSSION

1. Observed Spectra

The observed spectra are presented in figure 23. The experimental conditions for each are summarized in Table II. Table III presents the 17 bands observed in this study together with the assignments given by Rubalcava, Jones, and

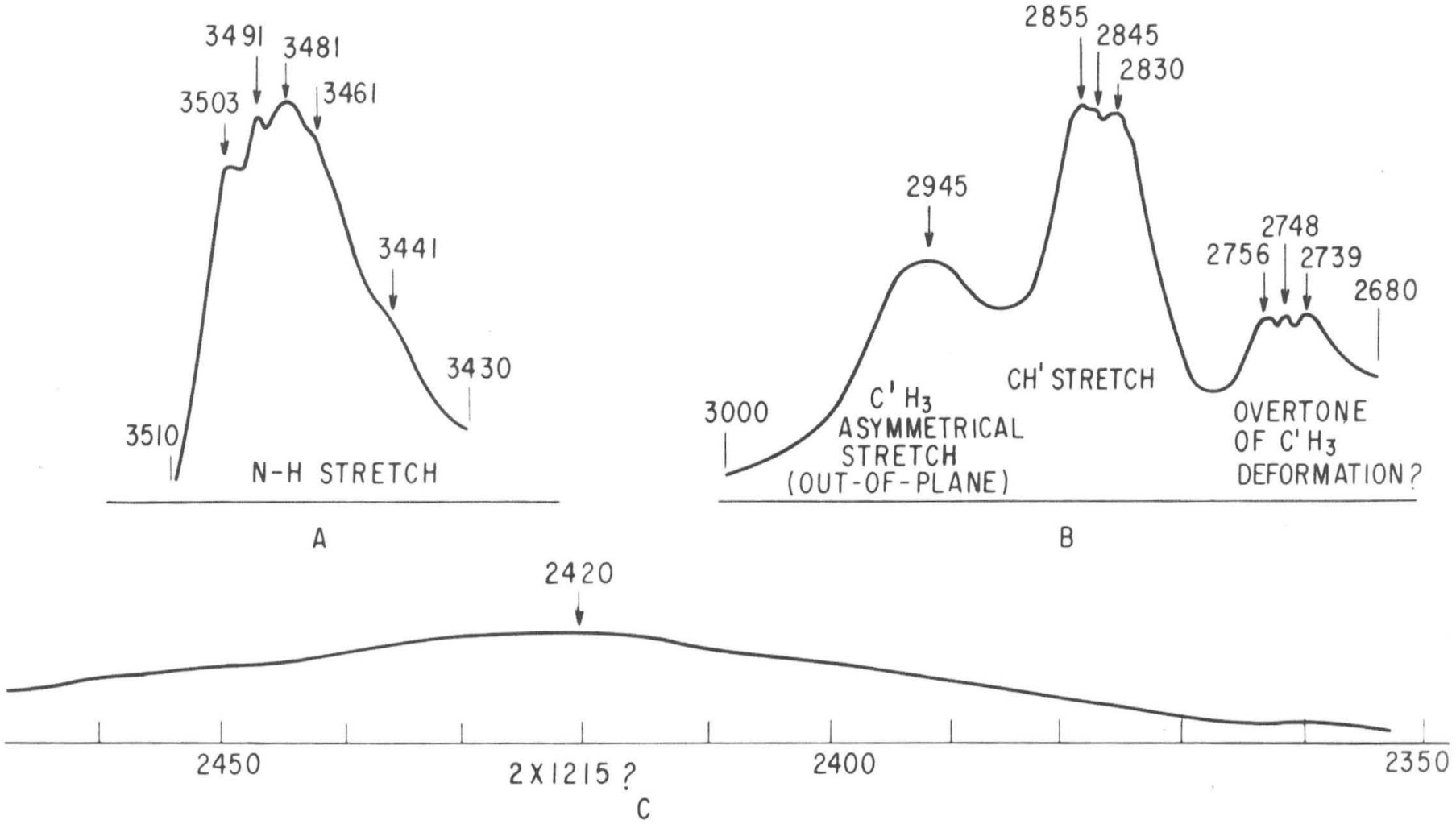

[C' REFERS TO METHYL CARBON
C REFERS TO CARBONYL CARBON
H' REFERS TO CARBONYL HYDROGEN
H REFERS TO AMIDE HYDROGEN]

N-METHYL FORMIDE SPECTRA

FIGURE 23-1

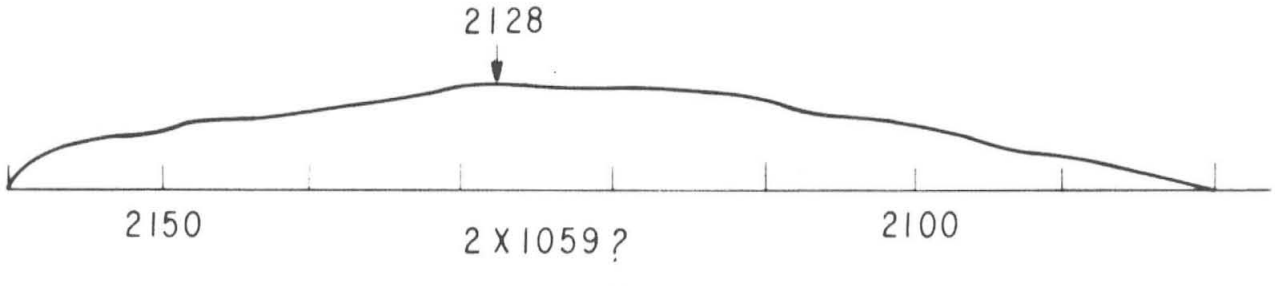

D

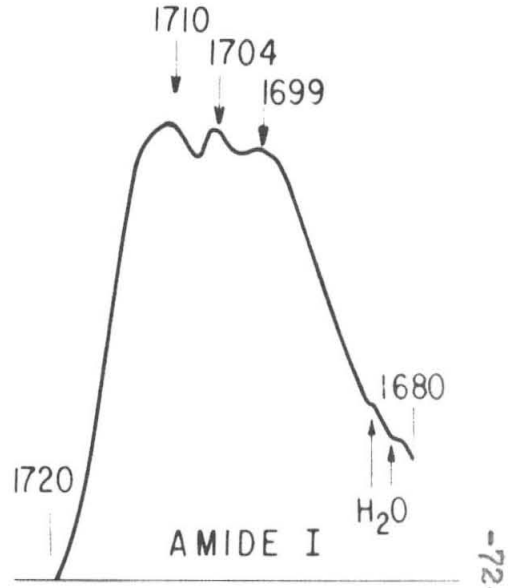

E

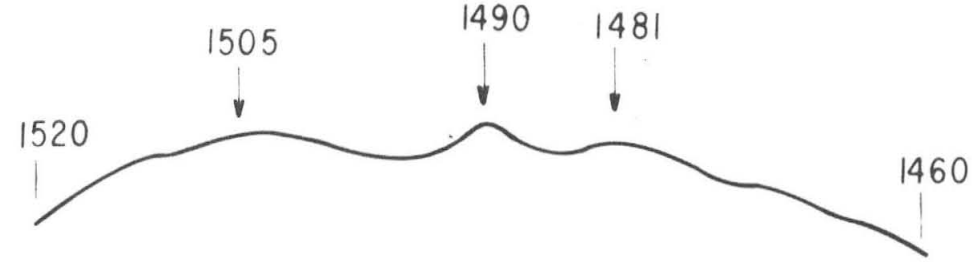

F

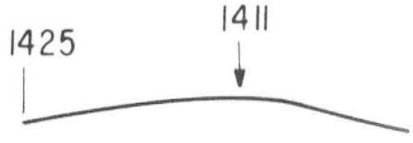

G ASYMMETRICAL $C'H_3$ DEFORMATION

FIGURE 23-2

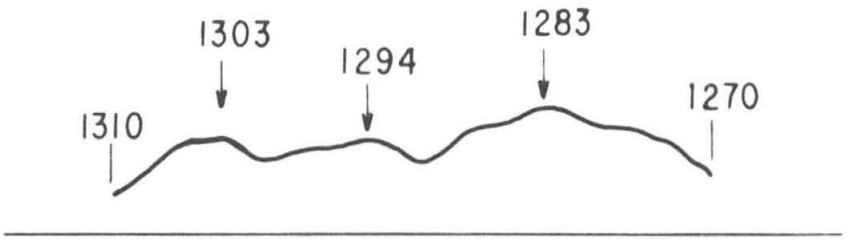

$C'H_3$ WAGGING MODE
(IN-PLANE)

H

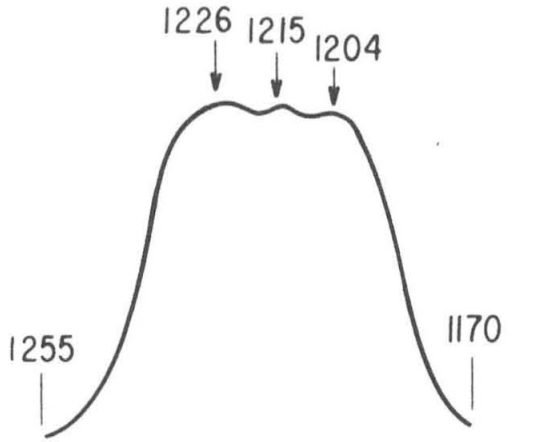

AMIDE II b

I

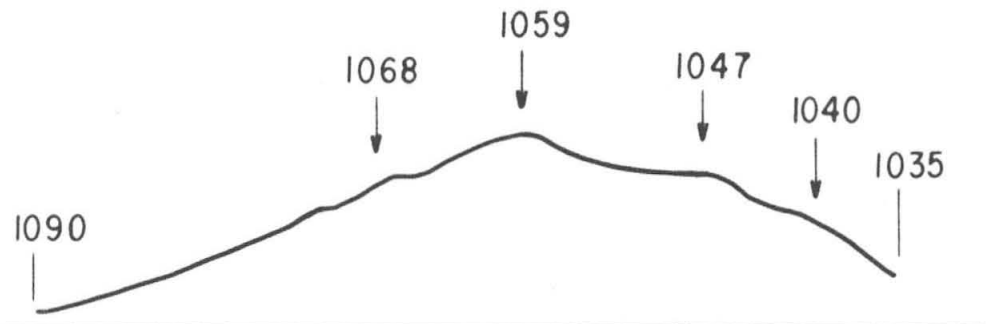

$C'H_3$ ROCKING MODE
(OUT-OF-PLANE)

J

FIGURE 23-3

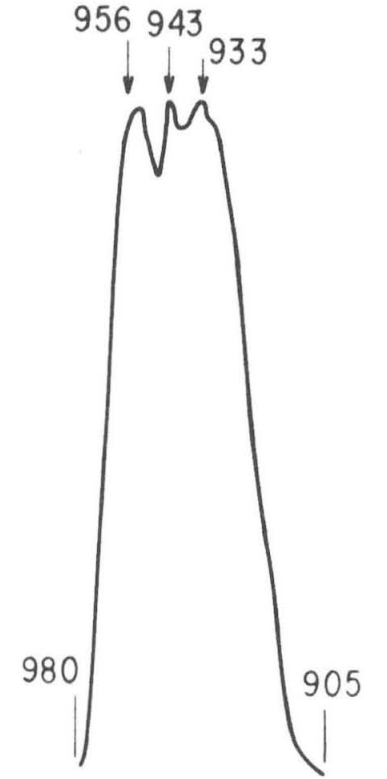

PREDOMINANTLY C'-N STRETCH

K

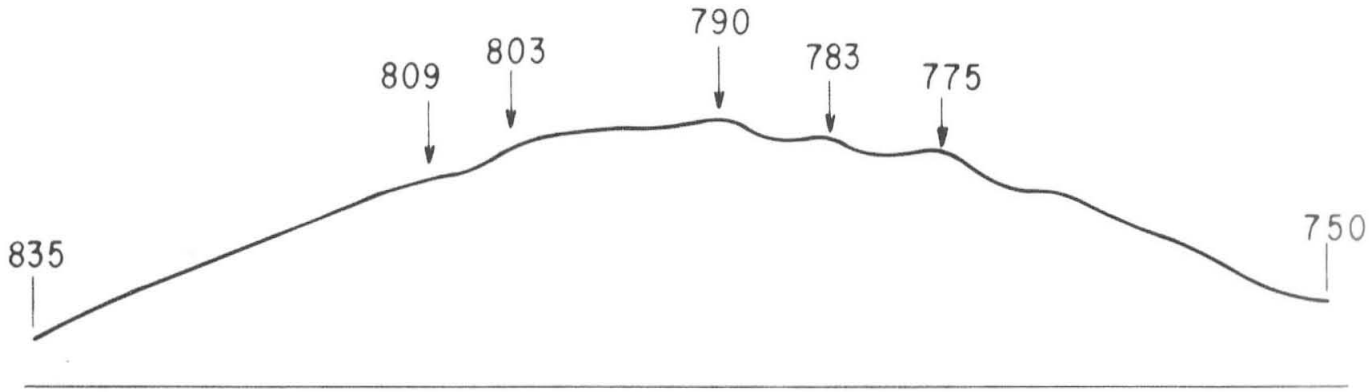

CH' OUT-OF-PLANE MODE

L

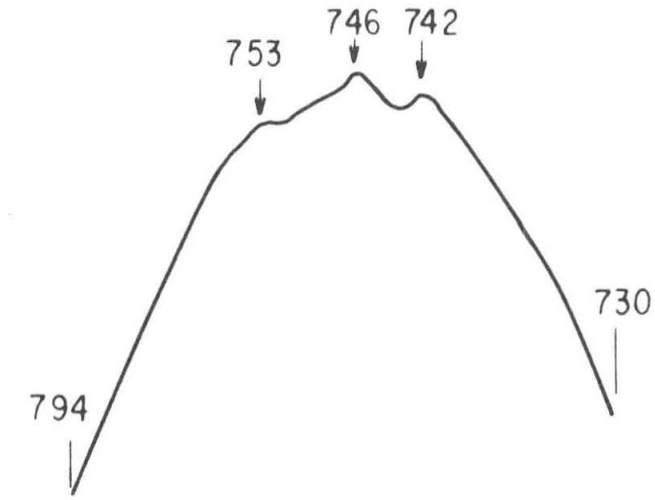

2X C=O OUT-OF-PLANE ?

M

FIGURE 23-4

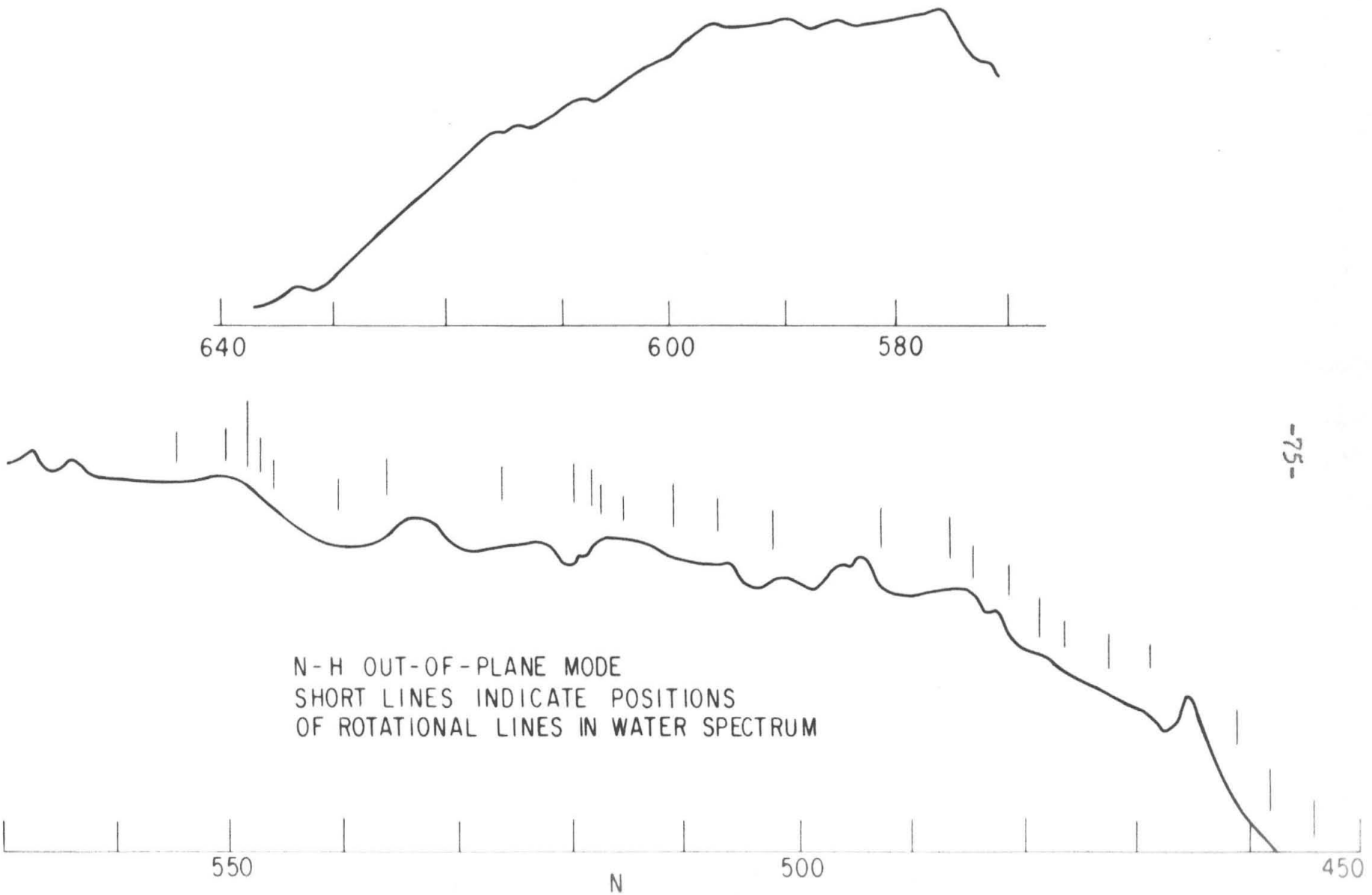
640
600
580
N-H OUT-OF-PLANE MODE
SHORT LINES INDICATE POSITIONS
OF ROTATIONAL LINES IN WATER SPECTRUM
550
500
450
N

FIGURE 23-5

NOTES FOR TABLE II

a. B.L. is Bausch and Lomb echelle grating; J.H. is 7500 lines/mm. echelette ruled on the Johns Hopkins engine.

b. These bands are traced directly from recorder charts. All others are taken from logarithmic plots described in the text.

c. These spectra were run with manually adjusted prism.

d. These gas samples were not in equilibrium with liquid.

e. Temperature effects were studied.

TABLE II--EXPERIMENTAL DATA

SPECTRUM	WAVELENGTH RANGE	CELL	GRATING AND ORDER[a]	SPECTRAL SLIT WIDTH ($CM.^{-1}$)	TEMPERATURE °C.	PRESSURE MM. Hg
A[b,e]	3510 to 3430	glass	J.H.--1st	4.48	95	43
B[b,e]	3000 to 2680	glass	J.H.--1st	2.82	47	12
C	2472 to 2353	glass	B.L.--1st	11.6	147	112
D	2160 to 2080	glass	B.L.--1st	8.9	147	112
E[b,e]	1720 to 1680	steel	B.L.--3rd	2.40	46	11
F[e]	1520 to 1460	steel	B.L.--3rd	1.54	90	38
G	1425 to 1400	steel	B.L.--3rd	1.23	90	38
H	1310 to 1270	steel	B.L.--1st	1.51	88	37
I	1255 to 1170	steel	B.L.--1st	1.32	88	37
J	1090 to 1035	steel	B.L.--1st	3.89	104	54
K[b,c]	980 to 905	glass	B.L.--1st	4.03	88	32[d]
L[c,e]	835 to 750	glass	B.L.--1st	2.97	88	32[d]
M[e]	794 to 730	glass	B.L.--1st	1.88	65	20
N[c,e]	640 to 450	glass	B.L.--1st	0.96	80	30

NOTES FOR TABLE III

a. A, B, and C refer to three, two, or one branches, respectively.

b. See figures 24 and 25 for meaning of atomic symbols.

c. Not observed.

d. Predominantly C character, but shows some structure.

TABLE III--OBSERVED BANDS

FREQUENCY (CM.$^{-1}$)	CHARACTER[a]	ASSIGNMENT[b]			SPECTRUM (FIGURE 23)
		RUBALCAVA	JONES	THIS STUDY	
3491	A-22	NH Stretch	NH Stretch	NH Stretch (trans)	A
3450	B-20	c	c	NH Stretch (cis)	A
2945	C	Asym. Methyl Stretch	Asym. Methyl Stretch	Asym. Methyl Stretch (out-of-plane)	B
2845	A-25	CH'Stretch	CH'Stretch	CH'Stretch	B
2748	A-25	?	Sym. Methyl Stretch	2X Methyl Deformation?	B
2420	C	c	c	2X Amide IIb?	C
2128	C	c	c	2X Methyl Rock?	D
1704	A-11	Amide I	CO Stretch	Amide I	E
1490	A-24	Amide IIa	NH In-plane Bend + CN Stretch	Amide IIa	F

TABLE III (Continued)

FREQUENCY (CM.-1)	CHARACTER[a]	ASSIGNMENT[b]			SPECTRUM (FIGURE 23)
		RUBALCAVA	JONES	THIS STUDY	
1411	C	c	Sym. Methyl Deformation	Asym. Methyl Deformation	G
1294	A-20	Methyl Deformation	Methyl Wag	Methyl Wag	H
1215	A-22	Amide IIb	CN Stretch + NH In-plane Bend	Amide IIb	G
1059	C[d]	c	Methyl Rock	Methyl Rock	J
943	A-23	C'N Stretch	C'N Stretch	C'N Stretch	K
790	C[d]	c	CH' Rock	CH' Rock	L
746	A-21	c	2X CO Out-of-plane Bend?	2X CO Out-of-plane Bend?	M
530	C[d]	c	NH Out-of-plane Bend	NH Out-of-plane Bend	N

this study. In general, the assignments of this study agree with those of Jones. A number of previously unresolved bands can be seen from this study to have the PQR structure with approximately the 20 cm.$^{-1}$ P-R spacing found by Jones in the bands at 1201 and 946 cm.$^{-1}$ These include 3491, 2845, 2748, 1704, 1490, 1294 and 746 cm.$^{-1}$ The observation of a Q branch in the 1294 cm.$^{-1}$ band supports the assignment by Jones of this band to the wagging mode of CH_3. At the same time, the lack of such a structure in the band at 1411 cm.$^{-1}$ makes it difficult to assign this band to the symmetrical methyl deformation as Jones did. A much better assignment, because of the similarity of its shape to that of the asymmetrical methyl stretch at 2945 cm.$^{-1}$ is to the asymmetrical methyl deformation. Such a frequency is not unreasonable in view of the work by Deschamps, Forel, Fuson, and Josien.[46,47]

Three bands were observed in this study which have not been previously reported in the literature. These are at 2420, 2125, and 746 cm.$^{-1}$ The first two have also recently been observed by Jones.[48] The 746 cm.$^{-1}$ band is discussed below. The 2420 and 2125 cm.$^{-1}$ bands are likely the first overtones of 1215 and 1059 cm.$^{-1}$

The presence of the band at 1490 cm.$^{-1}$ (amide IIa) is worthy of comment. Badger,[23] in his study of the

normal modes of the amide group done with the aid of the mechanical model, found the nature of this vibration in the cis form of the linkage to be such that it would probably be of very low intensity in the infrared spectrum. This was because of the cancellation of opposing dipole moment changes. Huisgen, Brade, Walz, and Glogger[30] in their study of large ring lactams found this band missing in the spectra of smaller ring molecules to which they assign the cis form, but present in the larger ring molecules which they believed to have the trans form. In the molecule with a nine-membered ring, they found evidence of both forms. In the spectrum of this molecule, the amide IIa band showed an intensity change corresponding to the change in relative concentration of the two types. It is believed that this band would be missing in the N-methyl formamide spectrum if it were of the cis form.

2. Band Envelopes

A complete determination of the structure of N-methyl formamide is not practical from an analysis of the rotational spectrum in the rotation-vibration bands. It would not be possible to resolve the rotational spectrum in the infrared because of the high molecular weight and the con-

sequently large values of the moments of inertia. Even if the rotational spectrum could be resolved, and the rotational constants obtained, several different combinations of isotopic substitutions would have to be studied to obtain the complete structure. In their study of formamide, Costain and Dowling studied ten different species. Several more would be required in the case of N-methyl formamide. Because of this, one must consider, instead of the rotational spectrum, the gross envelopes of the bands to obtain similar information. The information obtained from such a consideration, of course, will amount to much less than a complete structure determination.

From previous discussion of the amide group, it is probably correct to say the structure of the N-methyl formamide molecule in the vapor phase is nearly planar and is composed of the two resonance forms shown in figures 16A and 16B. On this basis, it is possible to make some new proposals regarding the structure of the molecule based on the envelopes of the various bands.

As pointed out in more detail below, the shape of the envelop of a vibration band depends on the moments of inertia of the molecule. The approach here is to calculate the moments of inertia of each form of the N-methyl formamide molecule from the best available information on bond lengths

and bond angles. These moments of inertia will then be used to obtain the predicted band envelopes for each form of the molecule. These band envelopes will then be compared to observed envelopes.

Two significant differences can be expected between the band envelopes of the two forms of the molecule. In the first place, the trans form of the molecule is significantly different from a symmetrical rotator, while the cis form is nearly symmetrical, and could be expected to give rise to bands not greatly different from those of a symmetrical rotator. In the second place, while none of the bands on either model are pure A or B type there are some significant differences to be expected in the relative contribution of A and B character for some of the corresponding normal modes in the two forms of the molecule. For example, the N-H and C-H' stretches in the cis form should probably give changes in dipole moment more nearly parallel to the intermediate axis than in the trans form, and thus give rise to a band more nearly pure B type.

The molecular parameters used in the calculation of the moments of inertia for the two forms were based on those found by Costain and Dowling for formamide. The results of this calculation, together with the atomic coordinates used for each molecule, are shown in figures

24 and 25 for the trans and cis form respectively.

Two approaches will be used in obtaining the predicted envelopes of the bands. First, actual molecules can be found whose moments of inertia have nearly the same ratios as those of the two forms of N-methyl formamide. Since the shape of the band envelope depends only on the ratio of the moments of inertia, and not on the absolute moments of inertia, the bands of a model molecule can be compared with the observed bands of N-methyl formamide. It is necessary to make a change in the frequency scale of the band to correct for the difference between absolute moments of inertia. The molecules selected for comparison in this study are shown in Table IV.

Table IV gives the Badger-Zumwalt asymmetry parameters for each molecule.[49] These are defined in Appendix I, but here it may be said that they are a measure of the relative asymmetry of a molecule. Band shapes will be similar in molecules with similar Badger-Zumwalt parameters. Table IV gives the observed spacing between the P and R branches for each molecule together with the spacing corrected for the change in frequency scale for N-methyl formamide. This spacing is a useful quantitative expression for the shape of a band. The observed spacing and the spacing calculated by the Badger-Zumwalt method described below are also given

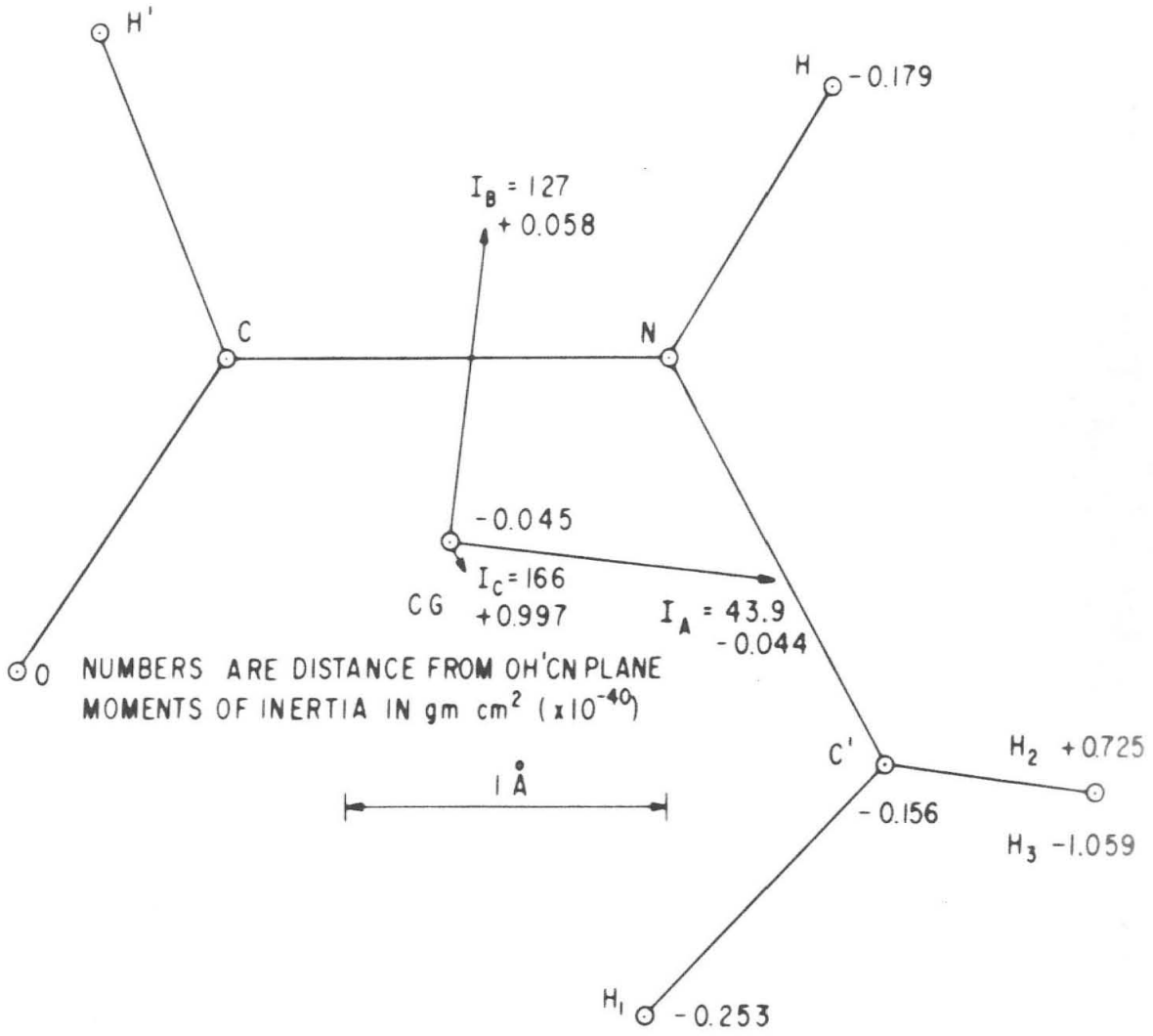

TRANS N-METHYL FORMAMIDE

FIGURE 24

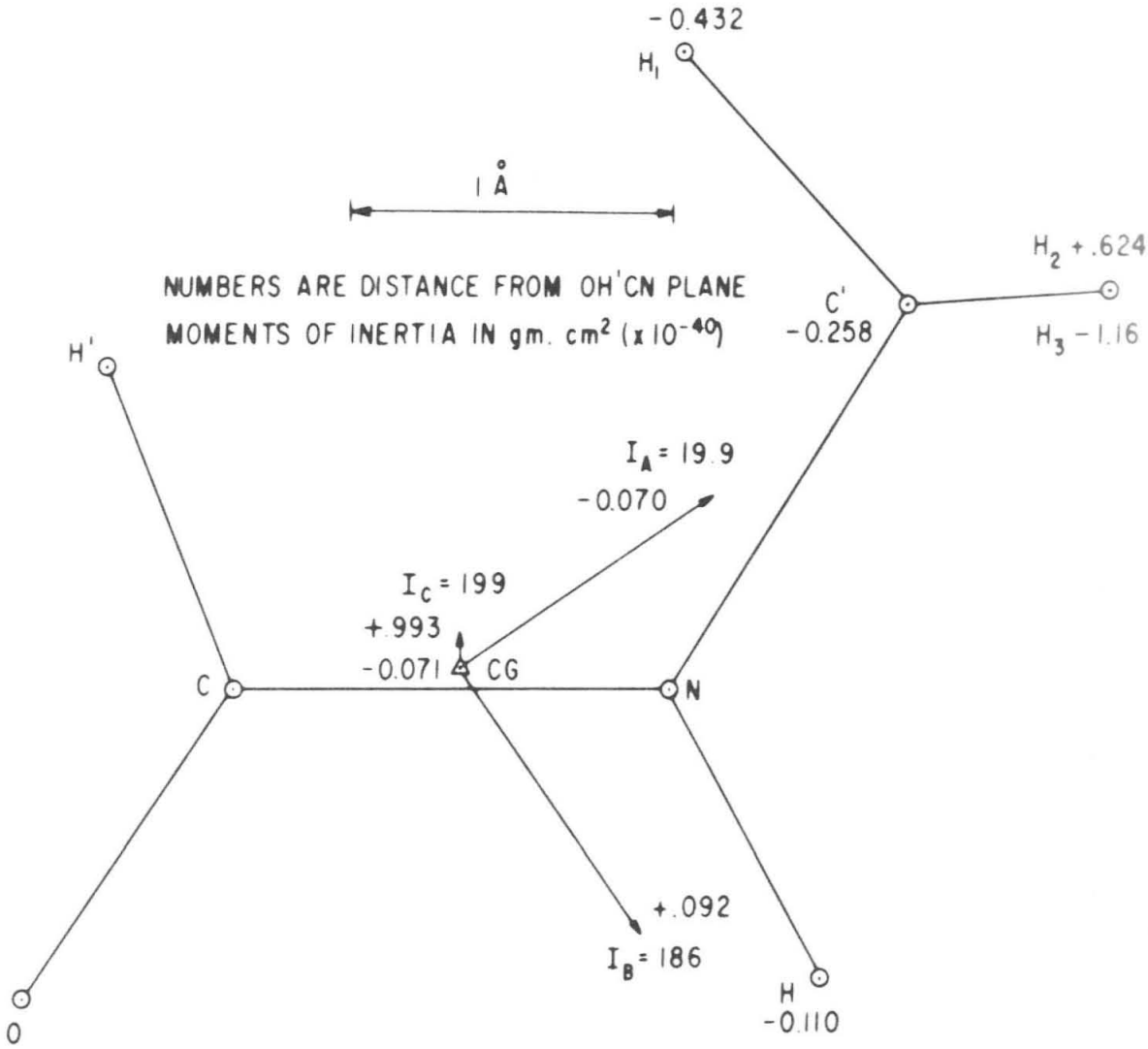

CIS N-METHYL FORMAMIDE

FIGURE 25

TABLE IV--MODEL MOLECULES

MOLECULE	BADGER-ZUMWALT PARAMETERS		SCALE CHANGE	PR SPACING ($CM.^{-1}$) OBSERVED			CORRECTED[a]			REFERENCE
	S	ρ		A	B	C	A	B	C	
trans $CHONHCH_3$ (calculated)	-0.78	2.08	--	--	--	--	26	29	b	This work
trans $CHONHCH_3$ (observed)	--	--	--	--	--	--	20	--	b	This work
C_2D_4	-0.82	2.53	1.83	40	30	b	21.8	16.4	b	52,53
cis $CHONHCH_3$ (calculated)	-0.98	7.80	--	--	--	--	24	32	b	This work
cis $CHONHCH_3$ (observed)	--	--	--	--	--	--	--	20[c]	--	This work
O_3	-0.97	7.10	1.72	31	43	--	18	25	--	54,55,56
HCOOH	-0.96	5.98	1.57	41.2	39.3	--	26.2	19.4	--	52,57,58,59
CH_3Cl	-1.0	9.40	1.80	32.9	--	--	18.2	--	--	60

notes
a. Frequency scale corrected for comparison with N-methyl formamide.
b. Gaussian error curve.
c. Separation of shoulders of NH stretch band.

for both forms of N-methyl formamide.

The second approach to obtaining the predicted band envelopes is to calculate them from the moments of inertia. Band envelopes for symmetrical rotators were first calculated as functions of the moments of inertia by Gerhard and Dennison.[50] The expression for the intensity of a rotational line in a vibration band[51] is given by

$$I = L A \left[N \frac{g}{r} e^{-\epsilon/KT} \right]. \qquad (1)$$

Here L is the oscillator strength of the vibrational transition, A is a factor involving the matrix elements for the particular rotational transition being considered, and the factor in brackets gives the number of molecules in the rotational state from which the transition is being made. This is the product of N, the total number of molecules present; r, the rotational partition function; g, the degeneracy; and the factor $e^{-\epsilon/KT}$ where ϵ is the energy of the original rotational level.

If, as is the case here, comparisons are to be made between identical bands in two structures, L, N, and r may be neglected since they only contribute to a change in scale. The energy ϵ of the initial rotational level for a symmetrical rotator can be written

$$\frac{\epsilon}{kT} = \sigma J(J+1) + \beta K^2$$

where

$$\sigma = \frac{h}{8\pi^2 kTB}$$

and

$$\beta = \frac{h}{8\pi^2 kT}\left(\frac{1}{A} - \frac{1}{B}\right).$$

A and B are the unique and equal moments of inertia, respectively. The value of β in this study is equal to β/σ in the paper by Gerhard and Dennison. It is convenient to combine the expressions for A and g into one expression A'. Values for A' are given in the paper by Gerhard and Dennison for the symmetrical rotator, and Appendix I for the unsymmetrical case.

When substitutions are made for A' and ϵ, equation 1 becomes a function of the quantum numbers J and K. In general, for a given value of the wavelength, there will be several combinations of J and K. In principle, one would sum equation 1 over all values of J and K which contribute to the intensity of the band at a given wavelength and divide by the spacing between rotation lines at the given wavelength to get the average absorption coefficient in the given spectral region. When this is done over the entire band, the result is the envelope of the absorption

coefficient for the band. For heavy molecules and not-too-low temperatures, it is justified, and also much easier, to make approximations which become valid when J and K are much larger than one. The expression for the total intensity at a particular wavelength is also simplified by the approximation that the appropriate sums can be replaced by integrals. The resulting expressions for the absorption coefficient envelopes of the parallel and perpendicular bands of a symmetric rotator are given by Gerhard and Dennison. It should be noted that the effects of Coriolis interactions in the perpendicular degenerate vibrations were ignored in their paper. Consequently, the results for the perpendicular band apply only to an accidentally symmetrical rotator which does not have degenerate vibrations.

An approach similar to this was used by Richardson[61] in the analysis of Raman data. Here the problem is the same except for the values of A which are different for the Raman case. Richardson did an exact calculation on a digital computer. The results were helpful in the assignment of individual Raman lines to their correct transitions. They were also useful in the refinement of the molecular parameters. In using the exact summations instead of the approximate integrals of Gerhard and Dennison, Richardson introduced the problem of determining the exact point at

which to break off the summations. Broderson[62] has published improved criteria for the discontinuance of these summations. Boyd and Edwards[63] have also reported a computer program designed to solve the problem of the envelopes of the bands of a symmetrical rotator.

The extension of the method of Gerhard and Dennison to unsymmetrical rotators was made by Badger and Zumwalt[49] with the introduction of certain approximations regarding the energy le els and transition probabilities. For any unsymmetrical molecule, the energy levels corresponding to a given J were divided into two regions. The energy levels and transition probabilities for the higher energy levels are adequately represented by one symmetrical rotator approximation. In a fairly small intermediate transition region, both approximations fail badly, but this was ignored in the Badger-Zumwalt theory. An abrupt discontinuity between the two regions above mentioned was assumed. The cases actually calculated by Badger and Zumwalt appear to be in reasonable agreement with observation, but are for very unsymmetrical rotators and cannot be directly compared with N-methyl formamide, neither form of which is highly unsymmetrical.

The approximate expressions for the energy levels referred to above were obtained from an approximate solution of the secular determinant of Wang.[64] If a, b, and c are

the reciprocals of the three moments of inertia A, B, and C, respectively, where $A \leq B \leq C$ then the upper energy levels can be regarded as corresponding to a symmetrical rotator whose two like reciprocal moments of inertia are equal to the mean of b and c, and the lower levels to a symmetrical rotator whose two like reciprocal moments of inertia are equal to the mean of a and b. The final expressions for the energy levels are identical to the corresponding ones for a symmetrical rotator except for correction factors which multiply σ and β . The approximate expressions for the factors A are taken directly from the expressions for the appropriate symmetrical rotator.

These approximations are convenient for making calculations in that the resulting expressions for the energy levels and the factors A' involve J and K in exactly the same manner as the same expressions for the symmetrical rotator. Thus, it is possible to substitute directly in the formulae of Gerhard and Dennison once the correction factors for the energy levels are obtained. The calculations themselves are summarized in Appendix I. The results are presented in figure 26.

The values of the asymmetry parameters S and ρ for the two forms of N-methyl formamide are too far removed from any considered by Badger and Zumwalt to allow any very

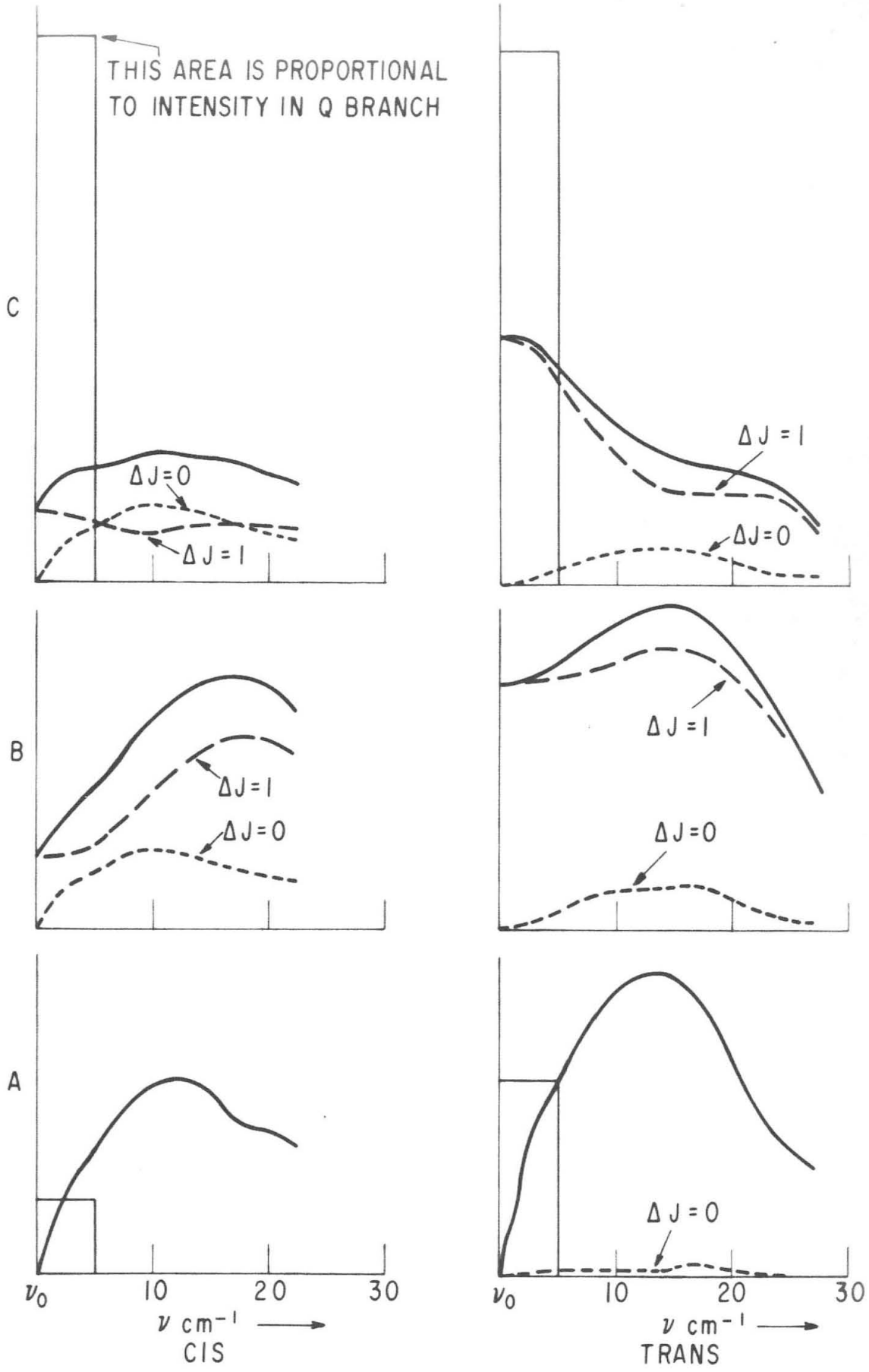

CALCULATED BAND CONTOURS FOR N-METHYL FORMAMIDE

FIGURE 26

significant comparison. One can only note such things as the decreasing importance of the $\Delta J=0$ branch of the A bands in their paper as S decreases and ρ increases. The beginning of the appearance of intensity in the center of the B type band and in the $\Delta J=0$ branch of the C band is noticed in their figure 5. These features dominate the shape in the present calculation.

In comparing these calculations with the models of actual molecules mentioned above, one sees that, while the A and C type bands agree with observation fairly satisfactorily, the spacing between the two maxima in the B band is considerably greater as calculated than as observed.

The only sign of a B type band in the observed spectra of N-methyl formamide is the two shoulders on the side of the N-H stretch at 3491 $cm.^{-1}$ The spacing of these shoulders agrees nicely with the two model molecules for the cis form. The agreement with calculation is poor. No explanation is offered for this fact. It is only noted that the molecules under consideration here are much more symmetrical than any considered thus far by the Badger-Zumwalt method.

In his paper proposing the cis structure for the vapor phase of N-methyl formamide, Jones used the approach outlined above. He calculated the moments of inertia, obtained

the band contours, and finally compared these to the experimentally observed envelopes. Unfortunately, several errors were made in the procedure. In the first place, the calculations for the moments of inertia were made assuming point masses for the N-H, C-H, and CH_3 groups. This made the cis form of the molecule seem much more symmetrical than it actually is. It was felt that, since it was nearly a symmetrical rotator, it would be a justifiable approximation to use the method of Gerhard and Dennison for calculating the envelopes of the bands of the cis form. It is not stated how the envelopes of the trans form were obtained. One imagines that it was by some sort of an extrapolation from the data of Badger and Zumwalt. Both the calculations made here and the observations made on model molecules show that the work was inadequate and gave erroneous results.

The first thing one notices about the band envelopes obtained in this study, either from model molecules or from the calculations, is the difficulty of making a decision between the two forms of the molecule on the basis of band envelopes alone. The differences between the two sets of bands are much too small to permit a definite decision between the two forms to be made on this basis alone. It is necessary to consider all the available data, and choose the form of the molecule which corresponds most

closely to the entire body of information.

One more comment about the envelopes of the cis bands needs to be made. Although the approximations made here predict a smooth shape for the B band, the low moments of inertia allow one to predict that the envelope will show some structure. On the basis of the calculated moments of inertia, one would predict that sub-bands spaced about 2.95 $cm.^{-1}$ apart should appear. The failure to notice any such structure in any observed band is evidence that the cis form does not predominate. On the basis of this fact, as well as the observation of the amide IIa band and the comments made below regarding the N-H stretch, it is concluded that the trans form of the molecule predominates in the vapor.

3. Planarity of the Molecule

In view of the work by Costain and Dowling, it was one of the aims of this study to investigate carefully the evidence for or against the planarity of the molecule about the nitrogen atom. The best evidence would seem to come from the N-H out-of-plane bending vibration. On the basis of deuteration data, this vibration is attributed[41] to a band at 714 $cm.^{-1}$ in the liquid. With the absence of the

effects of hydrogen bonding one might expect it to be shifted to lower frequencies provided there are no significant structural changes in the vapor. It seems probable that it is the band observed at around 500 cm.$^{-1}$ in the vapor as proposed by Jones, but it would be interesting to have deuteration data on the vapor to confirm this.

Suppose that the molecule is nonplanar about the nitrogen atom, and that this is due to a small potential barrier in the center of the N-H out-of-plane vibration. This was the conclusion reached by Costain and Dowling for formamide. The effect of the potential barrier would be to increase the energy of the even-numbered vibrational states, while leaving the odd-numbered states relatively constant. The effect would be largest on the lower states, and would soon disappear as higher states are reached. The effect of this shift of energy levels on the vibration frequencies would be to shift the fundamental ($0 \rightarrow 1$) to longer wavelengths and to shift the first "hot band" ($1 \rightarrow 2$) to shorter wavelengths. The hot band would then be found in the region studied here, while the fundamental would be found at longer wavelengths. Because of the low energy of the first excited level, it would have an abnormally high population, and this would contribute to an abnormally high intensity for the hot band. Thus, it is quite possible that the band at 500 cm.$^{-1}$ (or

another band nearby) is not a fundamental, but a hot band. If this were the case, it would be evidence for the non-planarity of the molecule.

If the 500 cm.$^{-1}$ band were a hot band, it would be expected to show an increase in intensity with increasing temperature. This would reflect the increasing population of the first excited state. A careful investigation of a possible temperature effect in this band was made, but none could be found within experimental error. Experimental error is estimated at around 5% of the total intensity. The reason for this large experimental error lies in the fact that this band had to be scanned by manually adjusting the prism at intervals throughout the scan. To allow for the possibility of an error in indentification of the N-H out-of-plane vibration, the bands at 790 and 746 cm.$^{-1}$ were also investigated at different temperatures. Temperature effects were observed in each of these bands, but were of the wrong sign to account for a hot band. The explanation for this is given below.

The 500 cm.$^{-1}$ band is very broad and diffuse. It stretches from 420 to 640 cm.$^{-1}$ with an ill-defined center at 533 cm.$^{-1}$ Some of the structure in the point-by-point plot in figure 23 is undoubtedly due to the rotational spectrum of water. The water lines in this region are shown

in the plot.[65] Jones ascribes the broadness of this band to the hindered rotation about the C-N bond. This seems unreasonable in view of the high potential barrier expected for this rotation of the basis of the resonance structure for the molecule.

4. The Cis Isomer

From the standpoint of new information which this study is able to contribute, the most interesting band in the spectrum is the band centered at 3481 cm.$^{-1}$ This can only be assigned to the N-H stretch mode. Three peaks and two shoulders can be observed in this band. All but the single most-long-wavelength shoulder have been observed by Jones since his paper was published.[48] In two spectra run on the same specimen of vapor at two different temperatures, the three peaks remained the same intensity, while the two shoulders increased in intensity with temperature. The three peaks are at the proper wavelength intervals to correspond to the P, Q, and R branches of an A band of either molecule. It is true that the intensity distribution between the three peaks is unusual, but this could easily be explained by a hot band superimposed on the peak at 3481 cm.$^{-1}$

If the two forms of the molecule are in equilibrium,

one expects the trans band to lie slightly to the short-wavelength side of the cis band. The reason for this concerns the intra-molecular hydrogen bonding which the molecule can be expected to undergo in the cis form. (See figure 19.) This has the effect of weakening the N-H bond and shifting this band to a slightly longer wavelength than the corresponding trans band in the vapor. The N-H stretch band should be much more nearly a pure B type band than the trans. This explains the absence of a Q branch if the two shoulders are assigned to the cis form of the molecule.

In a similar experiment the band at 790 cm.$^{-1}$ showed a decrease in intensity with increasing temperature. This could be explained as due to the conversion of some of the trans form to cis with increasing temperature, the corresponding band for the cis form being either far removed from this one, or too weak for observation. On the basis of this assumption, a simple calculation using the Boltzmann expression gives an energy difference for the two forms of 1.4 kcal. per mole and an equilibrium mixture at 300° K of 10% cis and 90% trans.

One other band showed a similar temperature effect. This was observed at 746 cm.$^{-1}$ No band has been reported in this location by other workers. Rubalcava[40] showed a tracing of the vapor spectrum in this region which shows

a small shoulder on the NaCl absorption as it begins to obscure the spectrum here. Jones[43] reports a weak band at 715 cm.$^{-1}$ which was not observed in this study. One is tempted to assume that these are the same bands. Jones assigned the band to the second overtone of the CO out-of-plane bend, which seems a reasonable assignment. The PQR structure of the band argues for its assignment to either an in-plane vibration or an even-numbered overtone of an out-of-plane vibration. The most convenient choice is the overtone due to CO.

The 790 cm.$^{-1}$ band shows the Gaussian error curve shape expected for a C band, and can only be assigned to the CH out-of-plane bend. It shifts very little on deuteration in the liquid where it is observed at 778 cm.$^{-1}$ [41] Such behavior is expected for the CH out-of-plane bend, and this seems a reasonable assignment. It is difficult, then, to understand what becomes of the corresponding band in the cis form of the molecule. There seems no very good reason why it should not be quite close, and may indeed overlap the trans band.

The above is the evidence for the coexistance of the two forms of the molecule. If it is assumed that only the N-H stretch band of the cis form of the molecule is intense enough for observation under the conditions of this study, a consistent case can be made for the coexistance of a second

species with an energy level 1.4 kcal. above the more abundant species. From the appearance and behavior with temperature of the band at 3481 cm.$^{-1}$, it can be concluded that the more abundant species is trans.

It is interesting to consider some observations of Russell and Thompson[66] in this connection. They report seeing a splitting of the N-H stretch band in dilute CCl_4 solutions of a considerable number of N-substituted amides. In the case of N-methyl formamide, the main peak was at 3466 cm.$^{-1}$ and a much weaker subsidiary one at 3429 cm.$^{-1}$ Such a subsidiary N-H is common in peptide and amide spectra and a unique interpretation is difficult. In this case, Russell and Thompson attribute the satellite band to a cis amide molecule, though they attempted no observations on temperature effects and offer no really convincing proof. Their interpretation, however, receives support from the present study.

Taking into consideration an expected shift to shorter wavelengths on vaporization, the frequency shift observed by Russell and Thompson is not in unreasonable agreement with the present observation. In particular, the shift of the band assigned to cis is less than that of trans, as expected on the basis of the hydrogen bonding considerations given above. It may be mentioned that Miyazawa[23] made a calcu-

lation using Jones' (incorrect) moments of inertia and the relative abundance given by Russell and Thompson. He arrived at a value for the energy difference of 1.6 kcal./mole and a relative abundance of 0.14 at 200° C.

5. The CH Stretch Region

The higher resolution available in this study makes possible a better understanding of the bands in the CH stretch region. Three bands are observed in this region. The first is the C type band at 2945 cm.$^{-1}$ This is due to the asymmetrical stretch of the methyl hydrogens. Forel et al.[46,47] reported a study of the methyl vibrations in a large number of molecules. In each molecule the short wavelength band is due to the asymmetrical stretch. When the molecule has lower symmetry than C_{3v}, this is split into two bands by the lifting of the degeneracy by the lower symmetry of the rest of the molecule. The splitting in an N-substituted amide might be expected to be of the same magnitude as that in a methyl ester, which was found to be around 30 cm.$^{-1}$ The out-of-plane component is always the higher frequency component and has the greater intensity. In the present case it seems likely that the band at 2945 cm.$^{-1}$ is the out-of-plane asymmetrical methyl stretch vibration and that there

is an unobserved band near 2915 cm.$^{-1}$ due to the in-plane component of the asymmetrical stretch.

The band at 2845 cm.$^{-1}$ is reasonably assigned to the CH' stretch due to the hydrogen attached to the carbonyl carbon. It shows the expected PQR structure for an in-plane vibration of predominantly A character. It is quite near the corresponding band (2880 cm.$^{-1}$) in formamide.[40]

The band at 2748 cm.$^{-1}$ presents a problem. Jones' assignment to the symmetrical methyl stretch seems unreasonable on account of the low frequency, particularly in view of the work by Forel et al. At the same time the assignment by Rubalcava to the combination tone of 1508 + 1270 cm.$^{-1}$ cannot be correct in view of deuteration data in the liquid. This band shows little shift upon deuteration, while the 1508 cm.$^{-1}$ band shifts from 1543 to 1436 cm.$^{-1}$ upon deuteration.[41] Overtones of methyl deformations have been observed in this region[46,47] but there is no positive evidence for such an assignment. A study of N-methyl formamide with a deuterated methyl group would be very interesting in this connection.

CONCLUSIONS

A study of N-methyl formamide in the vapor phase has been made. High resolution was used, and the band envelopes examined in detail. The assertion of Jones that the cis form is required to account for the observed envelopes has been shown to be fallacious, both by a calculation of the band envelopes and by comparison with spectra of known molecules. Indeed, it is concluded that for nearly planar molecules which do not deviate greatly from symmetrical rotators, it is not easy to estimate the degree of asymmetry from the band envelopes alone.

While these observations cannot provide conclusive proof that the predominant form of N-methyl formamide is the trans form in the vapor phase, they are consistent with this conclusion and would be difficult to account for in toto in terms of the cis form. Evidence for the trans form consists of (1) the presence of the amide IIa band, (2) the absence of strong bands of predominantly B type, (3) the failure to resolve rotational structure in any of the bands, and (4) the behavior with temperature of the NH stretch region.

Observations of the effect of temperature on the bands in the NH stretch region indicate the existence of two iso-

meric forms in equilibrium. Both band contours and frequencies indicate that the predominant form is trans, while the minor form is cis. Consideration of the quantitative changes of intensity with temperature in the 750 $cm.^{-1}$ region indicates that the minor form is approximately 1.4 kcal. above the major form.

Evidence for the nonplanarity of the molecule was sought, but none was found.

On the basis of the higher resolution obtained in this study, it was found necessary to reassign several bands.

SECTION III

PROPERTIES OF AN ECHELLE GRATING IN THE INFRARED

Because of its high cost and limited availability, the diffraction grating was for a long time neglected as a dispersive element in infrared spectrometers. In 1949 Strong[67] pointed out the advantages of the grating over the prism in a spectrometer in which the performance is energy limited rather than diffraction limited. Recently, high quality replica gratings have become available, with the result that commercial instrument makers now offer, or have announced their intention to offer, infrared spectrometers employing these replicas.

While a small group of spectroscopists have built up a considerable amount of experience in the use of diffraction gratings for high resolution work in small regions of the spectrum, there has been little effort devoted to the problems involved in extending the wavelength range of grating spectrometers. In order to compete commercially, a commercial grating instrument must be able to match the wavelength range of existing prism instruments --two to sixteen microns in the case of rock salt. Successful operation of a grating over such a wide wavelength range is far from the trivial problem it might seem. Let us consider first some

characteristics of diffraction gratings.

The simplest grating consists of an array of parallel line scatterers separated by the grating spacing. The efficiency of such a grating in its various orders can be calculated using Huygens' construction[68] with the result similar to that shown in figure 27. Such a grating shows its maximum efficiency in the zero order, i.e., the order in which it behaves as a plane mirror and shows zero dispersion. The efficiency of the higher orders drops rapidly with increasing order number, making it difficult to achieve high resolution with such a grating, since it is the higher orders which must be used for high resolution.

Michelson[69] developed the echelon in an effort to overcome this problem (figure 28). This instrument is designed to be used in a very high order, and thus gives extremely high resolution. Because the echelon can be used so that the individual scatterers behave as tiny mirrors with angle of incidence equal to angle of reflection, quite high efficiency is also possible. The difficulty is that, because the instrument is used in a high order, the angular separation of neighboring orders is small. This makes the echelon most useful in applications where an interferometer might be used--where the high resolution is necessary and another dispersive element can be used to separate the

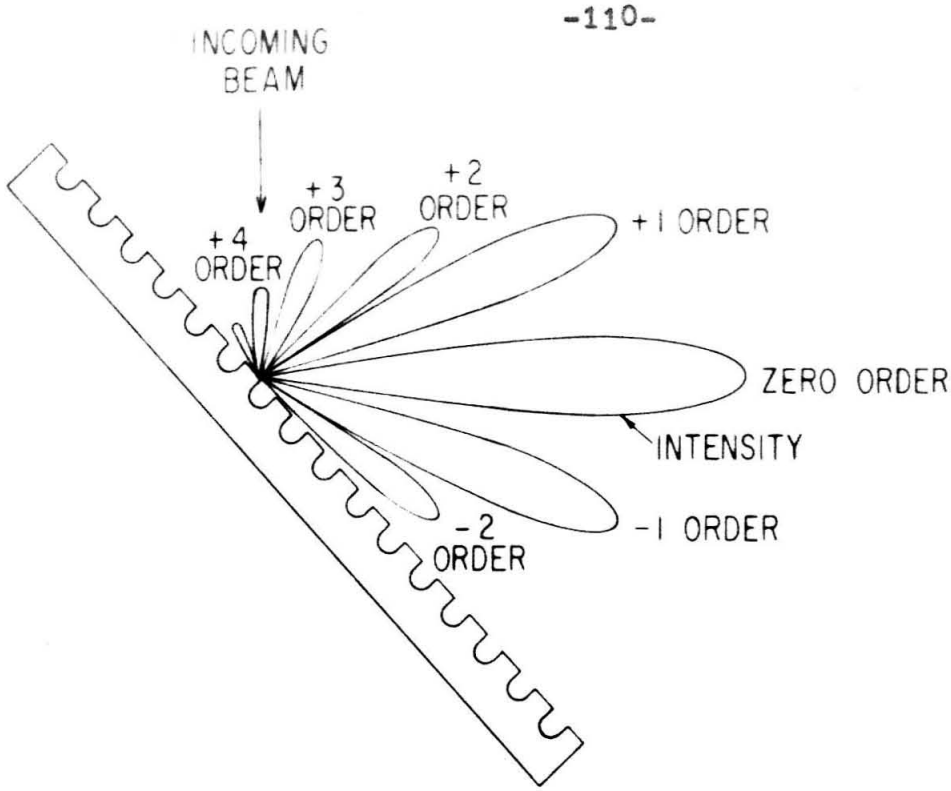

FIG. 27
SIMPLE DIFFRACTION GRATING

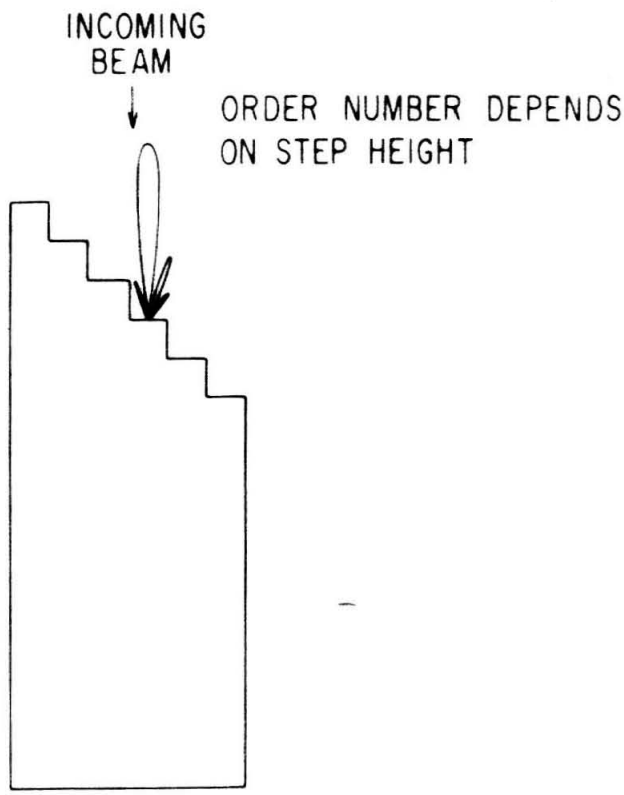

FIG 28 ECHELON

closely spaced orders.

What is needed for infrared spectroscopy is a compromise between the simple grating and the echelon. In the course of a study of the effect of groove shape on intensity distribution, Wood[70] discovered such a compromise, the echelette grating. This grating has its grooves ruled in steps and shows the intensity distribution shown in figure 29. Because it achieves its maximum efficiency at a fairly large grating angle where it also has fairly good resolution, the echelette grating is the grating which is the most widely used at the present time in the infrared. The echelette grating will show its maximum efficiency at the grating angle at which the long sides of the grooves are perpendicular to the bisector of the angle between the incident radiation and the diffracted radiation. This grating angle is referred to as the blaze angle of the grating. It is an unfortunate characteristic of echelette gratings that the efficiency falls off rapidly as one departs from the blaze angle. As a rule of thumb, the width of the useful region about the blaze angle in microns is equal to the wavelength of the blaze angle in microns.

A number of methods are used to overcome this rapid fall-off in efficiency. The grating in the Beckman IR7 is used over as wide an angle as possible. The grating order

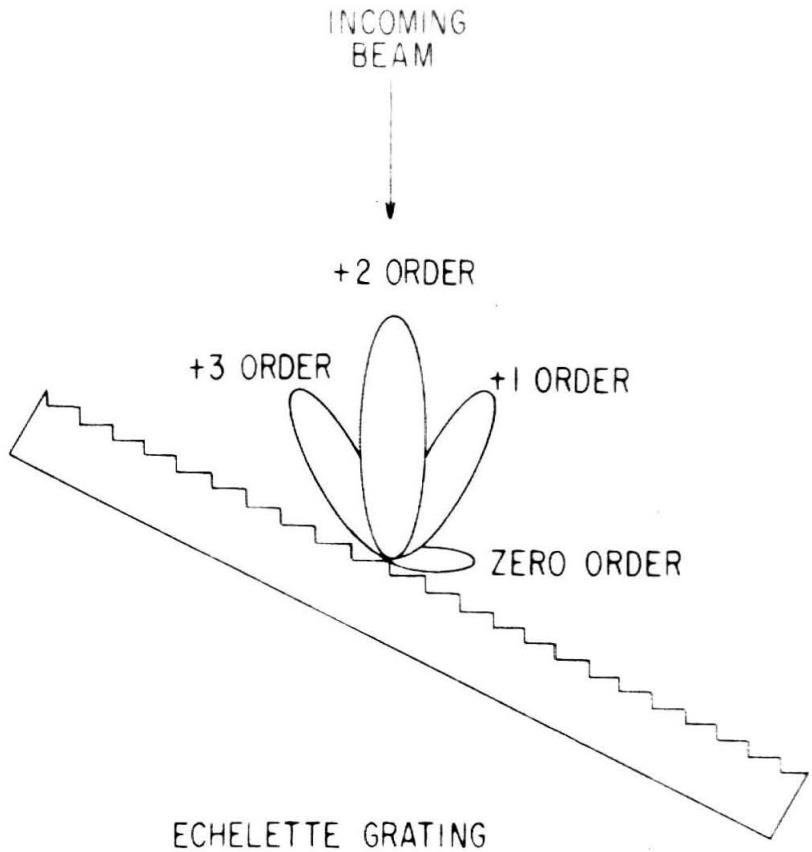

ECHELETTE GRATING
FIG 29

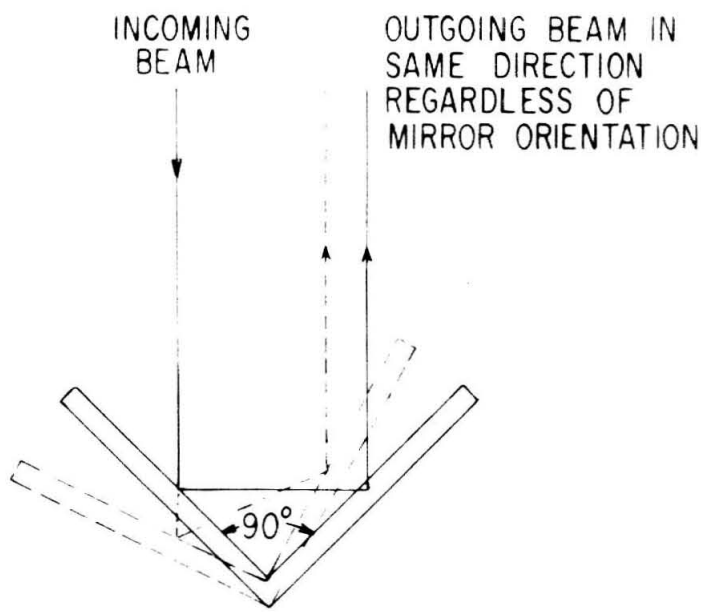

ROOF MIRROR
FIG 30

is then changed to bring the grating back past the blaze angle. This may be satisfactory if the slits are programed to give constant intensity during these fluctuations, and if the user is aware of what is happening to the resolution during the excursions of the slit width. Some workers use a series of gratings, changing from one to the other as the spectrum is scanned. Conn[71] has suggested that two gratings could be used to advantage by alternating from one to the other and changing orders at the same time.

No matter which solution for the problem of varying efficiency is adopted, some mechanical means must be provided to manipulate the grating through its various orders, or to change gratings during the scan. There has been no practical mechanical device made which is capable of doing this, and still maintains the precision demanded of a grating mount in order to achieve the wavelength accuracy inherent in the grating.

Even if a practical mechanical device could be worked out which would preserve the wavelength accuracy of the grating while it manipulated the grating to provide a long scan, another problem exists. One often wishes to make comparisons of spectra taken in different parts of the spectrum, and wishes to do so under identical resolution conditions. It is well known by users of prism instruments

that this is impossible with a prism because of the widely varying dispersion of prism materials. It is also impossible on instruments using present-day gratings because of the varying efficiency.

Martin[72] has pointed out that if the dispersive element in a spectrometer had constant efficiency and dispersion with respect to wavelength, then to the extent that the Rayleigh-Jeans law is obeyed, a spectrometer using movable entrance and exit slits would give constant wavenumber resolution. The argument proceeds as follows: In the instrument contemplated, the energy passing through the instrument is proportional to the square of the width of the two slits. It is presumed that the entrance and exit slits both have the same width. Since the Rayleigh-Jeans law predicts a decrease in energy from a black body radiator which is proportional to the fourth power of the wavelength, the slits must be opened at a rate proportional to the square of the wavelength as the spectrum is scanned to maintain constant energy at the detector. From $\nu = 1/\lambda$ one has $\delta\nu = -\lambda^{-2}\delta\lambda$. But $\delta\lambda$ is proportional to the slit width, so $\delta\nu = K\lambda^{2}\lambda^{-2}$ where k is the constant relating $\delta\lambda$ to the slit width. The wavelength thus cancels out of the expression for the wavenumber resolution leaving the resolution constant with respect to wavelength.

From the result of Martin, it is seen that a grating with a widely varying efficiency will not show constant wavenumber resolution in a spectrometer. Only when constant efficiency is achieved over a large range of grating angle will the ideal of constant wavenumber resolution be attained.

This portion of the thesis will deal with the two problems just mentioned--the problem of making a long scan while maintaining wavelength accuracy, and the problem of achieving the ideal of constant wavenumber resolution during this scan. Both problems would be solved if one had a grating which showed constant efficiency with respect to grating angle. The echelle grating to be described here closely approaches this ideal. Instead of a single blaze angle, it shows a blaze region, a region where the efficiency is nearly constant, and is at the same time high enough to be useful. The discussion will begin by presenting some background which shows an echelle grating to be a logical choice to show the blaze region. Next, three experiments will be described which support the contention that the echelle should show a blaze region. Following this two mathematical analyses will be presented which predict the blaze region instead of a single blaze angle. The first analysis, based on the Kirchhoff theory, gives a deeper insight into the

physics of the blaze region, while the second, based on the Rayleigh theory, makes some predictions regarding the polarization characteristics of the grating.

Both the echelon and the echelette achieve their highest efficiency when they are used in such a manner that a geometrical optics approximation would predict that light is being specularly reflected from planar scatterers. The implication is that highest efficiency is achieved when a single scatterer would specularly reflect light coming from the entrance slit to the exit slit. This implication is supported by simple theory. The Huygens' construction argument[68] expresses the intensity of diffracted radiation as the product of a term characteristic of the periodic properties of the grating and a term describing the Fraunhofer diffraction pattern of one of the individual scattering elements. The Fraunhofer diffraction pattern of a planar reflecting scatterer reaches its maximum in the direction predicted by geometrical optics for specular reflection.

There exists an optical element for which the geometrical optics approximation predicts that incident light will be reflected in the same direction regardless of the angle in which it is used. This is the roof mirror shown in figure 30. It can be seen that the incident light is reflected back parallel to itself. This is very nearly

the geometry used in the Littrow grating mount. The efficiency of a roof mirror scatterer will be nearly constant with respect to angle through a considerable angular range. Thus, one might expect that a grating constructed of scatterers shaped like roof mirrors would show nearly constant efficiency in any order when used in a Littrow mount, so that incoming and outgoing beams nearly coincide.

Figure 30 implies a process in which light is being doubly reflected in the roof mirror. In an element as small as a scattering element in a grating, one certainly does not expect reflection to take place in the geometrical optics sense. Nevertheless, the term "double reflection" will be retained to describe a scattering process in which two surfaces participate, as opposed to a process in which only one surface participates. The latter process will be termed "single reflection".

The groove shape of an echelette grating resembles a roof mirror, but when the grating is used in its customary manner with the long side of the groove doing the scattering, the geometry is favorable for the double reflection of a roof mirror to take place over only a narrow angular range. If an echelette grating, on the other hand, is used on the "wrong" side, i.e., with the narrow side of the groove doing the scattering, the conditions for double reflection,

similar to that in a roof mirror, are favorable over a much wider angular range.

It was in connection with the "wrong" side of an echelette grating that a wide blaze region was first observed. Wiggins and Saksena,[73] in a note on the relative dispersion of one-pass and two-pass spectrometers, remark that their grating showed a wide blaze region on the opposite side from that on which it was designed to be used, i.e., the side on which the short groove sides were doing the scattering. Rautian[74] later observed a wide blaze region under these conditions and gave a theoretical discussion similar to the Kirchhoff treatment given below to account for it. Both of these studies were made in the visible, and neither of the authors seems to have noticed the application of such a grating to an infrared spectrometer. Probably because of the poor optical quality of the short sides of the grooves in these gratings, the wide blaze region in both cases was of much less intensity than the blaze on the opposite side, and would not have suggested itself as useful when the other was available.

In an effort to improve on the echelon, Harrison[75] proposed the echelle grating. This is similar to the echelette, but is blazed at an angle greater than 60°, and is intended for use in a high order in visible light. Two

facts about the echelle are of concern here. First, the echelle is intended for use with the light reflected from the short side of the groove. Second, this grating is intended for use in the visible where the requirements of groove perfection are more stringent than in the infrared. Since greater care must be taken to rule such a grating, there is a good chance that, for the first time, one has a grating with two good groove sides at his disposal. One might expect, then, that an echelle showing a good secondary blaze (from the long side of the groove) near 90^{o} from the primary blaze will behave as an assemblage of very narrow roof mirrors and show a wide blaze region rather than a single blaze angle as is the case with the echelette.

To recapitulate, the intensity characteristics of gratings suggest that a condition in which the geometrical optics approximation would predict specular reflection taking place in the scattering element of the grating is important in achieving high efficiency. A grating with the scattering elements shaped like roof mirrors fulfills this condition, and at the same time should show constant intensity of scattered light with respect to grating angle. An echelette grating, when used on the "wrong" side, should approximate such a grating. Two papers have been published describing a blaze region which was observed on the "wrong"

side of echelette gratings. Probably because of poor groove shape, this blaze region was in both cases weak and not useful. The echelle grating, since it is intended to be used in the visible region, should have grooves of higher quality, and might be expected to show a much stronger blaze region. The following section which describes experiments made on an echelle grating shows this to be indeed true.

EXPERIMENTAL

The echelle used was obtained from Bausch and Lomb. It is a replica of a master which was ruled 80 lines/mm. over an area 194 x 104 mm. The primary blaze is in the 41st order of the mercury green line and is observed visually at $63^{\circ}30'$. A secondary blaze is observed visually near 27° and is found to correspond to the -15th order of the mercury green line. The experiments described here were done with the spectrometer discussed in Section I.

When one examines the grating from near either blaze angle, one sees an image such as might be seen from a very poor-quality mirror. This is similar to the same observation made on an echelette grating. This grating, however, shows a distinctive effect when viewed from a direction

nearly perpendicular to its face. From this direction one observes a large amount of light being reflected, but, in this case, no suggestion of an image can be seen. When mounted in the spectrometer, a strong zero order is observed. These observations are not unexpected in view of the discussion given above of a grating of roof mirrors, but it is of some interest that there was no image in the perpendicular direction. It is in this direction that the double reflection in the roof mirror is taking place.

The purpose of the experiments to be described is to test the hypothesis that a grating of roof mirrors will show a broad blaze region. The experimental procedure is to measure the efficiency of the grating as a function of grating angle. While such an experiment is quite simple in principle, it is extremely difficult in practice. The procedure is to use the grating in the spectrometer with a radiation source of known temperature and to measure the intensity of light at the detector as a function of wavelength. From the temperature of the source the intensity of incident light is calculated using Planck's formula. Thus, the efficiency of the grating can be calculated. The difficulty is that several corrections must be applied to the data to obtain the true efficiency.

The corrections which must be applied are as follows:

First, the globar used as a source is not a black body, so the energy emitted as calculated from Planck's formula must be corrected using the emissivity of the globar. Second, the mirrors in the spectrometer do not have unit reflectivity. Instead, their reflectivity varies as a function of wavelength. Thus, the light observed at the detector is diminished by the value of the reflectivity of aluminum for each single reflection in the spectrometer. Third, the light must pass through two potassium bromide windows at the entrance and the exit of the spectrometer and through a potassium bromide prism in the foreprism monochromator. Thus, the data must be corrected for the absorption of potassium bromide. Fourth, the light passing through the slits is a function of their width. Thus, the data must be corrected for the slit width. Fifth, the energy as calculated from Planck's formula is expressed as proportional to the wavelength interval observed. This interval may be a function of the slit width and of the dispersion of the two dispersive elements. A dispersive element of high resolution spreads the spectrum out over a wider area than one of lower dispersion. With the same energy input, the output through the exit slit will vary with the dispersion of the dispersive element. Thus, the data must be corrected for the dispersion of both the prism

and the grating. Finally, there are two ways of expressing the efficiency of a grating. The first is to express the efficiency in terms of an infinite grating illuminated by a finite beam of light. In this case, all of the light reaches the grating regardless of grating angle. The second way of expressing the efficiency is in terms of a grating of fixed size and a somewhat larger beam of light of fixed size. In this case, the amount of light falling upon the grating depends on the aspect which the grating presents to the collimator. This latter method measures the efficiency of the grating in a spectrometer. For a detailed discussion of these corrections, Strong[67] and Conn[71] may be consulted.

In the first experiment, the corrections described above were cancelled out by averaging the data. The procedure was to measure the intensity of each order of the grating for a number of different wavelengths. The available lines in the infrared spectrum of a mercury lamp were used where possible. At longer wavelengths, an artificial band which was the pass-band of the foreprism was used. The intensity of a line was taken as proportional to the height of the line at its maximum on the recorder tracing when the line appeared to be narrow with respect to the slit width. When a line became of a breadth comparable to

the slit width, it was not used. The intensity of an artificial band was taken as proportional to its area as measured on the recorder tracing with a planimeter. When changing ranges on the spectrometer a correction had to be made for the change of length on the chart paper for unit wavelength. This was determined by measuring a portion of a band which appeared in both ranges.

For each wavelength observed, the average was determined of the intensities in all of the observed orders. The intensity of each individual order was divided by this average. In a series of measurements of different orders of the same wavelength, the only factor varying is the grating angle. Each of the corrections described above can be expressed as a factor which multiplies the observed intensity. Upon dividing each observed intensity by the average of intensities for that wavelength all correction factors which do not depend on grating angle, therefore, cancel out of the problem.

The only correction which may depend on the grating angle is the correction for the dispersion of the grating. This correction does not apply to this particular experiment for the following reason: As explained above, the correction to be applied is a function of the wavelength interval observed. Because of the way in which the intensity

is determined, the wavelength interval observed depends solely on the width of the line in the case of the observations of the mercury spectrum, and on the pass-band of the foreprism in the case of the observations on the artificial band. Thus, the ratio of the observed intensity of an order to the average of all orders observed at the same wavelength is proportional to the efficiency of the grating when mounted in the spectrometer.

Such a procedure depends on the observation of a large number of orders for each wavelength and for this reason is best at shorter wavelengths. It tends to ignore such isolated effects as Wood anomalies or atmospheric bands in a single order. These effects would tend to average out if a large number of orders were observed, but can become quite troublesome at long wavelengths where few orders are observed. The value of the ratio for the first order is plotted in figure 31.

In the second experiment, an attempt was made to evaluate each of the corrections discussed above. A background spectrum was observed in a single grating order over the complete range of wavelength available to the spectrometer. The energy variations encountered over this range are so great that a single slit width would give variations in observed intensity which are too large for measurement.

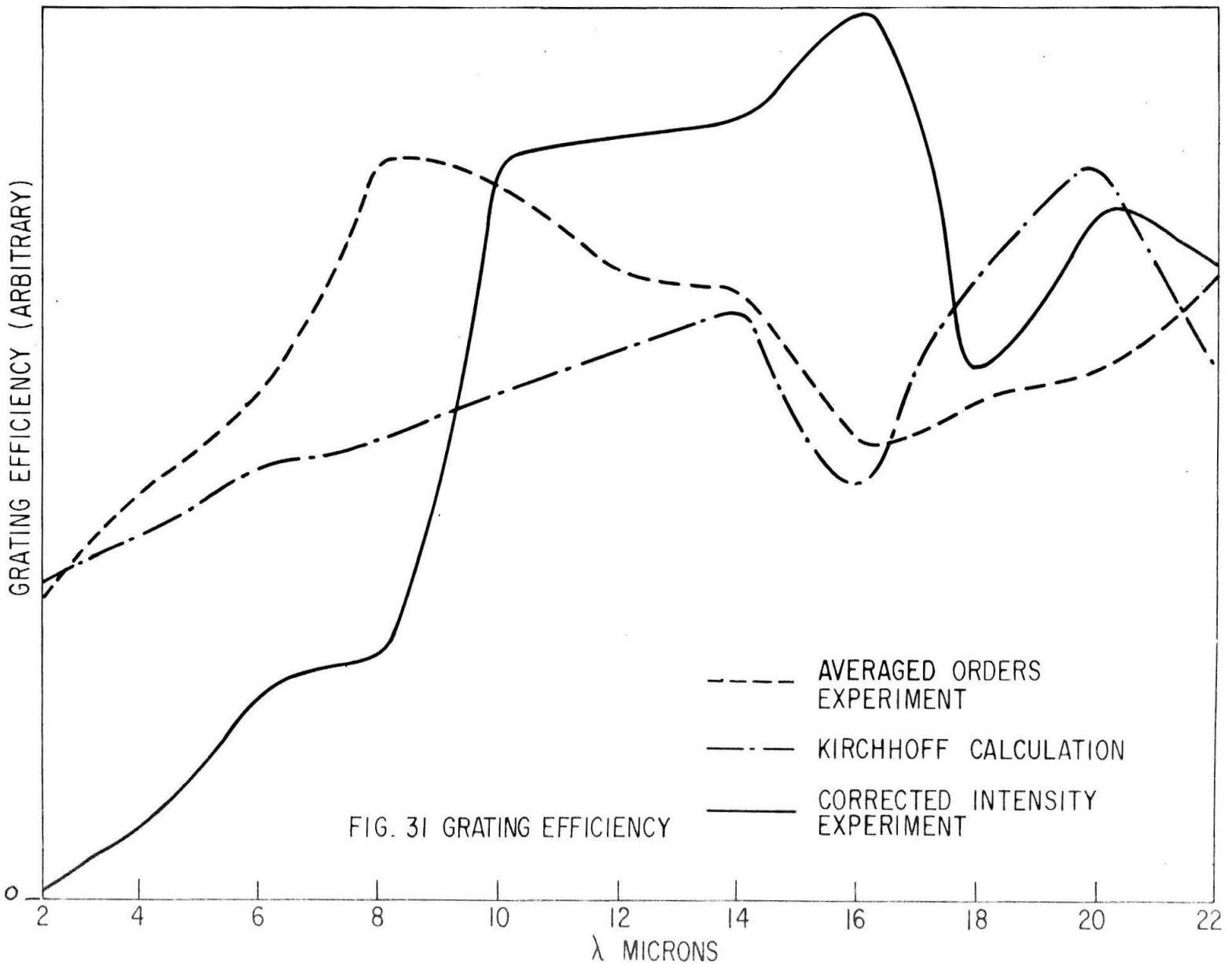

FIG. 31 GRATING EFFICIENCY

Therefore, the slits were varied as required to give a satisfactory level of intensity at the detector at all times. The intensity observed, together with the slit width used, was recorded at closely spaced wavelength intervals. When these intensities are corrected properly, they are proportional to the efficiency of the grating.

The corrections to be applied are as follows:

1. The intensity is divided by the square of the slit width to obtain the intensity for a slit of unit width.
2. It is divided by the absorption of potassium bromide to correct for the absorption in the windows and prism.
3. It is divided by the reflectivity of aluminum to the fifteenth power to correct for the fifteen reflections in the spectrometer.
4. The intensity is divided by the linear dispersion of potassium bromide.
5. For the same reason it is divided by the cosine of the grating angle to correct for grating dispersion.
6. It is divided by the intensity of a black body at the temperature of the globar, as measured with an optical pyrometer, to correct for variation in source intensity.
7. Finally, the intensity is divided by the emissivity of the globar to correct the black body intensity to that of the globar.

The corrections are presented in Table V and the results are plotted in figure 31. Figure 31 represents the performance of the grating in a spectrometer using a Littrow mounting and does not contain the correction for aspect angle. These results are each divided by the average value of the efficiency over the entire range in order to express them on a basis similar to the results of the first experiment.

Both of the above experiments rely heavily on corrections and approximations for their interpretation. Another experiment was performed which is much easier to interpret. It gives less information about the grating itself, but does give a clearer picture of the performance of the spectrometer as a whole. In view of Martin's results discussed above one would expect the echelle grating to give constant wavenumber resolution over some broad wavelength region. The wavenumber resolution was measured as follows: Some convenient intensity level at the detector is selected. As the spectrometer is adjusted to various wavelengths through the spectrum, the slit is adjusted to give the selected intensity at the detector. The resultant slit width is used to calculate the resolution at each wavelength and this resolution is plotted as a function of wavelength. If the intensity selected were the minimum intensity which the

NOTES FOR TABLE V

A Potassium bromide absorption[76]

B Aluminum reflectivity[77]

C Potassium bromide dispersion[78]

D $\cos^2 \theta$ (caculated)

E Black body intensity at source temperature (calculated)

F Globar emissivity[79]

G Total correction ($=AxB^{15}xCxDxExF$)

a. Observed intensity is corrected for slit width and divided by G.

b. Entries in parentheses are estimated.

TABLE V--CORRECTIONS TO OBSERVED INTENSITY

WAVELENGTH (microns)	A	B	C	D	E	F	G[a]
2	0.91	0.970	0.003	0.994	125	0.73	1.56
4	0.91	0.977	0.020	0.975	61.4	0.79	0.600
6	0.91	0.980	0.022	0.944	24.5	0.84	0.287
8	0.91	0.981	0.022	0.896	7.74	0.85	0.0878
10	0.91	0.982	0.020	0.840	3.55	0.86	0.0284
12	0.90	0.984	0.018	0.769	1.86	0.80	0.0146
14	0.90	(0.985)[b]	0.017	0.686	1.06	0.81	0.00726
16	0.90	(0.985)	0.015	0.590	0.652	(0.80)	0.00325
18	0.90	(0.985)	0.014	0.481	0.422	(0.80)	0.00164
20	0.90	(0.985)	0.012	0.360	0.283	(0.80)	0.000726
22	0.86	(0.985)	0.011	0.226	0.198	(0.80)	0.000270
24	0.83	(0.985)	0.010	0.083	0.142	(0.80)	0.0000634

spectrometer could measure, the resolution data would represent the resolution limit of the spectrometer. The minimum intensity which the spectrometer can measure is a somewhat subjective term, since it depends upon such things as the response time one is willing to tolerate in making the measurements. For this reason, some arbitrary higher intensity level was chosen. In this case the resolution observed is proportional the resolution limit of the spectrometer.

Such an experiment was performed with the echelle grating and vacuum spectrometer as well as with an echelette grating and the Beckman IR7 spectrometer. This echelette grating is somewhat smaller than the echelle and is ruled 75 lines/mm. and blazed at 12 microns in the first order. The Beckman spectrometer uses a Nernst glower as a source, and consequently has a higher source temperature than was used with the vacuum spectrometer. For this reason, it must be emphasized that the comparison to be made here is between spectrometers and not primarily between gratings. In addition, because of the selection of the arbitrary intensity level, absolute resolutions cannot be compared between different instruments. The significant result is the shape of the resolution curve as a function of wavelength. The smaller size of the grating in the Beckman spectrometer would tend to lower its resolution limit,

while the higher source temperature would tend to increase it. Since the constants of the grating in the Beckman spectrometer correspond most closely to those of the echelle in the second order, an experiment was also performed on the echelle in the second order. The results of these experiments are presented in figure 32. Resolution for the observed slit width is plotted against wavelength.

THEORETICAL

Twersky[80] has given an excellent review of the literature on the theory of diffraction and multiple scattering. While the theory is well understood in its principles, there are not satisfactory mathematical methods for applying these principles. Because of this one must make approximations regarding the magnitude of some of the parameters in the problem with the result that the theory will apply only to certain ranges of these parameters. Calculations applying to the intensity distribution of the diffraction pattern of a grating which have been reported in the literature are nearly all[71,74,81-84] based on an analysis presented by Rowland.[85] (Analyses pertaining to Wood anomolies are not included.) The Rowland theory is in turn based on the Kirchhoff theory developed here, but some authors do not seem to be aware of this fact. Any grating used in the

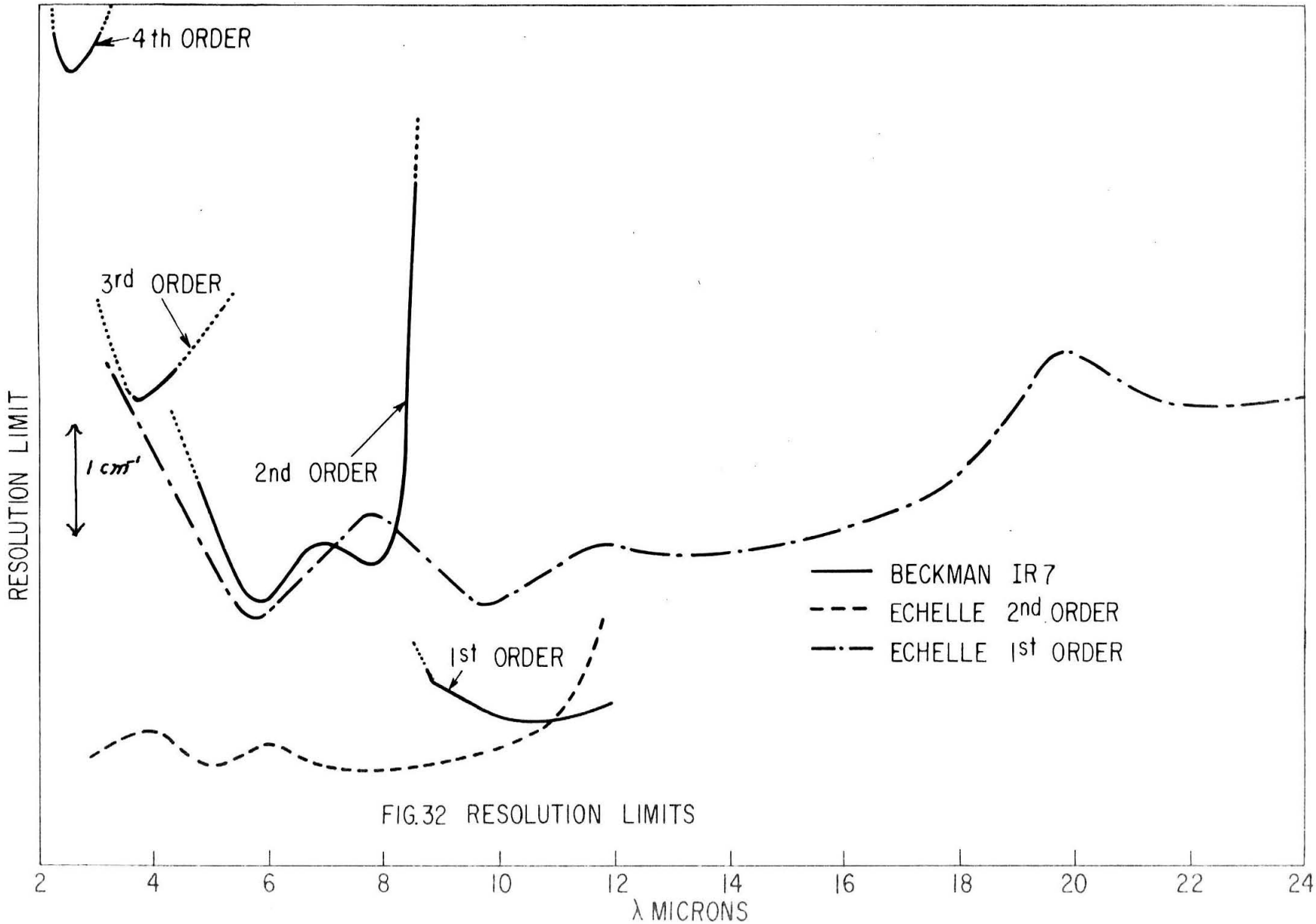

FIG. 32 RESOLUTION LIMITS

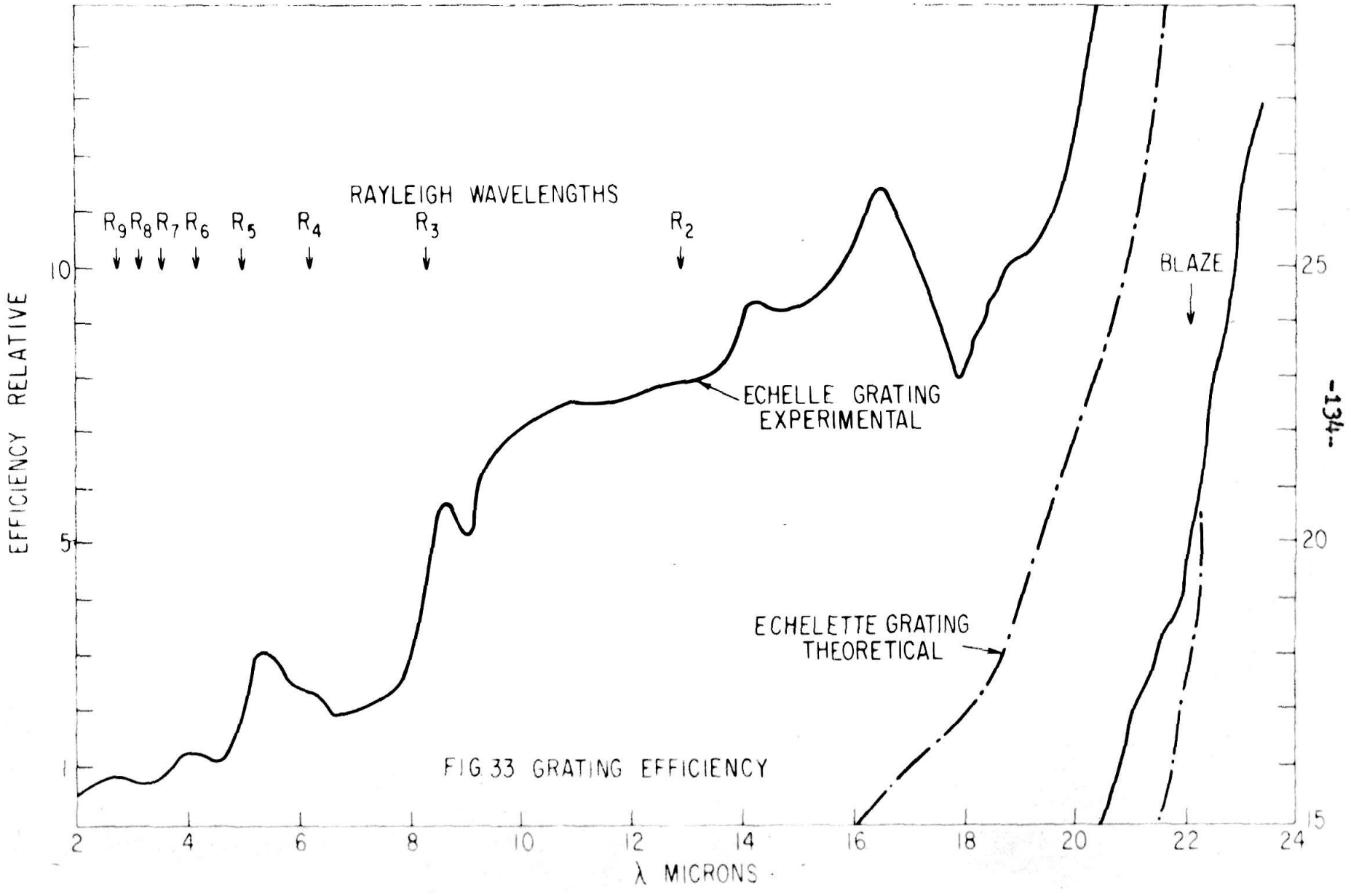

FIG 33 GRATING EFFICIENCY

first order is in a wavelength range dangerously near the limit of validity of the Kirchhoff theory. At a grating angle of thirty degrees in a Littrow mount the wavelength actually becomes greater than the grating spacing. As will be seen below, this evidently does not completely destroy the validity of the results, but one should be aware that the theory on which they are based no longer applies. Three papers have appeared based on other analyses. The first is the one by Rautian[74] which uses the same method as that given below for calculating the diffraction pattern of a roof mirror. The second two are the papers by Meecham[86,87] on which the Rayleigh theory analysis given below is based.

Two mathematical analyses are given here. They differ in the approximations made and the range of validity. The first is based on Kirchhoff's formulation of the Fresnel-Huygens diffraction theory which assumes that the wavelength is much less than the grating spacing. In this analysis, each scatterer is treated separately and the resulting diffraction patterns finally added to obtain the pattern for the grating. The second is based on Rayleigh's dynamic theory[88] and assumes that the depth of the groove is much less than the wavelength. This analysis treats the grating as a whole. One expects that the Kirchhoff analysis will be most valid at short wavelengths and that the Rayleigh

analysis will be best at long wavelengths.

1. THE KIRCHHOFF THEORY

It is difficult to find in one place in the literature a complete treatment of this theory as applied to diffraction gratings. The one by Born and Wolf[89] is the most complete, but there are gaps in this as applied to the grating problem. It is hoped that this analysis will correct this deficiency. The analysis will begin with the wave equation. The derivation of Kirchhoff's integral by Green's theorem will be presented, and this integral will be applied to the case of Fraunhofer diffraction by a single slit. This much of the theory is in standard texts, and is presented here to emphasize the approximations made. Next an intuitional idea of diffraction by the roof mirror will be obtained by considering diffraction from two separate slits and adding the amplitudes of the resulting waves. Squaring these amplitudes and suitably normalizing the resulting intensity will then give the desired results.

Following Born and Wolf one begins with the wave equation

$$\nabla^2 \phi = \frac{1}{c^2} \frac{\partial^2 \phi}{\partial t^2} \qquad (2)$$

as derived from Maxwell's equations. Here ϕ is one of the scalar components of either the electric or magnetic vectors. Ideally, equation 2 should be a vector equation, but to the extent that the waves under consideration can be regarded as plane waves, a single scalar component will adequately represent them. If ϕ fulfills the conditions of the Fourier integral theorem,(90) as it does in this problem, then

$$\phi(\vec{r},t)=\frac{1}{\sqrt{2\pi}}\int_{-\infty}^{+\infty}\psi_\omega(\vec{r})\,e^{i\omega t}\,d\omega, \tag{3}$$

where ω refers to the angular frequency. By the Fourier inversion formula

$$\psi_\omega(\vec{r})=\frac{1}{\sqrt{2\pi}}\int_{-\infty}^{+\infty}\phi(\vec{r},t)\,e^{-i\omega t}\,dt. \tag{4}$$

Since ϕ satisfies equation 2, ψ will satisfy

$$(\nabla^2+K^2)\,\psi_\omega=0 \qquad K=\frac{\omega}{c} \tag{5}$$

If ψ' also satisfies equation 5, then, by Green's theorem,(91)

$$\int_V(\psi_\omega\nabla^2\psi'-\psi'\nabla^2\psi_\omega)\,dV$$
$$=-\int_S\left(\psi_\omega\frac{\partial\psi'}{\partial n}-\psi'\frac{\partial\psi_\omega}{\partial n}\right)dS, \tag{6}$$

where V and S are a volume and its enclosing surface,

respectively, within which ψ_ω and ψ' fulfill the conditions for Green's theorem. Here $\partial/\partial n$ denotes differentiation with respect to the inward normal to S. Since both ψ_ω and ψ' satisfy equation 5, the left side of equation 6 vanishes and

$$\int_S \left(\psi_\omega \frac{\partial \psi'}{\partial n} - \psi' \frac{\partial \psi_\omega}{\partial n}\right) dS = 0. \qquad (7)$$

Now consider the situation in figure 34. P is the point at which the effects of an incident beam originating at P_0 and falling upon aperture A will be calculated. Take $\psi' = s^{-1} e^{-iks}$ where s is the distance from P to the point at which ψ_ω is to be evaluated. This function has a singularity at P which must be eliminated from the region of integration. This is done by enclosing P in a sphere S' with center P and radius ϵ which is small. The value of ψ' is now substituted into equation 7 and the limit as $\epsilon \to 0$ taken. The integral over S' becomes $4\pi \psi_\omega(P)$, and equation 7 becomes

$$\psi_\omega(P) = \frac{1}{4\pi} \int_S \left[\psi_\omega \frac{\partial}{\partial n}\left(\frac{e^{-iks}}{s}\right) - \frac{e^{-iks}}{s} \frac{\partial \psi_\omega}{\partial n}\right] dS. \qquad (8)$$

In equation 8, ψ_ω is only one of the monochromatic components of ϕ. To get the complete expression for ϕ, substitute equation 8 into equation 3 and change the order of integration:

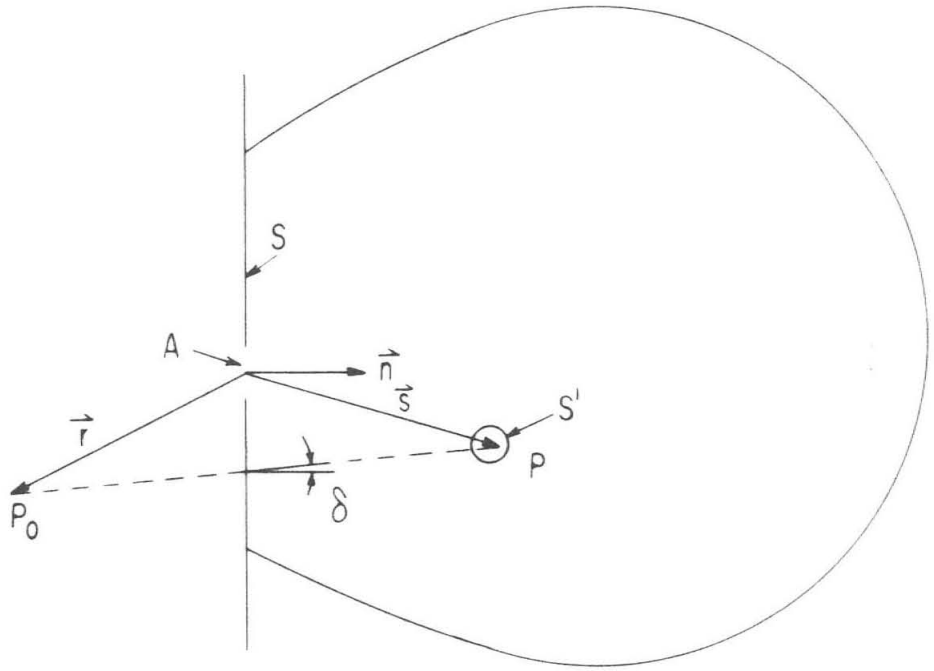
S
A
$\vec{n}$
$\vec{s}$
S'
$\vec{r}$
P
P_0
δ

FIG. 34

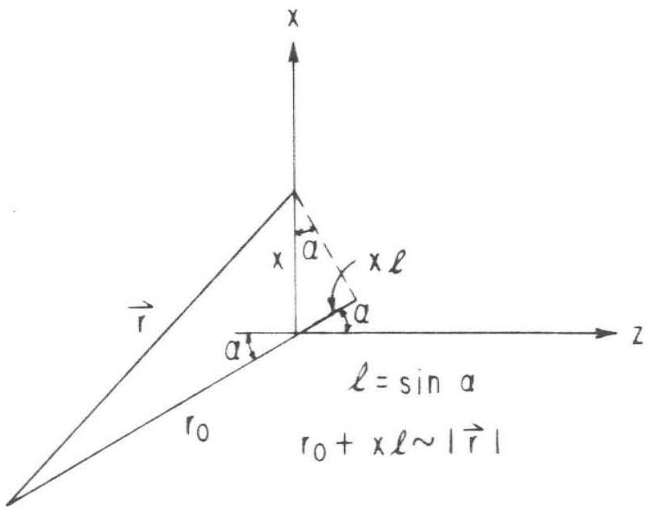
x
x
α
$x\ell$
α
$\vec{r}$
α
z
$\ell = \sin \alpha$
r_0
$r_0 + x\ell \sim |\vec{r}|$

FIG. 35

$$\phi(P,t)=\frac{1}{4\pi}\int_S \frac{1}{\sqrt{\pi}}\int_{-\infty}^{+\infty}\left\{\psi_\omega\left[\frac{\partial}{\partial n}\left(\frac{1}{s}\right)-\frac{i}{s}\frac{\omega}{c}\frac{\partial s}{\partial n}\right]e^{i\omega(t-s/c)}\right.$$

$$\left.-\frac{e^{i\omega(t-s/c)}}{s}\frac{\partial}{\partial n}\psi_\omega\right\}d\omega\, dS. \qquad (9)$$

If ϕ is substituted for its value on the right hand side of equation 9 using equation 3,

$$\phi(P,t)=\frac{1}{4\pi}\int_S \phi(s,t-s/c)\frac{\partial}{\partial n}\left(\frac{1}{s}\right)-\frac{1}{cs}\frac{\partial s}{\partial n}\left[\frac{\partial\phi(s,\tau)}{\partial\tau}\right]_{\tau=t-s/c}$$

$$-\frac{1}{s}\left[\frac{\partial\phi(s,\tau)}{\partial n}\right]_{\tau=t-s/c} dS. \qquad (10)$$

The similarity between ϕ and the well-known retarded potential[92] is to be noted here. If, instead of choosing a component of one of the wave vectors for ϕ in equation 2 one had chosen the scalar potential, $\phi(s,t-s/c)$ would represent the potential at a distance s due to a wave propagating with the velocity c. This is the starting point of many treatments such as this one.

It is now necessary to obtain the expression for ϕ on the surface over which the integration is to be performed.

It is assumed that the source P_o is emitting spherical waves of amplitude unity and wavelength $\frac{2\pi}{k} = \frac{c}{\omega}$. A factor $e^{i\omega t}$ will be removed from the expression. In aperture A (figure 34)

$$\phi_o = \frac{e^{ikr}}{r} \tag{11}$$

$$\frac{\partial \phi_o}{\partial n} = \frac{e^{ikr}}{r}\left[ik - \frac{1}{r}\right]\cos(n,r).$$

The expression (n,r) represents the angle between r and the normal n to A. It should be noted that equation 11 is not strictly correct at the edges of the aperture. This is one of the reasons for restricting the validity of this treatment to wavelengths much shorter than the dimensions of A. It is convenient to make an assumption which causes the integrand to vanish except over A. This is easily done in the case of the screen S by assuming that it is perfectly opaque. For the remainder of the surface, Born and Wolf[93] point out that the assumption that the surface lies at infinity is not adequate because of the presence of s in the denominator in equation 10. They assume that the surface is so large that the wavefront cannot propagate to it during the time of an experiment. Substituting equation 11 into equation 10,

$$\phi = \frac{iK}{4\pi}\int_S \frac{e^{iK(r+s)}}{rs}\left[\cos(n,s)-\cos(n,r)\right]dS$$

$$-\frac{1}{4\pi}\int_S \frac{e^{iK(r+s)}}{rs}\left[\frac{\cos(n,s)}{s}-\frac{\cos(n,r)}{r}\right]dS. \qquad (12)$$

It will be assumed that r and s are large with respect to k^{-1} so that the second term of equation 12 can be neglected in comparison with the first. When the roof mirror is considered, this assumption will not be strictly true. When light is reflected from one side of the groove to the other, r becomes of the order of the groove width, which can actually be less than the wavelength. It will be further assumed that the variation of the factor

$$\frac{\cos(n,s)-\cos(n,r)}{rs} \qquad (13)$$

is small over the range of integration and that this factor can be taken outside the integral sign. There it will be written $\cos(\delta)/r_o s_o$ where δ is the angle between the normal to A and the line connecting P and P_o. The precise definition of r_o and s_o will be given later, but they are some mean value over A of r and s respectively. Making these changes, equation 12 becomes

$$\phi_o(P) = -\frac{ik\cos\delta}{4\pi r_{os}} \int_A e^{ik(r+s)}\, dS. \qquad (14)$$

Equation 14 is Kirchhoff's formulation of Huygens' construction. It assumes that the wave can be represented as a scalar, that the representation in equation 11 expresses the field in the aperture with sufficient accuracy, that the second term in equation 12 can be neglected, and that the expression in equation 13 can be removed from the integral. No provision is made for polarization of the light wave.

A set of co-ordinates is now defined with xy plane lying in aperture A and positive z directed toward the region containing P. From figure 35 it can be seen that the error in writing $r = r_o + l_r x + m_r y$ is of the order of the error in taking an angle for its sine when the angle is small. Here, r_o is the distance of P_o from the origin and l_r and m_r are the sines of the angles between the normal to A and the x and y components of $\vec{r}$. Treating s similarly, (r+s) becomes $r+s = r_o + s_o + lx + my$, where $l = l_r + l_s$ and $m = m_r + m_s$. Using these new variables, equation 14 becomes

$$\phi(P) = -\frac{ik\cos\delta}{4\pi r_{os}} e^{ik(r_o+s_o)} \int_A e^{ik(lx+my)}\, dx\, dy. \qquad (15)$$

If P_o is regarded as the image of a source on the same side of S as P, S as a perfect absorber, and A as a perfect reflector, equation 15 gives equally well the field at P due to waves originating at P_o and reflected from a mirror A. It should be noted that this does not include waves propagating directly from P_o to P.

The extension to a grating is made by adding the effects of a series of N identical mirrors of dimensions axb,

$$\phi_T = -\frac{ik\cos\delta}{4\pi r_o s_o} e^{ik(r_o+s_o)} \int_{-b/2}^{b/2} e^{ikmy}\,dy \cdot$$

$$\cdot\left[\int_{-a/2}^{a/2} e^{ikl x}\,dx + \int_{d-a/2}^{d+a/2} e^{ikl x}\,dx + \cdots + \int_{(N-1)d-a/2}^{(N-1)d+a/2} e^{ikl x}\,dx\right]. \qquad (16)$$

This is

$$\phi_T = -\frac{ik\cos\delta}{4\pi r_o s_o} e^{ik(r_o+s_o)} \int_{-b/2}^{b/2} e^{ikmy}\,dy \cdot \int_{-a/2}^{a/2} e^{ikl x}\,dx \cdot$$

$$\cdot\left[1 + e^{ikd} + e^{2ikd} + \cdots + e^{(N-1)ikd}\right]$$

which, on summing and evaluating the integrals, becomes

$$\phi_T = -\frac{ik\cos\delta}{4\pi r_o s_o} e^{ik(r_o+s_o)} \cdot \frac{1}{imk} \cdot \left(e^{ikmb/2} - e^{-ikmb/2}\right) \cdot$$

$$\cdot \frac{1}{ilk}\left(e^{iklb/2} - e^{-iklb/2}\right)\left(\frac{1-e^{iklNd}}{1-e^{ikld}}\right). \qquad (17)$$

The experimental quantity measured is the intensity, so

equation 17 is multiplied by its complex conjugate to get

$$I_T = |\phi_T|^2 = \frac{\cos^2\delta}{4\lambda^2 r_0^2 s_0^2} \cdot \frac{\sin^2(\pi mb/\lambda)}{(\pi mb/\lambda)^2} \cdot \frac{\sin^2(\pi la/\lambda)}{(\pi la/\lambda)^2} \cdot \frac{\sin^2(\pi Nld/\lambda)}{\sin^2(\pi ld/\lambda)} \quad (18)$$

using $K = 2\pi/\lambda$ where λ is the wavelength. As N becomes large, the last factor is small except for values of l for which $n\lambda = dl$ where n is an integer. This is the origin in this theory of the grating formula. There are small maxima between these values, but these can be neglected for the present purpose.

Equation 18 is the expression for a grating of N plane mirrors of dimensions axb. It will now be used to obtain a similar expression for the grating of roof mirrors. The fact that it involves the product of a factor describing the Fraunhofer diffraction of a narrow slit,

$$\frac{\cos^2\delta}{4\lambda^2 r_0^2 s_0^2} \cdot \frac{\sin^2(\pi mb/\lambda)}{(\pi mb/\lambda)^2} \cdot \frac{\sin^2(\pi la/\lambda)}{(\pi la/\lambda)^2}$$

and a factor characteristic of the periodicity of the grating suggests that the extension to another scatterer is to be made by calculating the Fraunhofer pattern of the new scatterer. The single roof mirror is regarded as equivalent to two mirrors (figure 36). The portion of the roof mirror involved in double reflection is replaced by a mirror of width a oriented perpendicular to the incoming beam

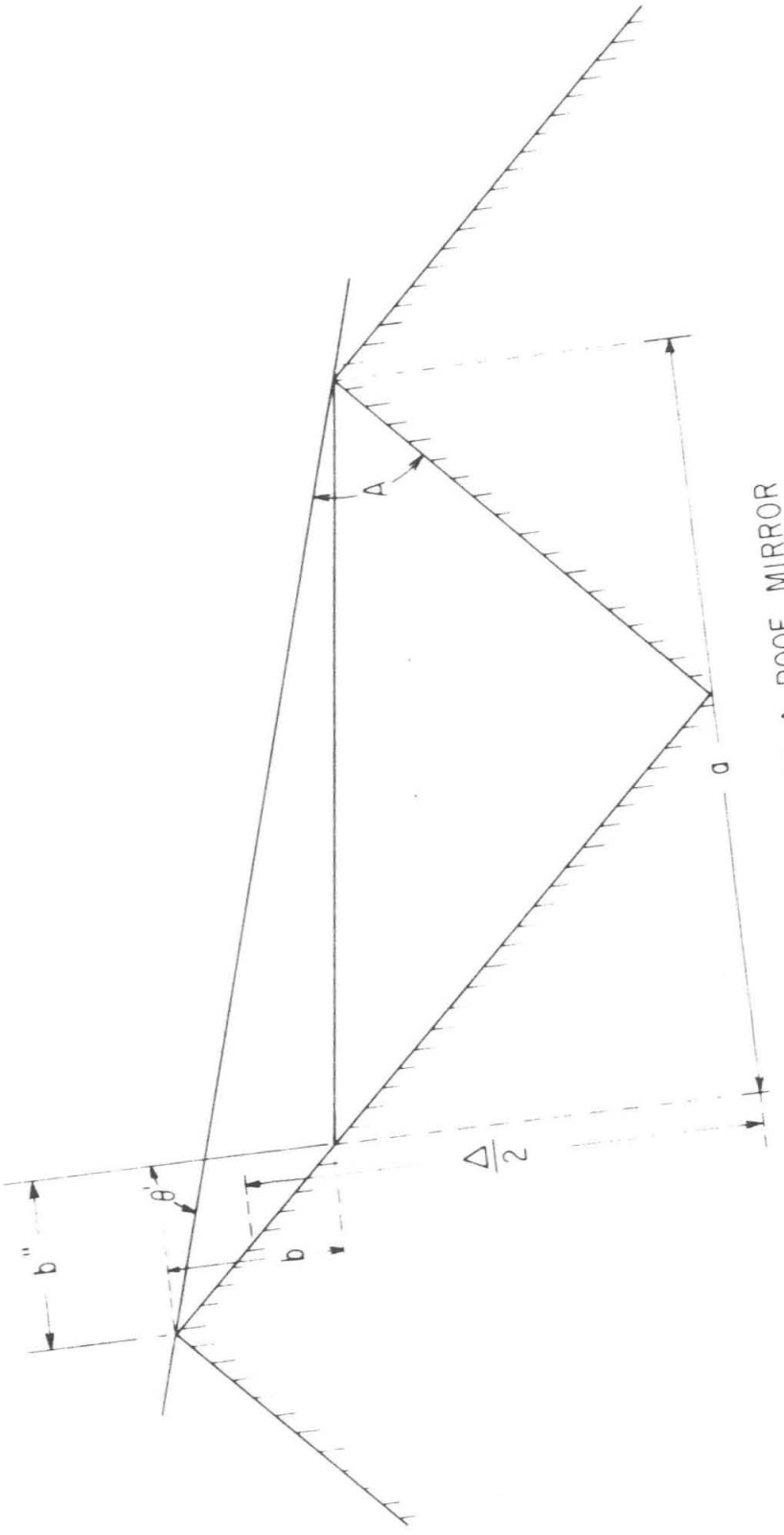

DIFFRACTION BY A ROOF MIRROR
FIG 36

(which is assumed here to be planar). The portion involved in single reflection is approximated by b which is perpendicular to the extreme ray involved in double reflection and is excited by light of intensity proportional to b", the portion of the incoming beam involved in single reflection. It must be remembered that the separate amplitudes scattered from these two mirrors are to be added with a phase change equivalent to Δ where Δ is twice the distance between the midpoints of the two mirrors, measured in the direction of the incoming beam. See figure 36. It is convenient to consider two cases separately--that in which b is a portion of the long groove side, and that in which b is a portion of the short groove side. In the first case, b is inclined to the direction of the collimator at such a large angle that the radiation scattered from it to the collimator can be neglected. The final expression for the intensity is

$$I(\theta) = 2NR^2 \cos A \sin \Phi \qquad \text{case b} \qquad (19a)$$

$$I(\theta) = N\left\{R^2(-2\sin A\cos\Phi) + R(\sin\theta' + 2\sin A\cos\Phi)\cdot \frac{\sin^2\left[\frac{\pi d}{\lambda}\sin(\Phi+A)\sin 2\Phi\right]}{\left[\frac{\pi d}{\lambda}\sin(\Phi+A)\sin 2\Phi\right]^2} + 2R^{3/2}\left[(-2\sin A\cos\Phi)\cdot(\sin\theta' + 2\sin A\cos\Phi)\right]^{1/2}\cdot \frac{\sin\left[\frac{\pi d}{\lambda}\sin(\Phi+A)\sin 2\Phi\right]}{\left[\frac{\pi d}{\lambda}\sin(\Phi+A)\sin 2\Phi\right]}\cdot \cos\left[d\cos\Phi(\cos A - \sin A\cos\Phi)\right]\right\} \qquad \text{case b} \qquad (19b)$$

where N is a constant factor which will drop out later, A is the groove angle, θ' is the angle shown in figure 36 (90°—the usual grating angle), R the reflectivity of the coating, d the grating spacing, and ϕ the angle $(A+\theta')$. The first two factors in equation 18 are included in N. Equation 19 is to be multiplied by the last factor in equation 18, but this is equal to one in the center of an order which is the case of interest.

Calculations have been made for a grating similar to the echelle used in the experimental work. A reflectivity of 0.90 was assumed. The results are presented in figure 31. The values calculated from equation 19 at each wavelength are averaged and each individual calculation divided by this average. This has the effect of expressing the results on the same basis as the results of the first two experiments.

2. THE RAYLEIGH THEORY

The above method deals with a single scattering element of the grating and then adds the contribution of each scattering element to obtain the scattered radiation from the entire grating. The treatment by Rayleigh[88] expands the solution to the wave equation in a series of plane waves

which correspond to the orders of the grating. The coefficients of those plane waves which propagate away from the grating are then proportional to the amplitude of radiation in each grating order.

Born and Wolf[94] point out that any solution of the wave equation 2 can be written

$$\phi(r,\theta) = \int f(\alpha)\, e^{ikr\cos(\theta-\alpha)}\, d\alpha \qquad (20)$$

where the path of integration and the function $f(\alpha)$ are suitably chosen. This is equivalent to saying that the solution can be expanded in a spectrum of plane waves, some of which propagate away from the grating and some of which are exponentially damped depending on whether the cosine term is real or imaginary. Rayleigh's approach is to express the integral in equation 20 as a sum using only those values of α which correspond to grating orders. This is probably a good approximation in the far field where only discrete grating orders are observed, but we are trying to match boundary conditions in the groove itself. It is probable that waves propagating from a groove surface to another groove surface farther into the grating will be important, particularly in the case of a grating of roof mirrors. Such waves would not have the convenient periodic properties of the outgoing waves in the far field, and the integral

expression, equation 20, would have to be used to include them.

Lippman[95] has pointed out this discrepancy with the Rayleigh method, and, in an unpublished report,[96] has obtained an expression for the portion of the field represented by waves traveling into the grating. Unfortunately, the expression does not easily lend itself to numerical calculations. Meecham[86] has considered this problem and quoted another unpublished report by Lippman as giving a condition which is sufficient for the neglect of this inward-scattered field. This condition is that the groove depth be much less than a wavelength. The grooves in the echelle grating are quite deep, but this condition should be fairly well satisfied at long wavelengths. Since this is the region in which the Kirchhoff theory is least valid, it seemed well to present an analysis based on the Rayleigh theory.

The equations given by Rayleigh are not easy to use. The problem, as defined by him, consists in solving an infinite set of algebraic equations, and it is not easy to see in what manner this set should be broken into a finite set which can be solved. Meecham has discussed another method which leads to a series that can be terminated at any point at which the results are sufficiently accurate.

Meecham and Peters[87] have published results of calculations made with the series method in which the electric vector is parallel to the grating grooves. In addition experimental data are presented in this latter paper for an echelette grating.

Two other features of the Meecham-Rayleigh approach will be useful. In the Kirchhoff theory, no distinction is made between waves polarized with the electric vector parallel and those polarized with the electric vector perpendicular to the grooves of the grating. Peters, Deibel, Pursley, and Zipf[97] have reported a study which shows that quite radical differences can occur between these two polarizations. The Meecham-Rayleigh approach, in writing down the material boundary conditions explicitly, includes the polarization. Second, the Rayleigh theory predicts the Wood-Strong anomalies which are observed in this grating, and which prove troublesome at times.

To begin, one writes

$$\phi_0 = \phi_i + \phi_r \tag{21}$$

where ϕ_0 is the time-independent field sought, ϕ_i is the incoming wave, and ϕ_r the scattered field. In particular,

$$\phi_i = e^{iK(x\sin\theta_i - z\cos\theta_i)} \tag{22}$$

where the x axis is perpendicular to the grating groove and the z axis perpendicular to the grating surface. The boundary conditions for equation 2 are

$$\phi[x, g(x)] = 0 \qquad \vec{E} \parallel y \tag{23a}$$

$$\frac{\partial \phi}{\partial n}\Big|_{z=g(x)} = 0 \qquad \vec{E} \perp y \tag{23b}$$

for the electric vector parallel to, and perpendicular to, the groove, respectively. Here $g(x)$ is the equation of the surface of the grating. The differentiation is normal to g. It is supposed that one can write

$$\phi_i = -\sum_{\nu=-\infty}^{\infty} C_\nu e^{-i k x \sin\theta_\nu + i k z \cos\theta_\nu} \tag{24}$$

where $K = \frac{2\pi}{\lambda}$ and θ_ν is the grating angle for the ν th order given by the grating equation

$$\sin\theta_\nu = \frac{\nu\lambda}{d} - \sin\theta_i . \tag{25}$$

In equation 25, θ_i is the angle of incident radiation. The implication of equation 24 is that the reflected field can be expressed as a sum of discrete waves which correspond to all real and imaginary grating orders. Using equation 22 and equation 24, the boundary conditions become

$$e^{ik(x\sin\theta_i - \varphi(x)\cos\theta_i)} - \sum_{\nu=-\infty}^{\infty} C_\nu e^{-ikx\sin\theta_\nu + ik\varphi(x)\cos\theta_\nu} = 0 \qquad \vec{E} \parallel y \tag{26a}$$

$$\frac{\partial}{\partial n}\left[e^{ik(x\sin\theta_i - \varphi(x)\cos\theta_i)}\right] - \sum_{\nu=-\infty}^{\infty} C_\nu \frac{\partial}{\partial n}\left[e^{-ikx\sin\theta_\nu + ik\varphi(x)\cos\theta_\nu}\right] = 0 \qquad \vec{E} \perp y. \tag{26b}$$

For a grating whose grooves have a triangular cross section, the function $\varphi(x)$ is specified as

$$\begin{aligned} \varphi(x) &= -cx && 0 \le x \le d' \\ &= -c'(d'-x) && d \le x \le d \end{aligned} \tag{27}$$

where c' is the tangent of the larger groove angle (A in figure 36) and c is the tangent of the other groove angle. The value of x where the two sides of the groove meet is d'. Clearly $\varphi(d')$ is the groove depth. Using equations 25 and 27, and dividing by a factor $e^{ikx\sin\theta_i}$, equation 26 becomes

$$\bar{\Phi}_i - \sum_{\nu=1}^{\infty} A_\nu F_\nu = 0 \qquad \vec{E} \parallel y \tag{28a}$$

$$\begin{aligned} &(c\sin\theta_i - \cos\theta_i)\bar{\Phi}_i(x) \\ &\quad - \sum_{\nu=1}^{\infty} A_\nu (c\sin\theta_\nu - \cos\theta_\nu) F_\nu(x) = 0 \qquad 0 \le x \le d' \\ &(c'\sin\theta_i + \cos\theta_i)\bar{\Phi}_i(x) \qquad \vec{E} \perp y. \\ &\quad - \sum_{\nu=1}^{\infty} A_\nu (c'\sin\theta_\nu + \cos\theta_\nu) F_\nu(x) = 0 \qquad d' \le x \le d \end{aligned} \tag{28b}$$

Here

$$\bar{\phi}_i = e^{ik\zeta(x)\cos\theta_\nu},$$
$$F_\nu(x) = e^{-i\frac{2\pi}{d}\nu x - i\frac{2\pi}{\lambda}\zeta(x)\cos\theta_\nu}, \tag{29}$$

and

$$\begin{aligned} A_1 &= C_0 \\ A_2 &= C_1 \\ A_3 &= C_{-1} \\ A_4 &= C_2 \\ &\text{etc.} \end{aligned} \tag{30}$$

the substitution being made for convenience in adapting the problem to a computer. The A_ν then represent the solution of the problem. Those A_ν for which $\cos\theta_\nu \leq 1$ represent the complex amplitudes of each propagating order, while the remainder represent the evanescent waves.

To calculate A_ν Rayleigh solved the set of equations 28. Meecham proceded by defining a new set of functions which are a linear combination of the F_ν

$$G_K = \sum_{\ell=1}^{K} \Gamma_\ell^K F_\ell, \tag{31}$$

and have the orthogonality property

$$(G_k, G_\ell) = \delta_k^\ell . \tag{32}$$

Here δ_k^ℓ is the Kronecker delta and the scalar product is written

$$(g,h) = \frac{1}{d}\int_0^d g^* h \, dx. \tag{33}$$

The integration in equation 33 is over only one groove because of the periodicity of the grating, and not because only one groove is to be considered. It will be noticed that the extra terms which the boundary conditions for the perpendicular polarization introduce in equation 28b can be included in a factor which multiplies the scalar products. Doing this has the advantage of making the remaining equations identical for the two polarizations.

In terms of the G_k, using equation 28a,

$$\bar{\phi}_i = \sum_{\alpha=1}^{\infty} B_\alpha G_\alpha , \tag{34}$$

the B_α being defined by equation 34. A similar equation holds for equation 28b. The advantage of using the G_k is that the series can be terminated at any term N giving

$$\phi_i^N = \sum_{\alpha=1}^{N} B_\alpha G_\alpha . \tag{35}$$

The B_α are calculated by using the orthogonal properties of the G_k. One has, from equation 35,

$$(G_\alpha, \phi_i^N) = (G_\alpha, \sum_{k=1}^{N} B_k G_k),$$

or

$$(G_\alpha, \phi_i^N) = B_\alpha, \tag{36}$$

using equation 32. Using equation 31,

$$B_\alpha = (\sum_{\beta=1}^{N} \Gamma_\beta^\alpha F_\beta, \phi_i^N). \tag{37}$$

Now from equations 31 and 35

$$\begin{aligned} \phi_i^N &= \sum_{k=1}^{N} B_k \sum_{\ell=1}^{k} \Gamma_\ell^k F_\ell \\ &= \sum_{\ell=1}^{N} \sum_{k=1}^{N} B_k \Gamma_\ell^k F_\ell. \end{aligned} \tag{38}$$

By analogy with equation 28a, this implies

$$A_\nu = \sum_{k=1}^{N} \Gamma_\nu^k B_k. \tag{39}$$

The Γ_ℓ^k are calculated[98] by the Schmidt procedure. First,

$$\begin{aligned} \gamma_k^k &= 1 \\ \gamma_\ell^k &= -\sum_{\beta=\ell}^{k-1} \sum_{\alpha=1}^{\beta} \Gamma_\alpha^{\beta *} (F_\alpha, F_k) \Gamma_\ell^\beta \qquad \ell \neq k. \end{aligned} \tag{40}$$

When the unnormalized quantities γ_ℓ^k have been computed for

all $\ell \leq \kappa$, the normalization factor

$$N_\kappa = \sum_{\mu=1}^{\kappa} \sum_{\nu=1}^{\kappa} \gamma_\mu^{\kappa *} (F_\mu, F_\nu) \gamma_\nu^{\kappa} \tag{41}$$

is computed. Dividing, one obtains

$$\Gamma_\ell^\kappa = \gamma_\ell^\kappa / \sqrt{N_\kappa} . \tag{42}$$

These are the equations necessary for the calculation of the intensities. One computes the scalar products (F_i, F_j), uses them in equations 40, 41, and 42 to obtain the Γ_ℓ^κ, calculates the B_α from equation 37, and finally the A_ν from equation 39.

There are two other relations to be established which are useful in checking the results. The first is the energy balance. Noting that the energy in the incoming beam is unity according to equation 22 while that in the outgoing beams is $|A_\nu|^2$ for each real order, we have, using the proper aspect angle for each order and canceling equal factors,

$$\cos \theta_i = \sum_\nu \cos \theta_\nu |A_\nu|^2 , \tag{43}$$

where the summation is over all values of θ_ν for which the cosine is real. Also, the mean square error in matching the boundary conditions can be calculated. It is expressed as

$$|\Delta|^2 = \frac{1}{d}\int_0^d |\bar{\phi}_i[x,\varphi(x)] - \phi_i^N[x,\varphi(x)]|^2\, dx.$$

Using equation 33

$$|\Delta|^2 = (\bar{\phi}_i - \phi_i^N,\ \bar{\phi}_i - \phi_i^N)$$

$$= \frac{1}{d}\int_0^d (\bar{\phi}_i^* - \phi_i^{N*})(\bar{\phi}_i - \phi_i^N)\, dx$$

$$= \frac{1}{d}\int_0^d \bar{\phi}_i^*\bar{\phi}_i - \phi_i^{N*}\bar{\phi}_i - \bar{\phi}_i^*\phi_i^N + \phi_i^{N*}\phi_i^N\, dx.$$

Using equation 35

$$|\Delta|^2 = (\bar{\phi}_i, \bar{\phi}_i) - \sum_{k=1}^{N} \frac{1}{d}\int_0^d \bar{\phi}_i B_k^* G_k^* + \bar{\phi}_i^* B_k G_k - B_k^* G_k^* B_k G_k\, dx$$

$$= (\bar{\phi}_i, \bar{\phi}_i) - \sum_{k=1}^{N} B_k^*(G_k, \bar{\phi}_i) + B_k(\bar{\phi}_i, G_k) - B_k^* B_k$$

$$= (\bar{\phi}_i, \bar{\phi}_i) - \sum_{k=1}^{N} B_k^* B_k + B_k B_k^* - B_k^* B_k$$

$$= 1 - \sum_{k=1}^{N} |B_k|^2. \qquad (44)$$

The problem was programed on the Burroughs 220 digital computer. The program was written for a grating with triangular grooves in a Littrow mounting, but, by adding new

subroutines, it can be adapted to any mounting and any groove shape for which the scalar product can be programed. The input consists of the grating parameters d, c, and c', the wavelength, the order in which the grating is to be used, and the number of terms (up to 10) to be included in the series. The output includes the cosine of the grating angle for each order together with the real and imaginary parts of the A_ν. At the option of the operator the expressions for equations 43 and 44 are also computed. Each individual calculation takes about six minutes. The program is described in more detail in Appendix II.

Calculations were performed for various wavelengths in the first and second orders of the echelle grating and are presented in figure 37. The values from the computer output were multiplied by the reciprocal of the right side of equation 43 to correct for any error in energy balance, and were divided by the average of all wavelengths to express them on the same basis as the other results.

DISCUSSION

The experiment which measured the resolution of a spectrometer in which the grating is used is the most straightforward, and is therefore the most easily interpreted. When one considers the result of Martin it is

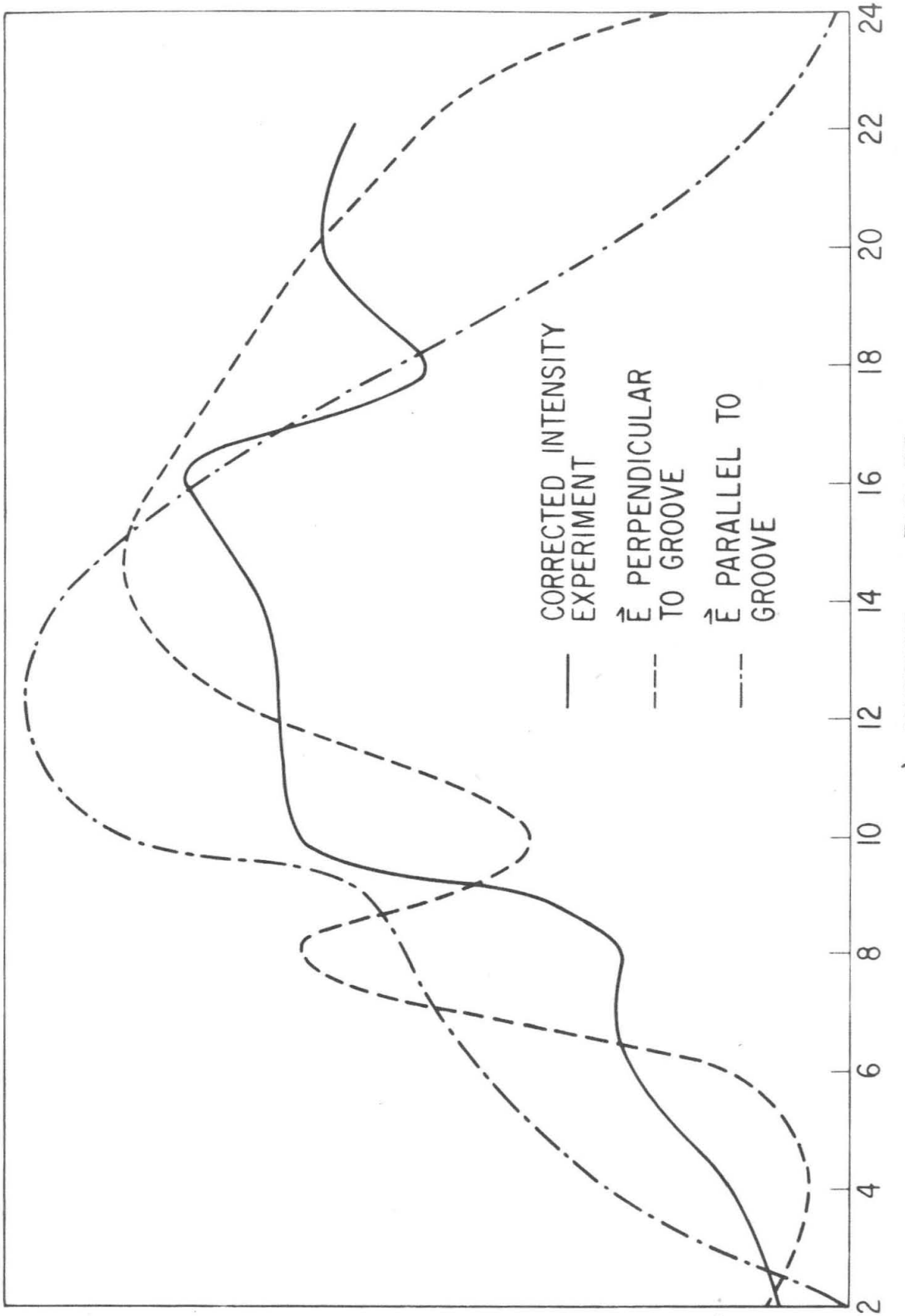
CORRECTED INTENSITY
EXPERIMENT
$\vec{E}$ PERPENDICULAR
TO GROOVE
$\vec{E}$ PARALLEL TO
GROOVE
2
4
6
8
10
12
14
16
18
20
22
24
λ MICRONS

FIG. 37

quite clear from figure 32 that the efficiency of the grating must be quite constant over a wide range of grating angle. Martin, it will be remembered, showed that, if the Rayleigh-Jeans law is obeyed, a grating of constant efficiency will show constant wavenumber resolution when used with movable entrance and exit slits. The comparison made in figure 32 between the vacuum spectrometer using the echelle-type grating and the Beckman IR7 spectrometer using an echelette grating shows quite clearly the advantages of the former grating. Not only does one have the mechanical advantage of being able to make a long scan without changing grating orders, but also, during this long scan, the resolution of the instrument is much more constant. This is a real advantage in a research instrument where the interpretation of the spectra depends on the resolution.

While the data in figure 32 are perhaps the most interesting from a practical standpoint, they constitute a description of an entire spectrometer and not of a grating alone. One can learn much more about the behavior of the grating itself from the data in figure 31. Three sets of data are presented here--the data from the first experiment labeled"averaged orders experiment", the data from the second experiment labeled "corrected intensity experiment", and the data from the Kirchhoff calculation. While there

are large individual discrepancies, the general form of each curve is the same. The efficiency is low at the short wavelength limit, but rapidly increases to reach a broad maximum beginning at about 8-10 microns. A minimum is reached at 16-18 microns which is followed by a second peak at 20-22 microns. This is followed by a decline in efficiency which extends to the long wavelength limit of the grating at 25 microns (beyond the range shown in figure 31).

If one remembers that the resolution of a spectrometer is inversely proportional to the efficiency of the grating, the same general pattern can also be seen in figure 32. An additional feature here--the loss in efficiency at eight microns--is explained by absorption due to atmospheric water.

The general features pointed out in figure 31 are most easily understood in terms of the Kirchhoff analysis. Between 2 and 14 microns the portion of the grating groove which is not involved in double reflection lies on the long side of the groove. There is no contribution to the efficiency from this portion because of the large angle which it makes with the radiation diffracted toward the collimator. The portion of the grating groove which is lost as a result of single reflection decreases with increasing wavelength and finally vanishes at 14 microns. This explains the monotonic (increasing) efficiency curve in the Kirchhoff results

and also the broad maximum in the experimental results. Beginning at 14 microns the portion of the groove involved in single reflection is on the short side of the groove and is in a favorable angular position to contribute to the diffracted intensity. Between 14 and 16 microns, however, its contribution is too small to be noticeable and the efficiency curve is still dominated by the contribution of the portion of the groove involved in double reflection, which is now decreasing. At 16 microns, single reflection becomes dominant, and the grating now behaves as a conventional echelette, approaching a maximum and then declining. The maximum is displaced slightly from its expected position due to interference effects between the singly and doubly reflected light. This latter effect appears in the calculations as a contribution of the last term in equation 19b.

Some explanations for the individual variations in the results presented in figure 31 can be advanced. The value for the efficiency obtained from the corrected intensity experiment is likely to be low at the short wavelength end of the curve. This is due to the scattering of light from the surface of the potassium bromide prism and windows. This scattering was not considered in making the corrections. A Wood anomaly at eight microns may well explain the peak here in the averaged order experiment which is not observed

in the other sets of data. This peak results from a single observation made at the grating angle where the third order grazes the surface of the grating. This is the necessary condition for the appearance of a Wood anomaly. It was not possible to obtain data on either the reflectivity of aluminum or the emissivity of a globar beyond 14 microns. For this reason, the data from the corrected intensity experiment are in some question in this region. Finally, it must be remembered that the averaged orders experiment is expected to be less reliable at the long wavelength limit because of fewer orders over which to average. This accounts for the lack of detail in the results from this experiment beyond 16 microns.

The data presented in figure 31 represent the performance of the grating in a Littrow mounting in a spectrometer. Figure 33 presents the same data used for the plot of the corrected intensity data in figure 31, but divided by the cosine of the grating angle. These data thus represent the reflectivity of the grating, i.e., the performance of an infinite grating in a finite beam of light. The interesting feature here is the extremely large increase in efficiency at long wavelengths. This increase is necessary to compensate the decrease in efficiency of the Littrow-mounted grating due to the cosine of the grating angle. For com-

parison, the calculated efficiency of an echelette grating blazed at the same angle is also presented. The difference between the two gratings is the shoulder extending from 8-16 microns in the echelle. It is this shoulder that is responsible for the constant resolution seen in figure 32.

The data in figure 33 are plotted at shorter wavelength intervals resulting in a plot with higher "resolution". One can see here several Wood anomalies. These occur at the Rayleigh wavelengths where a grating order just grazes the surface of the grating. Wood anomalies are of some interest in grating theory, because only the more sophisticated theories are able to account for them. They are of even more practical interest because of their appearance in the spectra produced by some grating instruments.

The data from the Rayleigh theory calculations are presented in figure 37 together with the results of the corrected intensity experiment for comparison. The striking feature here is the relation of the experimental data to the calculated efficiencies for the two polarizations. It is at once clear that the efficiency for unpolarized light is not the average of the efficiencies for the two polarized components. From 2-18 microns the experimental curve more closely resembles the curve calculated for the electric vector polarized parallel to the grooves, while beyond 22

microns the experimental curve follows the curve calculated for the electric vector polarized perpendicular to the grating grooves. It should be noticed that, as a result of dividing each set of data by its average, the vertical scales of individual sets of data may not be the same.

It is significant that the point at which the experimental data crosses over from the parallel polarization curve to the perpendicular polarization curve is also the point at which the dominant contribution to the diffracted beam changes from doubly-reflected to singly-reflected light. The explanation is that double reflection tends to polarize the light parallel to the groove while single reflection tends to polarize the light perpendicular to the groove.

The above remark regarding the effect of double reflection on the resulting polarization is made on the basis of a comparison between experiment and theory, and is not supported by experimental work done on the echelle thus far. There are data on echelette gratings, however, that do lend it support. Table VI presents data from the report by Peters, Deibel, Pursley, and Zipf in which an echelette grating is studied in the microwave region. The data show

TABLE VI--POLARIZATION DATA ON ECHELETTE GRATING[97]

Grating spacing wavelength	PERCENT EFFICIENCY					
	PARALLEL POLARIZATION			PERPENDICULAR POLARIZATION		
	ORDER			ORDER		
	0	1	2	0	1	2
0.70	92	8	-	99	1	-
0.94	60	40	-	97	3	-
1.20	60	40	-	100	-	-
1.75	5	85	10	7	53	40

essentially the same polarization behavior as is observed here. Figure 38 shows a tracing taken by a Beckman IR7 spectrometer with a polarizer in one of the double beams. The two curves represent the parallel and perpendicular polarizations. It can be seen that the perpendicular polarization is stronger in the blaze, near 600 cm.$^{-1}$ while the parallel polarization becomes more strong in the Wood anomaly at 1100 cm.$^{-1}$. This again is similar to the results in figure 37.

CONCLUSION

It has been shown that a grating carefully ruled with both sides of the grooves flat and at right angles to each other, used in a Littrow mounting, will show an extremely wide blaze region. Indeed, it can be thought of as nearly constant in its efficiency throughout the range of angles in which the entire groove is illuminated. Such a grating, when used in a practical spectrometer, gives nearly constant wavelength resolution through a wide wavelength range. This wide wavelength range is scanned in a single order, making it unnecessary to change orders or to change gratings during the scan.

Three experiments have been performed to determine the

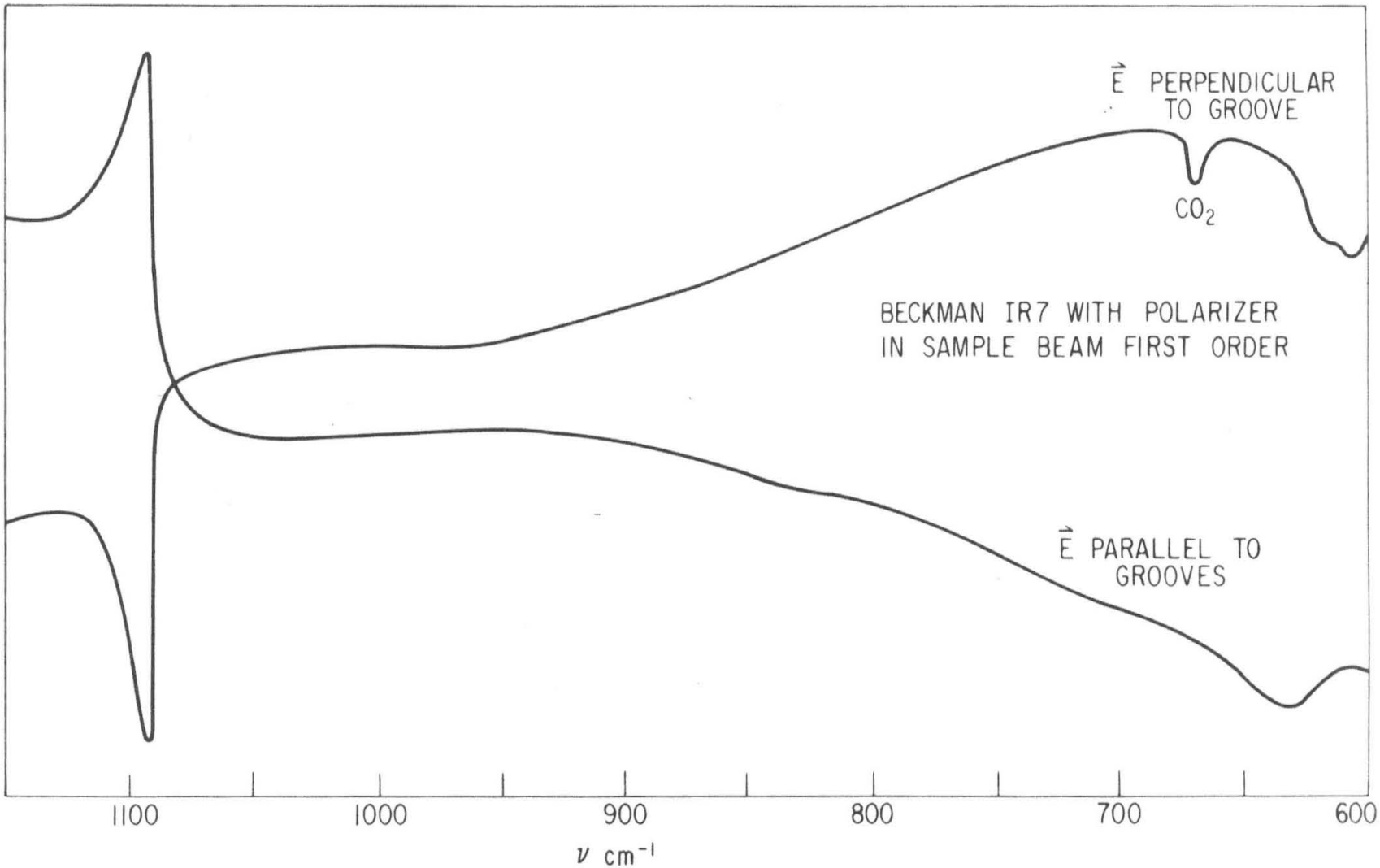

POLARIZATION IN BECKMAN IR7 COURTESY
R S McDONALD GE RESEARCH LABORATORY

FIG. 38

efficiency of such a grating. In the first, the corrections to the observed intensity were eliminated by an averaging process. In the second, these corrections were evaluated. In the third, the resolution performance of the spectrometer itself was observed. The three experiments agree that there is a wide range of reasonably constant efficiency.

Calculations based on two different theoretical treatments have been made. The first treatment is based on the Kirchhoff formulation of the Fresnel-Huygens diffraction theory. It is in general agreement with the experiments, but cannot predict all details. The second is based on Rayleigh's dynamic theory of the grating. The results of this calculation imply that quite strong polarization exists in most parts of the spectrum and that this polarization changes over the range of grating angles.

SECTION IV

AN INFRARED DETECTION SYSTEM

INTRODUCTION

Since the infrared spectroscopist does not enjoy the advantages of photography in recording his spectra, it is natural that he should be more conscious of electrical detection systems than those spectroscopists who specialize in the visible or ultraviolet regions. From the time the first galvanometer was attached to a thermocouple to the present day, one of the main parts of the infrared spectroscopist's endeavors has been to improve the detection system. Lately, with the rise of spectrophotometry, the visible and ultraviolet spectroscopists have also joined in this endeavor.

It is the purpose of this section to describe an amplifier which is the key component of a new infrared detection system. The term "detection system" will refer here to the entire system including the detector, amplifier, recorder, and any associated components. This system combines desirable features found only in several different systems at present. It is designed to use photoconductive detectors, but could be adapted to any detector with the appropriate time constant. The discussion will begin with

a description of several existing systems. It is believed that this set of existing systems is complete from the standpoint of different physical principles involved, but no attempt has been made to cover all possible variations of these. For a more complete discussion, the review of Williams[99] may be consulted. The discussion is intended to show the position of the new system in the spectrum of all possible systems, and to point out its advantages over existing systems.

EXISTING SYSTEMS

The simplest detection system consists of a transducer attached to a galvanometer with an optical lever for determining the swing. It is assumed throughout the discussion that the transducer produces a voltage which is, to a good approximation, proportional to the intensity of the light falling on it. This is true of the thermocouple, Golay cell, and photovoltaic detector. In the case of the bolometer or photoconductor, the voltage is produced across a load resistor or bridge circuit as the result of the change of resistance in the detector as the light falls upon it. The effect for the purposes of the detection system is essentially the same.

The galvanometer system shows several important defects. One is the long time constant of the system. Because of the low amount of energy available to the system from the transducer, very delicate galvanometers must be employed. These take a long time to reach their new rest point when a change in current is applied to their coils. Another drawback is the tendency of the system to drift. Changes in source intensity, monochromator characteristics, transducer characteristics, or galvanometer mounting all contribute drifts which cannot be separated from the observed data. A more important source of drift in this type of system lies in the thermocouple. In order to achieve high sensitivity, it is common to make the two junctions unsymmetrical. The sensitive junction is made with very low heat capacity, while the cold junction has high heat capacity. Consequently, if the temperature of the surroundings changes, the two junctions will be affected at unequal rates and drifts will result.

Although the drift drawback is still present, the next system to be discussed represents a significant advance. By inserting a DC amplifier between the transducer and the galvanometer, sufficient energy is now made available to operate any indicating or recording device. The amplifier will likely be a chopper-stabilized amplifier. Such ampli-

fiers possess greater stability which is important here in the elimination of drift. What distinguishes this system from the AC systems described below is the DC output of the transducer.

It can be shown that the DC system is considerably more sensitive than the AC system to be described below. There are times when the advantages of this extra sensitivity will outweigh the disadvantages of the system's inherent drift. For example, when an experiment is severely energy-limited, one may be content to obtain the best spectrum possible under the circumstances, and will accept a certain amount of drift in the background. At other times, however, the drift makes the work impossible. In a study such as the one in Section II on N-methyl formamide, it was necessary to scan the background of the region of interest and then scan the same region with the vapor in the light path. Any change in detector system characteristics would be reflected as a change in intensity or shape of the particular band envelope under consideration.

The answer to such a problem is to change to an AC detection system. In such a system, some portion of the detection system is made sensitive to only one particular frequency. Any signal falling on the detector can be resolved into a set of Fourier components of various frequen-

cies. The detection system then selects only the component, or the small group near the given frequency, to which the system is sensitive. If the light beam is modulated in such a manner that the strongest Fourier component will be that to which the detection system is sensitive, the output of the detection system will be the information contained in the intensity of the beam.

In considering the drift performance of such a system, consider a thermocouple. The same argument will apply to other detectors with appropriate changes. For a given intensity falling on the thermocouple, the junction will be at a given temperature. When the beam is chopped, the intensity falling on the detector will, in general, vary between two temperatures. These two temperatures will correspond to two particular voltages across the thermocouple. If the sensitivity of the thermocouple changes, the absolute values of these voltages will change, but, if the sensitivity is linear and the intensity falling on the hot junction has not changed, the difference between the two voltages will not change. It is this difference to which the detector system is sensitive.

The usual application of such a system modulates the beam by chopping it mechanically. The beam is then passed through the monochrometer and sample to the detector.

Upon detection, the information included in the spectrum of the sample plus the background of the optical system is recorded.

A somewhat different application was used by Dickey and Hoffman.[100] They wished to study the absorption due to the OH radical which was obscured by absorption due to water in the region of interest. They modulated the concentration of OH by observing it in a flame whose fuel supply was varied by a rotating gas valve. The modulated concentration resulted in a modulated intensity of the OH spectrum. The water concentration in the flame did not vary, and this allowed them to "look through" the water vapor absorption at the OH radical.

There are various means of making the detection system sensitive to only the modulation frequency. These can be classified as synchronous and nonsynchronous rectifiers. A synchronous rectifier is a switch which is opened and closed in synchronization with the modulation of the beam. In the simplest mechanical system the beam is modulated by a rotating chopper with teeth cut into it which alternately stop and pass the beam. Attached to the shaft of the chopper is a set of switches which are placed in the output circuit of the amplifier where they accomplish either full-wave or half-wave rectification of the alternating output voltage

which is proportional to the light falling on the transducer.

A slightly more complicated system is used in the amplifier supplied with the Golay detector. Here a photocell and lamp are placed so that the lamp beam is chopped at the same rate as the spectrometer beam. The voltage from the photocell is used to open and close an electronic switch with the same effect as before.

Either of the two synchronous rectifier systems passes a portion of the white noise spectrum which is assumed to exist in the beam. The bandwidth of noise passed is the reciprocal of the time constant of the detection system. Thus, the noise is that portion of the noise spectrum from $\omega = 0$ to $\omega = 1/\tau$ where τ is the time constant of the output filter. In general, this time constant is determined by a RC filter in the output circuit.

The nonsynchronous rectifier is simply a diode tube which rectifies the alternating voltage from the detector. To make it sensitive to the modulation frequency, a tuned filter is inserted in the amplifier before the rectifier. If it were possible to make the bandwidth of the tuned filter zero, only the portion of the noise spectrum with exactly the same frequency as the desired signal would be passed by the amplifier. For two reasons, this is impossible

practically. First, a bandwidth of zero would imply an infinite time constant. Second, and more important, the filter must be able to pass any excursions of the modulation frequency. It is easy to see the effect of such a system operating on the sharp slope of the bandpass characteristic. Any small change of modulation frequency would be presented to the output as a large change in apparent signal intensity.

Since the filter must have finite width, a considerable bandwidth of noise will be passed. This means that any frequency component of noise in the bandwidth will have a considerable side-band present which will result in the presence of low frequency components in the output. These low frequency components will be slightly larger than in the case of the synchronous rectifier system. This is because only the portion of the noise spectrum which is in phase with the signal is passed by a synchronous rectifier, while in this system the full range of phases is presented to the output. As before, the frequency range of noise passed is $0 \leq \omega \leq \frac{1}{\tau}$ but, in addition there is a constant component added to the background representing the noise at the modulation frequency.

The systems described above are all single-beam systems. They provide no means of allowing for drift in the components

which produce this single beam. For example, the monochromator can change its characteristics with temperature, the source can change in intensity over a period of time, atmospheric absorption can change, or the slope of the detector sensitivity curve can change. To make allowance for these changes, one must employ a double-beam system. The second beam is used to monitor the intensity of the source. The double-beam system has the advantage that the reference beam can also be used to keep track of additional information as well as the apparent intensity of the source. It would have been convenient, for example, to make the temperature effect studies described in Section II by placing identical samples of vapor in the two beams of a double-beam system. One sample would be at the lower temperature and one at the higher temperature. The system would measure the difference between the two beams and thus the difference between the intensity of light passing through the vapor at the two temperatures.

There are various means available for determining the difference between the two beams. The first is a hybrid between a single-beam system and a double-beam system. One makes a single-beam scan of the background and records the results on magnetic tape. Then one introduces the sample and repeats the scan, this time using the tape recording of

the previous scan to correct the results for variations in the background as a function of wavelength. This system has the disadvantage that it cannot compensate for changes in the system with time.

A second approach uses two complete beams. Light from the monochromator is split into two beams, either by a static beam splitter,[101,102] by rotating mirrors,[103] or by vibrating mirrors.[104] One beam is used for the reference information and one for the sample information. Two complete systems are commonly used--separate optics, separate detectors, and separate amplifiers. The system requires either exactly matched components in the two beams, which is impossible in practice, or some means of compensating for differences which will exist. Typical compensating methods are the loaded potentiometers of the Applied Physics Model 14 Spectrophotometer or the graphic recording method of Cook and Smith.[105] The important feature of a compensating method is that it must be convenient, as it will be necessary to apply it often. Even then one cannot be certain that new changes have not crept into the system since the last compensating run was made.

A third approach splits the two beams with a rotating mirror, but recombines them later with a second rotating mirror. The information in the two beams is thus separated

in phase. A synchronous rectifier allows the amplifier to separate this information and obtain a signal proportional to the difference in intensity between the two beams. This signal is used to drive a servo motor which controls an attenuator in the reference beam. The system operates to adjust the intensity in the reference beam with the aid of the attenuator until it is equal to that in the sample beam. The recorder pen is also driven by the same servo and thus gives a record of the intensity in the sample beam divided by the intensity in the reference beam. The noise passed by the system is determined by the time constant of the loop. It is this system that is commonly used in commercial spectrometers in the infrared. This system has the disadvantage that varying amounts of energy fall on the detector depending on the intensity of the sample beam. This results in a varying response for the system. In addition, it is difficult to build a perfectly linear attenuator. The defects in the attenuator may be difficult to separate from features in the spectrum.

A fourth double-beam system splits and recombines the two beams as before, but does not attenuate either beam. The information in each beam is separated by some means in the amplifier. This information is used to compute the ratio between the intensities of the two beams, which is presented

as output. Such a system allows greater flexibility in designing the optical system. For example, Ahlers and Freedman[106] were interested in differences of absorption between two samples of liquid. These were placed in cells which could be placed on the chopper blade. Upon rotation, the two samples were alternately placed in the beam. A system of switches was used to allow the amplifier to decode the information in the beam. The ratio was finally computed and presented as output on a recorder.

The two beams can be distinguished by making use either of their difference in frequency[107] or their difference in phase.[108,109] If they are to be distinguished by their frequency difference, the beams are separated by a static mirror or beam splitter and each is chopped at a different frequency. Their information is separated in the amplifier by tuned filters. In the phase-difference system, the two beams are presented to the detector, usually by rotating or vibrating mirrors, at different portions of the same cycle. The usual means of separating the information at the output of the amplifier is by mechanical switches operating as a synchronous rectifier.

Various means of computing the ratio after the information is decoded are used. When a photomultiplier detector or some other detector whose response can be varied elec-

trically is used,[102,104] or where it is possible to vary the intensity coming from the monochromator,[103] the information in the reference beam can be used to maintain the energy input to the amplifier constant in the absence of a sample. Hariharan and Bhalla[110] have described the use of a logarithmic amplifier in which the two signals are subtracted from each other at the output, thus giving the logarithm of the ratio of the two signals. The most widely used method is to apply the reference information to the slidewire of a potentiometer recorder. The sample information is applied to the movable contact through the recorder amplifier and the recorder records the ratio of the two signals.

The ratio system has the advantage of compensating for drifts in all components common to the two beams. If care is used in keeping the two beams identical, except for the sample, only the desired signal plus some random noise should appear at the output. Noise components arising in components common to the two beams which are coherent over the period of beam alternation will be removed by the system. A large portion of the remaining noise will be removed by the output filter.

The question of synchronous or asynchronous rectification arises in the double-beam ratio system just as in

the case of the single-beam system. Neither system of rectification is phase sensitive in the sense that the expression is applied to microwave spectroscopy. The optical equivalent of this would be an interferometer. The question here seems to be between taking the ratio of noise observed over a short portion of a cycle in the case of the synchronous rectifier, or over the entire cycle in the case of the asynchronous rectifier. There seems, then, to be little difference between the two rectifiers in a practical sense. Any small advantage of the synchronous rectifier in noise is outweighed by the added complications of mechanical switches or phasing signals.

The various approaches to an infrared detection system have been described. Of these, only the single-beam AC system, the double-beam optical null system, and the double-beam ratio system find widespread use at present. The selection of a detection system to be used should be made on the basis of its intended use. The uses to which the system will be put fall into two categories. First, there is routine analytical work. Either the absorption of a sample or the ratio of intensity of light passing through two samples is to be determined. The requirements are quite routine and standard. The worker using this type of equipment will not be patient with complicated systems which are

designed for a flexibility for which he has no use. The double-beam null system is probably the most straightforward for this application. If the effects of the changing intensity in the system and the characteristics of the attenuator used are understood, this system is quite satisfactory.

The research spectroscopist's requirements are another matter. The greatest requirement here is one of flexibility. A detection system is needed which can readily be adapted from one experiment to another. The most flexible system is probably a single-beam AC system. If the disadvantages of source drift and difficulty in adapting to modulation techniques can be tolerated, there is little reason to change to another system. When, however, the system stability begins to limit the experiment, or the only way of performing an experiment is to use modulation techniques, it is necessary to contemplate some more complicated system. It seems that such a system will be some form of double-beam ratio system.

The system described here, it is hoped, will allow the use of these more sophisticated techniques, and at the same time retain as much flexibility as is possible. The system is designed around an amplifier which has been built and tested with a mock-up of the system, but not with a

spectrometer. The double-beam ratio system is used with the two beams separated by 180° in phase at a frequency of 90 cps. The system drift is compensated by chopping both beams at 420 cps. and using the information from these two frequencies to obtain the ratio at the output. The frequencies are separated by LC tuned circuits in a regenerative amplifier. If the double-beam system is not necessary in a particular experiment, either of the two frequency channels can be used separately as a single-beam system.

The mock-up used to test the amplifier (figure 39) used a rotating mirror to alternate the two beams, but this can be changed. Any optical system can be used which presents alternately the reference signal and the sample signal at 90 cps. and chops both in phase with each other at 420 cps. To eliminate cross talk between the two channels, it is required that the 420 cps. and 90 cps. signals be properly phased. The requirement is that the abrupt change in intensity as the beams are switched must not be seen by the detector. This requirement is easily met if synchronous motors are used.

AMPLIFIER

The circuit of the amplifier is presented in figure 40.

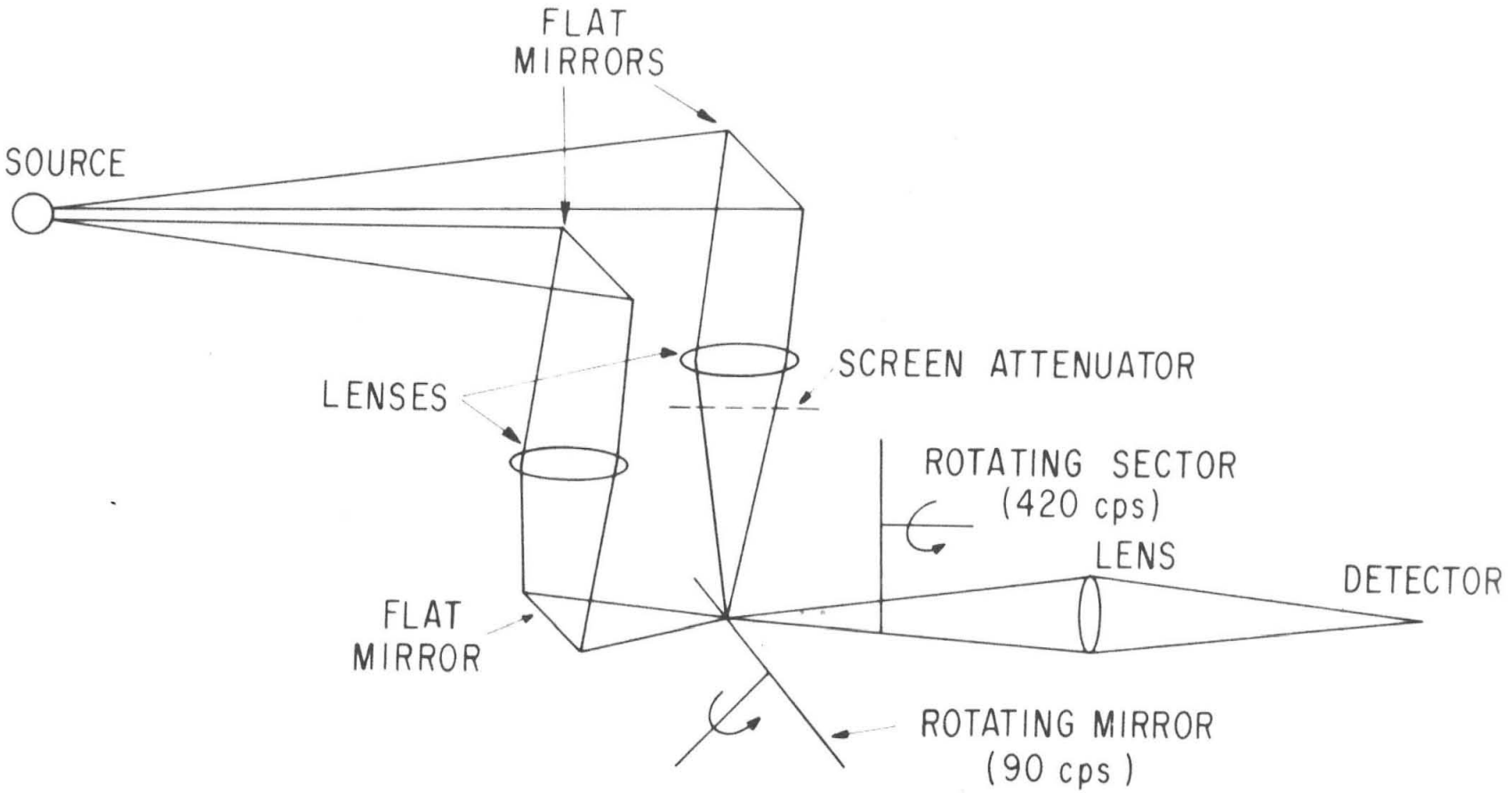

FIG. 39

DETECTION SYSTEM MOCK-UP

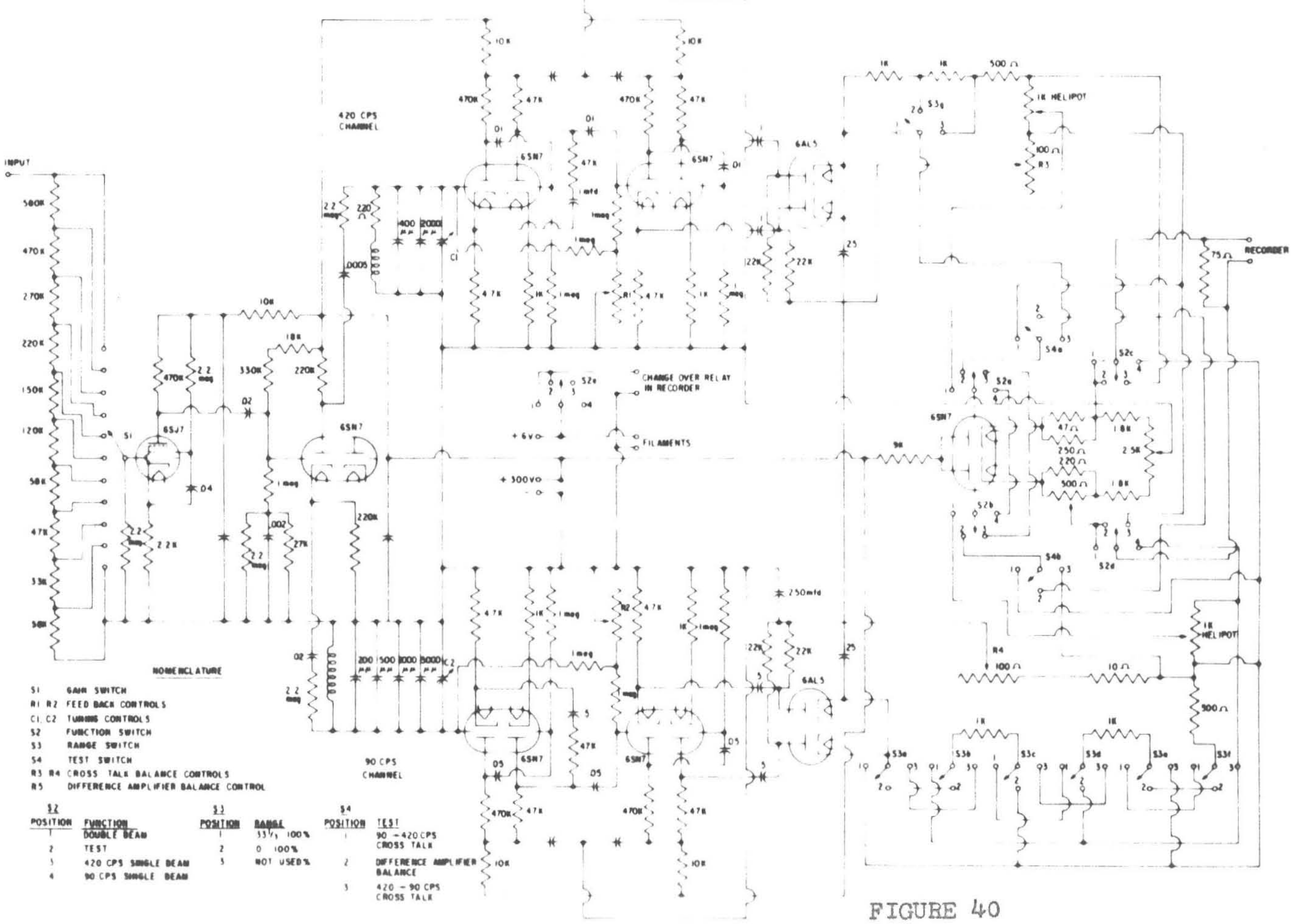
INPUT
RECORDER
420 CPS CHANNEL
90 CPS CHANNEL
CHANGE OVER RELAY IN RECORDER
FILAMENTS
+ 6V
+ 300V
1K HELIPOT
NOMENCLATURE
S1 GAIN SWITCH
R1 R2 FEED BACK CONTROLS
C1, C2 TUNING CONTROLS
S2 FUNCTION SWITCH
S3 RANGE SWITCH
S4 TEST SWITCH
R3 R4 CROSS TALK BALANCE CONTROLS
R5 DIFFERENCE AMPLIFIER BALANCE CONTROL
S2 POSITION FUNCTION
1 DOUBLE BEAM
2 TEST
3 420 CPS SINGLE BEAM
4 90 CPS SINGLE BEAM
S3 POSITION RANGE
1 33 1/3 100%
2 0 100%
3 NOT USED%
S4 POSITION TEST
1 90 - 420 CPS CROSS TALK
2 DIFFERENCE AMPLIFIER BALANCE
3 420 - 90 CPS CROSS TALK

FIGURE 40

It is taken from a design of a single-beam amplifier by Wilson[111] which was built and operated successfully in this laboratory previously. The input from a preamplifier is applied to the 6SJ7 tube through a stepped gain control, S1. The output of the 6SJ7 tube is applied to one side of a 6SN7 tube wired as a phase inverter. The plate signal from the phase inverter is the input to the 420 cps. channel, while the cathode signal is the input to the 90 cps. channel. Each channel is identical except for necessary changes in coupling condensers and tuning components for the two frequencies.

The first two stages in each individual channel provide the selectivity. They are isolated from the gain control by the 6SJ7 tube and the 6SN7 phase inverter. No evidence of interaction between channels due to varying the band width in one channel was noted. A tuned LC circuit is placed in the grid of the first section of the 6SN7. The two sections of this tube are connected in cascade with negative feedback from the plate of the second section to the cathode of the first, and with positive feedback from the plate of the second section to the grid of the first. The positive feedback can be controlled with R1 or R2 to vary the negative resistance presented to the LC circuit by the tube. This varies the Q of the circuit and thus the

selectivity. It is possible to present a high enough negative resistance to the LC circuit to send the circuit into oscillation. The sharpest tuning is reached just before this point, and it is here that it was found best to operate with the ratio system. This point seems quite stable. No trouble was noted with the circuit going into spontaneous oscillation when properly adjusted. The gain of the channel depends on the setting of the feedback control, but this stays fixed when using the amplifier in the ratio mode.

One of the condensers in the LC circuit (C1 or C2) is variable. This is used to tune the circuit to exactly the frequency of the signal which is determined by the frequency of the chopper or rotating mirror. Since these usually operate from synchronous motors, the system must be used on a power supply of quite constant frequency. A small variation in chopping frequency is reflected as a large change in apparent signal strength in an asynchronous rectifier system such as this. For this reason the band width must be large enough to include any variation in chopping frequency. At the same time it must be small enough to reject all of the opposite frequency in this system. Using the cross talk compensating circuit described below, it was found possible to meet these two conditions.

The next 6SN7 tube and the 6AL5 constitute a vacuum

tube voltmeter. Stability and linearity are improved by the negative feedback provided by returning the AC to the cathode of the first stage of the 6SN7. This results in a sharp saturation which tends to protect the computing and recording circuits in the event of overload. Wilson states that his circuit was linear from 0 to 1 ma. and saturated at 1.5 ma.

From the vacuum tube voltmeter circuits, the two channels are fed to a computer circuit which determines the intensity ratio. A simplified version of this circuit is shown in figure 41. The two signals are subtracted across a voltage divider, ABC. The two 500 ohm potentiometers in the voltage divider are the two sections of a dual three-turn Helipot mounted on the frame of a Brown recorder. The shaft of the Helipot is driven by the pen drive of the recorder with the arms moving as indicated by the arrows. These arms are connected to the grids of a difference amplifier. The output of the difference amplifier is connected directly to the input of the amplifier of the recorder, eliminating the slidewire. The difference amplifier serves as an isolating and impedance-matching device. The system is connected so that the pen drive will run in the direction necessary to reduce the difference of potential between the potentiometer arms and will stop when this difference is

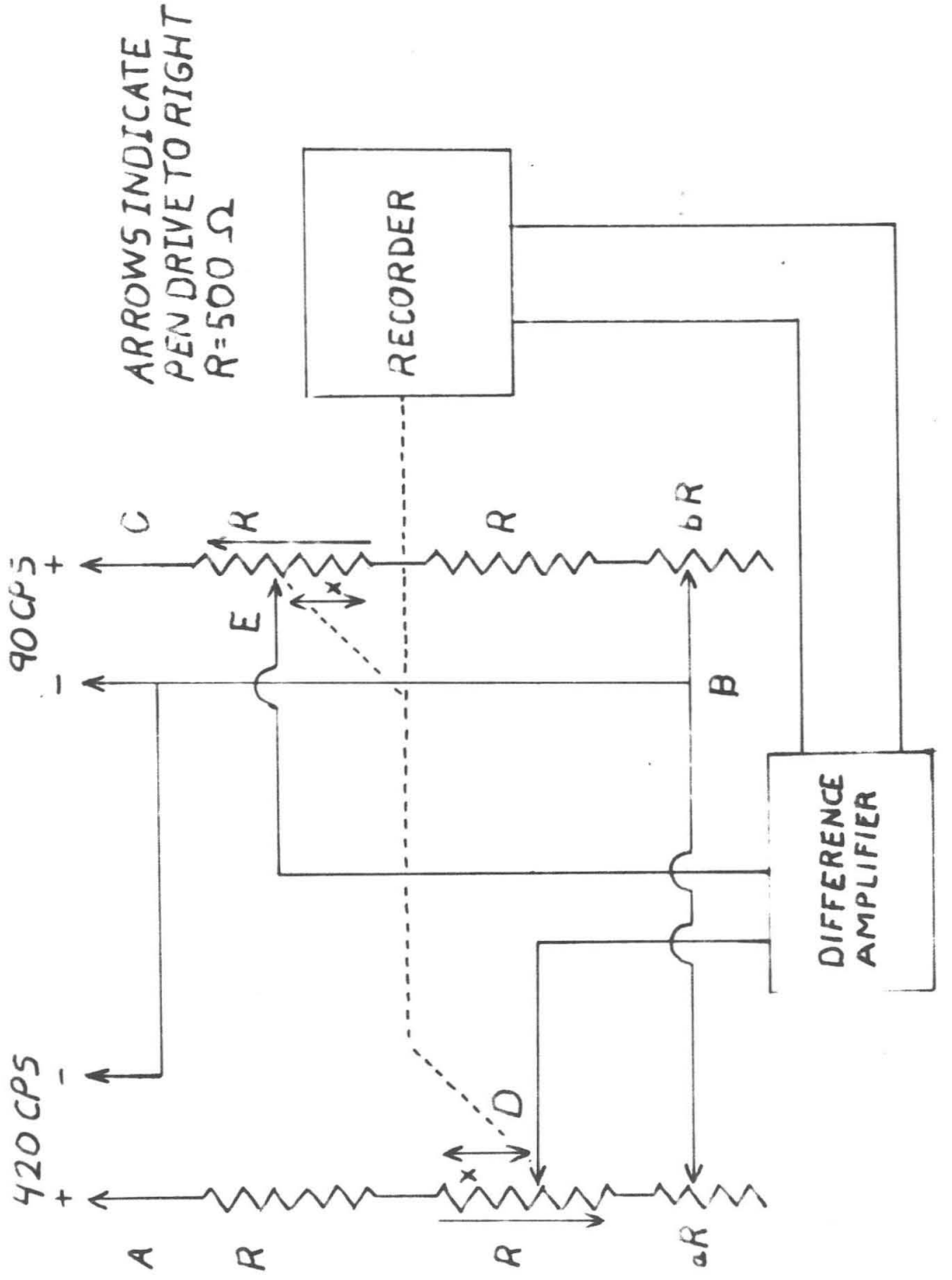
ARROWS INDICATE
PEN DRIVE TO RIGHT
R=500 Ω
RECORDER
90 CPS
420 CPS
C
A
E
D
B
R
R
R
R
bR
aR
DIFFERENCE
AMPLIFIER

FIGURE 41

zero.

The 90 cps. component of the input signal is proportional to the difference in intensity between the two beams. When each beam has the same intensity, this component will be zero and when one beam is completely missing (100% absorption) this component will be a maximum. The 420 cps. component of the signal is proportional to the sum of the intensities of the two beams, or, consequently, to the average intensity. Assume that the proportionality factors are the same for each component and let x represent the fraction of full scale at which the pen drive stops. For the time being assume a and b are zero. If I_o and I_s represent the standard and sample beam intensities, respectively, and R is the unit of resistance indicated in figure 41, we have, when the pen drive stops,

$$V_{DB} = V_{EB}$$

$$\frac{R(1-x)}{2R} V_{AB} = \frac{R(1+x)}{2R} V_{CB}$$

$$\frac{R(1-x)}{2R}(I_o+I_s) = \frac{R(1+x)}{2R}(I_o-I_s),$$

where V_{DB} is the difference in potential between D and B etc. Solving for X,

$$x = \frac{I_s}{I_o}.$$

Thus, in this somewhat simplified situation, it is seen that the pen of the recorder indicates the per cent trans-

mission.

Suppose the computer is arranged as shown in figure 42. Here, the relation at balance is

$$\frac{R(1-X)}{3R}(I_o+I_s)=\frac{R(2+X)}{3R}(I_o-I_s).$$

Solving for X we have

$$X=\frac{3}{2}\frac{I_s}{I_o}-\frac{1}{2}.$$

Now if we assume that $I_s/I_o=0.33$ corresponds to X=0 and $I_s/I_o=1.0$ corresponds to X=1 we again have $X=I_s/I_o$. The scale has simply been expanded and the lower third discarded. If the moveable tap is changed to the position indicated by the dotted lines in figure 42, a similar analysis yields $X=I_s/I_o$ for the full range.

Up to this point the possibility that the signals may not be completely separated by the tuned circuits has been neglected. Suppose that the 420 cps. component actually is proportional to $(I_o+I_s)+\beta(I_o-I_s)$ and the 90 cps. component to $\delta(I_o-I_s)+\alpha(I_o+I_s)$ where δ represents the ratio of gain in the 420 cps. channel to that in the 90 cps. channel. Let E=a+1 and D=b+1 where a and b are indicated in figure 41, and suppose that a and b are so small that $1/E \approx 1/D$. Now at balance

$$\frac{R}{R(E+1)}(E-X)[I_o+I_s+\beta(I_o-I_s)]=\frac{R\delta(D+X)}{R(D+1)}[I_o-I_s+\alpha(I_o+I_s)],$$

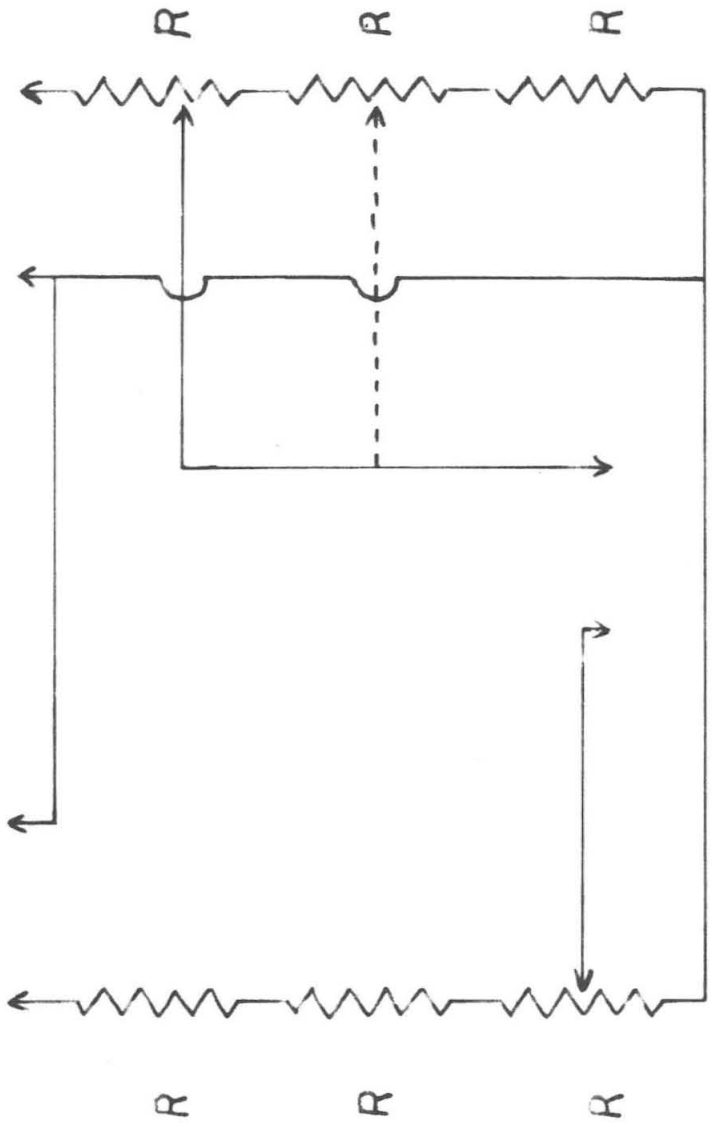

FIGURE 42

and

$$\chi=\frac{I_o[E(D+1)(\beta+1)-\delta D(E+1)(\alpha+1)]+I_s[E(D+1)(1-\beta)+\delta D(E+1)(1-\alpha)]}{I_o[(D+1)(\beta+1)+\delta(E+1)(\alpha+1)]+I_s[(D+1)(1-\beta)-\delta(E+1)(1-\alpha)]}.$$

Now, if

$$E(D+1)(\beta+1)-\delta D(E+1)(\alpha+1)=0$$

$$(D+1)(1-\beta)-\delta(E+1)(1-\alpha)=0 \qquad (45)$$

$$E(D+1)(1-\beta)+\delta D(E+1)(1-\alpha)=(D+1)(\beta+1)+\delta(E+1)(\alpha+1),$$

then

$$X=I_s/I_o$$

as before. Solving equation 45 for E, D, and δ, we have

$$E=\frac{1+\alpha}{1-\alpha}\simeq 1+2\alpha=1+a$$

$$D=\frac{1+\beta}{1-\beta}\simeq 1+2\beta=1+b$$

$$\delta=1.$$

We can see that, if the gain in the two channels is the same, and a and b are properly adjusted, the effect of cross talk between channels has been eliminated.

One particularly serious source of cross talk from the 90 cps. channel to the 420 cps. channel exists which can easily be eliminated. The fifth harmonic of 90 cps. is 450 cps. It is found that when it is strong, the fifth harmonic cannot be completely rejected by the 420 cps. tuned circuit. If the detector observes the abrupt change in in-

tensity as the two beams are switched, this harmonic is particularly strong. The motors, as pointed out above, are synchronous, and they can be phased so that this change occurs when the 420 cps. sector covers the detector. This was found to reduce cross talk by 60%.

Test circuitry is provided using position 2 of the function switch, S2, and the test switch, S4, to measure the amount of uncompensated cross talk between the two channels. The circuitry also allows the unbalance of the difference amplifier to be measured. Section E of S2 controls a relay on the recorder chassis which transfers the recorder input directly to the amplifier, bypassing the slidewire circuit in position 1 or 2. This is necessary to the operation of the ratio computer as stated above. In the case of the test circuit, this bypassing has the effect of making the recorder a much more sensitive indicator of an unbalance. The unbalance is indicated by any motion of the pen drive, while the balanced condition is indicated by a motionless pen drive.

In setting up the computer circuit, S2 is set to position 2 and S4 is in its normal center position. The difference amplifier is balanced with the aid of R5. A 90 cps. signal is then fed to the amplifier and S4 turned to position 1 while any cross talk to the 420 cps. channel

is compensated with R3. Next a 420 cps. signal is fed to the amplifier and, with S4 in position 3, cross talk to the 90 cps. channel is compensated with R4.

It should be noted that the 420 cps. component is a convenient source of a servo signal for a slit drive. It was with this in mind that provision was made for a DC input to the slit-drive servo described in Section I. This servo would maintain the average beam intensity constant and thus provide constant response in the detector system.

Operation as a single-beam instrument using either channel is provided by S2. In the single-beam mode, the relay on the recorder chassis restores the slidewire to the recorder circuit. The recorder input is taken from across either Helipot depending on the channel selected.

The high voltage supply for the amplifier is obtained from a commercially built power supply and is filtered again in the amplifier. It was found impossible to use AC on the heaters because of the seventh harmonic feeding into the 420 cps. channel. An Edison storage battery floating across a six volt DC supply worked quite satisfactorily as a heater supply.

Stability and linearity tests on the amplifier have been made in each of its three modes using the mock-up in figure 39. Calibrated wire screens were used for attenua-

tors. For the stability tests, the light was adjusted to give a reading near the middle of the recorder scale and the drift per hour was recorded. For the linearity tests the light was adjusted to give 100% transmission. A wire screen which gave a transmission of about 67% was placed in the sample beam. The recorder reading was recorded and the light in the sample beam adjusted with an attenuator to give this reading without the screen. The same screen was again introduced and another reading was taken. This procedure was repeated several times until the recorder reading had dropped to around 2% transmission. The percentage of light removed by the screen each time the screen was introduced was averaged. If the system is perfectly linear, the deviation of each reading from this average will be zero. Thus, regardless of the level of intensity in the beam, introducing the screen reduces the apparent intensity by the same factor. In an actual system, the deviation of each reading will show a non-zero value, and this value is taken as a measure of the nonlinearity of the system. It is reported as the percentage of the deviation from the absolute reading. The results of these tests are presented in Table VII. It can be seen that the system is linear in the higher ranges, but that the characteristic round-off of diode detectors occurs toward the bottom of the

TABLE VII--DRIFT AND LINEARITY

MODE	DRIFT PER HOUR (Times full scale)	LINEARITY[a] (%) 15-100%	10-100%	5-100%	2-100%[b]
DOUBLE BEAM	1.83×10^{-3}	1.79	2.51	3.79	4.90
SINGLE BEAM (90 cps.)	6.19×10^{-3}	1.19	1.46	3.66	3.36
SINGLE BEAM (420 cps.)	3.72×10^{-3}	2.17	1.73	2.80	4.09

notes
a. Average deviation of individual readings in linearity check over chart range shown.
b. Chart range.

scale.

CONCLUSION

A new detection system has been described. It combines the flexibility of an AC single-beam asynchronous rectifier system and the convenience of a double-beam ratio system. The amplifier which is the heart of the system has been completed and tested. It is found to work well and to show satisfactory linearity and stability characteristics.

APPENDIX I

BAND ENVELOPE CALCULATIONS

A great deal of trouble can be experienced in setting up a band envelope calculation such as the one described in Section II. It is with the hope that subsequent investigators may avoid this that the following summary of formulas used is included. The notation of Gerhard and Dennison and of Badger and Zumwalt is used as far as possible.

The initial parameters used are as follows:

Principal moments of inertia in gm. cm.^{2}

I_A	$a=1/I_A$
I_B	$b=1/I_B$
I_C	$c=1/I_C$

Badger-Zumwalt parameters

$$\rho = \frac{a-c}{b}$$

$$S = \frac{2b-a-c}{a-c}$$

Energy/kT for rotational level (J,K)

$$W = J(J+1)\sigma + K^2\beta$$

Note that this β is β/σ in Gerhard and Dennison.

$$\sigma' = \frac{h^2}{8\pi^2 kT} \cdot b \cdot \left[1 - \frac{\rho(5-3S)(1+S)}{8(3-S)} \right]$$

upper levels

$$\beta' = \frac{h^2}{8\pi^2 kT} \cdot b \cdot \left[\frac{\rho(17-14S+S^2)}{8(3-S)} \right]$$

$$\sigma'' = \frac{h^2}{8\pi^2 kT} \cdot b \cdot \left[1 + \frac{\rho(5+3S)(1-S)}{8(3+S)} \right]$$

lower levels

$$\beta'' = \frac{h^2}{8\pi^2 kT} \cdot b \cdot \left[- \frac{\rho(17+14S+S^2)}{8(3+S)} \right]$$

$$\frac{h^2}{8\pi^2 kT} = 1.342 \times 10^{-41} \text{ for } T = 300^\circ K.$$

Cutoff parameters for Gerhard and Dennison integrals

$$S' = \frac{2}{\pi} \tan^{-1} \left[\frac{b-c}{a-b} \right]^{1/2}$$

$$S'' = 1 - S'$$

Rotational line spacing in sec.$^{-1}$

$$\alpha' = \frac{h}{4\pi^2} \left(\frac{b+c}{2} \right)$$

upper levels

$$\alpha'' = \frac{h}{4\pi^2} \left(\frac{a+b}{2} \right)$$

lower levels

$$h/4\pi^2 = 1.678 \times 10^{-28}$$

The intensities for the pseudo-symmetric molecules (upper and lower levels) are as follows: (The constant factor is neglected)

$$I^{para.}_{\Delta J=0} = 4r\int_{J=0}^{\infty}\int_{K=\Delta J}^{J}\frac{K^2}{J}e^{-\sigma J^2-\beta K^2}\,dK\,dJ$$

$$= \pi^{1/2}r\left\{\frac{\Delta}{\beta(\beta\Delta^2+\sigma)^{1/2}} - \frac{1}{\beta(\beta+\sigma)^{1/2}} + \right.$$

$$\left. +\beta^{3/2}\ln\left[\frac{\beta^{1/2}+(\beta+\sigma)^{1/2}}{\Delta\beta^{1/2}+(\beta\Delta^2+\sigma)^{1/2}}\right]\right\} \quad (\beta>0)$$

$$= \pi^{1/2}r\left\{\frac{\Delta}{\beta(\beta\Delta^2+\sigma)^{1/2}} - \frac{1}{\beta(\beta+\sigma)^{1/2}} + \right.$$

$$\left. +(-\beta)^{-3/2}\left[\sin^{-1}\left(-\frac{\beta}{\sigma}\right)^{1/2} - \sin^{-1}\Delta\left(-\frac{\beta}{\sigma}\right)^{1/2}\right]\right\}$$

$$(\beta<0)$$

$$I^{para.}_{\Delta J=1}(\nu) = 2r \int_{\Delta J}^{J} \frac{J^2-K^2}{J} e^{-\sigma J^2-\beta K^2} dK$$

$$= 2r\, e^{-\sigma J^2} \left[\frac{1}{2\beta} e^{-\beta J^2} - \frac{\Delta}{2\beta} e^{-\beta \Delta^2 J^2} + \right.$$

$$\left. + \frac{J - \frac{1}{2\beta J}}{|\beta|^{1/2}} \int_{\Delta |\beta|^{1/2} J}^{|\beta|^{1/2} J} e^{-x^2} dx \right] \quad (\nu = \alpha J)$$

$$I^{perpr.}_{\Delta J=0}(\nu) = r \int_{K}^{K/\Delta} \frac{J^2-K^2}{J} e^{-\sigma J^2-\beta K^2} dJ$$

$$= \frac{r}{2} e^{-\beta K^2} \left[\frac{e^{-\sigma K^2}}{\sigma} - \frac{e^{-\sigma K^2/\Delta^2}}{\sigma} - \right.$$

$$\left. - K^2 \int_{\sigma K^2}^{\sigma^2 K^2/\Delta^2} x^{-1} e^{-x} dx \right] \quad (\nu = \frac{d\beta}{\sigma} K)$$

$$I^{perpr.}_{\Delta J=1}(\nu) = \frac{r}{2} \int \frac{(J+K)^2}{J} e^{-\sigma J^2-\beta K^2} dJ$$

$$I^{perpr}_{\Delta J=1}(\nu) = \frac{r}{2}\left\{ \int_{\frac{\Delta\nu}{\alpha(1+\beta\Delta/\sigma)}}^{\frac{\nu}{\alpha(1+\beta/\sigma)}} \frac{}{[\nu/\alpha+(1-\beta/\sigma)K]^2}\cdot \right.$$

$$\cdot e^{-\sigma(\nu/\alpha+\beta K/\sigma)^2-\beta K^2} dK +$$

$$+ \int_{-\frac{\nu}{\alpha(1-\beta/\sigma)}}^{\infty} \frac{[-\nu/\alpha+(1+\beta/\sigma)K]^2}{-\nu/\alpha+\beta K/\sigma}\cdot$$

$$\cdot e^{-\sigma(-\nu/\alpha+\beta K/\sigma)^2-\beta K^2} dK +$$

$$+ \int_{\frac{\Delta\nu}{\alpha(1-\beta\Delta/\sigma)}}^{\infty} \frac{[\nu/\alpha+(1+\beta/\sigma)K]^2}{\nu/\alpha+\beta K/\sigma}\cdot$$

$$\left.\cdot e^{-\sigma(\nu/\alpha+\beta K/\sigma)^2-\beta K^2} dK \right\}$$

$$(\beta/\sigma > 1)$$

$$I^{perpr.}_{\Delta J=1}(\nu) = \frac{r}{2}\left\{ \int_{\frac{\Delta\nu}{\alpha(1+\beta\Delta/\sigma)}}^{\frac{\nu}{\alpha(1+\beta/\sigma}} \frac{[\nu/\alpha + (1-\beta/\sigma)K]^2}{\nu/\alpha - \beta K/\sigma} \cdot e^{-\sigma(\nu/\alpha - \beta K/\sigma)^2 - \beta K^2} dK + \right.$$

$$\left. + \int_{\frac{\Delta\nu}{\alpha(1-\beta\Delta/\sigma}}^{\frac{\nu}{\alpha(1-\beta/\sigma)}} \frac{[\nu/\alpha + (1+\beta/\sigma)K]^2}{\nu/\alpha + \beta K/\sigma} \cdot e^{-\sigma(\nu/\alpha + \beta K/\sigma)^2 - \beta K^2} dK \right\}$$

$$(B/\sigma < 1).$$

These are the intensities of the $\Delta J=0$ and $\Delta J=1$ branches of the parallel and perpendicular bands at the distance ν from the center of the band. $I^{Para}_{\Delta J=0}$ is a single Q branch and appears as a line in this approximation.

It is convenient to make the total intensity of a band unity. This is accomplished by dividing the intensities by the following expressions for r, the rotational

partition function:

$$r_{para.} = I^{para.}_{\Delta J=0} + 2\int_0^\infty I^{para.}_{\Delta J=1}(\nu)\,d\nu$$

$$= \sqrt{\pi}\left[\frac{1}{\sigma\sqrt{\beta+\sigma}} - \frac{1}{\sigma\sqrt{\beta\alpha^2+\sigma}}\right]$$

$$r_{perpr.} = \int_0^\infty I^{perpr.}_{\Delta J=0}(\nu) + 2I^{perpr.}_{\Delta J=1}(\nu)\,d\nu$$

$$= \frac{\sqrt{\pi}}{2}\left[\left(\frac{1}{\sigma}-\frac{1}{\beta}\right)(\beta+\sigma)^{-\frac{1}{2}} + \left(\frac{1}{\beta}-\frac{1}{\sigma}\right)(\beta\alpha^2+\sigma)^{-\frac{1}{2}}\right].$$

In principle, $r_{para.}$ and $r_{perpr.}$ are equal. The fact that they are not equal is due to the approximations of the Badger-Zumwalt theory.

The band contours of the real molecule are expressed in terms of absorption by multiplying by the rotational line separation. (The Q branches must still be expressed in terms of their intensity which is concentrated in a single line.) The expressions for the absorptions are:

$$A^{A}_{\Delta J=0}(\nu) = \frac{1}{2}\left(I^{para.}_{\Delta J=0}\right)' + \frac{\sigma}{2\alpha\sqrt{\beta}}\left[I^{perpr.}_{\Delta J=0}(\nu)\right]''$$

$$A^{A}_{\Delta J=1}(\nu) = \frac{1}{2\alpha}\left\{\left[I^{para.}_{\Delta J=1}(\nu)\right]' + \left[I^{perpr.}_{\Delta J=1}(\nu)\right]''\right\}$$

$$A^{B}_{\Delta J=0}(\nu) = \frac{\sigma}{2\alpha|\beta|}\left\{\left[I^{perp}_{\Delta J=0}(\nu)\right]' + \left[I^{perp}_{\Delta J=0}(\nu)\right]''\right\}$$

$$A^{B}_{\Delta J=1}(\nu) = \frac{1}{2\alpha}\left\{\left[I^{perp}_{\Delta J=1}(\nu)\right]' + \left[I^{perp}_{\Delta J=1}(\nu)\right]''\right\}$$

$$A^{C}_{\Delta J=0}(\nu) = \frac{1}{2}\left(I^{para}_{\Delta J=0}\right)'' + \frac{\sigma}{2\alpha|\beta|}\left[I^{perp}_{\Delta J=0}(\nu)\right]'$$

$$A^{C}_{\Delta J=1}(\nu) = \frac{1}{2\alpha}\left\{\left[I^{para}_{\Delta J=1}(\nu)\right]'' + \left[I^{perp}_{\Delta J=1}(\nu)\right]'\right\}$$

$\left[I^{para}_{\Delta J=0}\right]'$ refers to the intensity of the Δ J=0 branch of the parallel band of the upper level pseudo-symmetrical molecule. The A's are the absorptions of the Δ J=0 and Δ J=1 branches of the A, B, and C type bands at a distance ν (in sec.$^{-1}$) from the center of the band. The first term for the Δ J=0 branch of the A and C bands is the Q branch intensity.

The ν here are in sec.$^{-1}$ They may be converted to cm.$^{-1}$ by dividing by c, the velocity of light. In this case the results will refer to a specific molecule at T=300°K. In the event that other temperatures are required, or other molecules with the same ratio of moments of inertia are of interest, it is more convenient to express the results in terms of the dimensionless parameter x of Badger and Zumwalt by multiplying ν by $\frac{\pi}{15\,OK}\sqrt{I_B}$. The results

can then be used for any temperature and for any absolute value of the intermediate moment of inertia.

The integrals in all but the last expression for the intensity of the pseudo-symmetrical molecule bands can be found in standard tables of functions. Gerhard and Dennison give an expression for the last integral (which contains several typographical errors). Because of the added complication of the lower limits, and the fact that one term in the resulting expression must still be integrated numerically, it was felt that the problem would be simplified by leaving the expression in the form given here. Each term can be expressed as

$$\int_a^b \frac{(c+dx)^2}{c+ex} e^{-\sigma(c+ex)^2-\beta x^2} dx$$

A computer program, described in Appendix II, has been written for the Burroughs 220 digital computer for the evaluation of this integral. The program is a straightforward application of a standard Simpson's rule subroutine.

APPENDIX II

COMPUTER PROGRAMS

The two computer programs used in the work described in the thesis are described in this appendix. The descriptions are intended primarily to serve as a guide to a user of the program. They presuppose some familiarity with the Burroughs 220 computer and its operation.

1. Integral Program

This program evaluates the integral

$$\int_b^{a\frac{(c+dx)^2}{c+ex}} e^{-\sigma(c+ex)^2+\beta x^2} dx$$

which arises in the Gerhard-Dennison theory for the absorption-constant envelope of an infrared band of a symmetrical molecule. The program is written to apply Simpson's rule using ten intervals in the range of integration. If it is desired to change the number of intervals, this can be done by inserting for the number of intervals any <u>even</u> number in floating point in location (0045).

In the case of integrals involving infinity as a limit, the value of b was made successively larger in a series of

calculations. Since the integrand cannot be negative, the largest of the results was taken for the value of the integral. In principle, the value of the integral should continuously increase with b, but because of errors in evaluating the exponential in the integrand and in applying Simpson's rule, this was not true in practice.

A set of input data consists of eight words. These are the variables a, b, c, d, e, σ , and β in floating point notation, plus a caption word to identify the particular set of data. Any number of such sets of data can be calculated on one run. The machine reads in a group of eight words, performs the calculation, prints out the result along with the caption word, and reads the next set of data.

In the preparation of the input tape, the first word is 6 0000 04 0199. This is followed by the first set of eight data words. After the first set of data only, the word 6 0000 30 0002 is punched. The remaining sets of data are punched consecutively, taking care that each contains eight words. It is convenient to leave a few inches of blank tape between each set. In the event that only the first few words in a set are to be changed, it is possible to punch the new data and the word 6 0011 03 0206 followed by the caption word. This command overrides the command to read eight words of data and leaves the remaining words of

the data set unchanged in memory. The caption word is entered in its proper location.

Two error halts are programed. One is the result of attempting to apply Simpson's rule to an uneven number of intervals. This usually is the result of a being larger than b. The other error halt is the result of attempting to find the exponential function of a number larger than 110. In the event the machine halts on either error it is convenient to restart by pressing the reset-and-transfer switch. This substitutes the word 1111 11 1111 for the results of the current set of data and starts reading the next set of data. The output command is 0020 06 PWR. Running time for the program is approximately 3 seconds for each set of data.

2. Meecham Calculation Program

The mathematical background of this calculation has been discussed in Section III of the thesis. The program uses 2500 words of memory. While it is in re-locatable form, the program should be located in the first 2500 of memory because of the use of the (0000) location in connection with the reset-and-transfer switch for initiating the program and correcting errors.

After the program is placed in memory, the data for the particular grating are entered as follows: The value of the grating spacing in microns is entered in memory location (0959). The tangent of the left-hand (when viewed from the collimator) groove angle is placed in (0960) and that of the right-hand angle in (0961). This is best done manually at the console. All numbers are in floating point notation. The proper control switches are next selected according to their function as described below. In particular, either CS1 or CS2 must be down, and CS9 must be up.

The program is started by depressing the reset-and-transfer switch. The machine will almost immediately stop with 7427 00 7427 in the C register. If a previous computation has been made the value of N, the number of terms to be included in the series, will appear in the A register. N is in fixed point notation. If this is the first computation the A register will be blank. The desired value of N (≤ 10) is inserted in the A register in fixed point and the start switch is depressed. The machine will stop on 7447 00 7447 with the previous value of the grating order, if any, in the A register in floating point. This is modified, if desired, and the start switch depressed. A halt on 8521 00 8521 will occur with the previous value of the wavelength in microns in the A register. This is changed,

as desired, and the start switch again depressed. The purpose of this procedure is to allow the operator to make only those changes in the input data that he may desire and to retain all others.

From this point, the program will proceed with the calculation as described in Section III. If it should be desirable to replace the cross product in order to treat another groove shape, this can be done as follows: Location (0054) contains a conditional branch command to (1298), the location of the beginning of the portion of the program which calculates the cross products. This portion of the program exits to (0085) on its completion. If this portion is eliminated, and another set of cross products substituted, a grating of some other groove shape can be treated. The calculated cross products (F_i,F_j) are stored in memory with real parts in (2258)-(2357) and imaginary parts in (2358)-(2457). The order is $(F_1,F_1).(F_2,F_1)...(F_{10},F_1)$, (F_1,F_2), (F_2,F_2), $(F_3,F_2)...(F_{10},F_{10})$. The $(F_i, \bar{\phi}_i)$ are stored in (2478)-(2487) (real parts) and (2488)-(2497) (imaginary parts). The values of sin R_i, and the real and imaginary parts of cos R_i can be found in (1658)-(1667), (1668)-(1677), and (1678)-(1687), respectively. In all cases i increases with increasing memory cell number. The value of sin I is in (0060).

The console control switches have the following functions: CS1 causes the program to make the computation using the boundary conditions for radiation polarized with the electric vector parallel to the grooves of the grating. CS2 is used for perpendicular polarization. If both control switches are depressed, the calculation will be for the perpendicular polarization. If neither control switch is depressed, a halt with R_C=3333 00 3333 will occur. In this event, the proper control switch can be selected, and the program resumed by pressing the start switch. CS4 and CS5 cause the values of $\sum_k |B_k|^2$ and $\sum_j \cos R_j |A_j|^2$ for all real R_j, respectively, to be calculated. These are for a check of the error in matching boundary conditions and for a check of the balance between incoming and outgoing energy. CS8 modifies the cross product routines to exclude regions in the geometrical shadow of any order from the range of integration. The word "ECHELLE" will be printed before the output data. This procedure did not appear to have any real value, and its use is not recommended.

The remaining control switches select diagnostic routines which were used in the de-bugging of the program. These routines can be extremely wasteful of computer time and should not be used except when necessary. CS3 causes a monitor routine to print out the words "F*F" and i,j

when the program calls for the value of (F_1, F_j) and "F*0" and 1 when $(F_1, \bar{\phi}_1)$ is called for. In addition, the numerical values of the cross products can be obtained by depressing CS7. CS6 causes the matrix (G_1, G_j) to be calculated and printed out as a check on the orthogonality of these functions. Actuating the reset-and-transfer switch with CS9 depressed places the program in an error halt-correction routine. During the de-bugging of the program error halts often occurred in the square root and exponential subroutines under conditions which suggested that the value of the function should be zero. The correction routine tests the contents of (0000) for the value which the P register would have at either of these halts. If the halt is recognized as belonging to either of these subroutines, the value zero is placed in the A register, and the program is transferred to the exit command of the appropriate subroutine. If the appropriate value of the P register is not recognized, the machine stops on 5555 00 5555. It is doubtful that this routine will be useful with the program running properly. Any occurrence of an error halt should be regarded with extreme suspicion.

CS10 causes the machine to vary the number of terms included in the series until a minimum for the value of the mean square error of the boundary conditions is reached.

The data for each calculation are printed out. One additional term is added with each calculation until either ten terms are reached or the value of the mean square error passes a minimum. In the latter event, one more calculation will be made with one less term, and the machine will halt on 7427 00 7427. If this mode is used, the initial value (usually one) of N must still be inserted as in the standard mode.

Two printout commands are used--the 09 SPO command for the calculated data, and several 1000 06 PWR commands for the monitor and certain other printouts. The output format contains the five letter word describing the polarization (PARAL or PERPR) followed by the wavelength and grating order in the first line. Following this line are cos R_1, the real part of A_1, and the imaginary part of A_1 for all i from 1 to N. Following this, if CS4 is depressed, is the word "ERROR CHECK" followed by the value of $\sum_{\kappa} |B_\kappa|^2$. Next, if CS5 is depressed, come the words "ENERGY CHECK" followed by the real part of $\sum_j |A_j|^2 \cos R_j$, and the real part of cos I. These data all are printed using the SPO command. All other output data come out on a 1000 06 PWR command. These include monitor data, cross product values, and G matrix.

Running time for the program is approximately 6 minutes.

BIBLIOGRAPHY

1. R. M. Badger, L. R. Zumwalt, and P. A. Giguere, Rev. Sci. Inst. 19,861-865 (1948).
2. For Example: M. K. Wilson and R. M. Badger, J. Chem. Phys. 17,1232-1236 (1949); L. H. Jones, R. M. Badger, and G. E. Moore, J. Chem. Phys. 19,1599-1604 (1951); K. Hedberg and R. M. Badger, J. Chem. Phys. 19,508-509 (1951).
3. G. K. T. Conn and D. G. Avery, Infrared Methods: Principles and Applications, New York: Academic Press (1960).
4. E. F. Daly and G. B. B. M. Sutherland, Proc. Phys. Soc. London A62,205-215 (1949).
5. P. Bratt, W. Engeler, H. Levinstein, A. MacRae, and J. Pehek, Infrared Phys. 1,27-38 (1961).
6. M. J. E. Golay, Rev. Sci. Inst. 18,347-356 and 357-362 (1947).
7. R. G. Greenler, J. Opt. Soc. Am. 46,433-434 (1956).
8. H. G. J. Kayser, Tabelle der Hauptlinien der Linien Spektra Aller Elemente nach Wellenlänge Geordnet, Berlin: J. Springer (1926).
9. H. M. Randall, R. G. Fowler, N. Fuson, and J. R. Dangl, Infrared Determination of Organic Structure, New York:

D. VanNostrand Company Inc. (1949) p.13.

10. K. T. Hecht, D. L. Wood, Proc. Roy. Soc. London, A235,174-188 (1956).

11. M. Beer, H. B. Kessler, G. B. B. M. Sutherland, J. Chem. Phys. 29,1097-1104 (1958).

12. G. B. B. M. Sutherland, Adv. Prot. Chem. 7,291-318 (1952).

13. S. Mizushima, Adv. Prot. Chem. 9,299-324 (1954).

14. L. Pauling, The Nature of the Chemical Bond, Ithaca, N. Y: Cornell University Press, (1960) 3rd Ed. p.229.

15. R. B. Corey, Adv. Prot. Chem. 4,385-406 (1948).

16. J. Ladell, B. Post, Acta. Cryst. 7,559-564 (1954).

17. L. Pauling, Ibid. p.281.

18. E. J. Ambrose, A. Elliot, R. B. Temple, Proc. Roy. Soc. London, A206,192-206 (1951).

19. T. Shimanouchi, K. Kuratani, S. Mizushima, J. Chem. Phys. 19,1479-1480 (1951).

20. N. B. Abbott, A. Elliot, Proc. Roy. Soc. London A234,246-268 (1956).

21. T. Miyazawa, T. Shimanouchi, S. Mizushima, J. Chem. Phys. 24,408-418 (1956).

22. W. C. Price, R. D. B. Fraser, Proc. Roy. Soc. London B141,66-67 (1953).

23. S. Mizushima, T. Simanouti, S. Nagakura, K. Kuratani,

M. Tsuboi, H. Baba, and O. Fujioka, J. Am. Chem. Soc. 72,3490-3494 (1950).

24. T. Miyazawa, T. Shimanouchi, and S. Mizushima, J. Chem. Phys. 29,611-616 (1958).

25. T. Miyazawa, J. Mol. Spect. 4,155-167 (1960).

26. R. M. Badger, Technical Report 8 and Final Report ONR Contract N6ori-102, Task Order VI Project NR-055-019 (1954).

27. E. R. Andrew, Nuclear Magnetic Resonance, Cambridge: University Press (1955).

28. W. D. Philips, J. Chem. Phys. 23,1363-1364 (1955).

29. H. S. Gutowsky and C. H. Holm, J. Chem. Phys. 25, 1288-1289 (1956).

30. M. E. Hobbs and W. W. Bates, J. Am. Chem. Soc. 74,746-749 (1952).

31. R. M. Badger and H. Rubalcava, Proc. Nat. Acad. Sci. 40,12-17 (1954).

32. R. Huisgen and H. Walz, Chem. Ber. 89,2616-2629 (1956); Chem. Abs. 51,14556d.

33. R. Huisgen, H. Brade, H. Walz, and I. Glogger, Chem. Ber. 90,1437-1447 (1957); Chem. Abs. 54,8624h.

34. G. R. Leader and J. F. Gormley, J. Am. Chem. Soc. 73,5731-5733 (1951).

35. C. P. Smyth, Dielectric Behavior and Structure, New York:

McGraw Hill Book Company Inc. (1955) pp.244-255.

36. L. R. Zumwalt and R. M. Badger, J. Chem. Phys. 7,87 (1939).

37. R. M. Badger and S. H. Bauer, J. Chem. Phys. 4,711-715 (1936).

38. C. C. Costain and J. M. Dowling, J. Chem. Phys. 32,158-165 (1960).

39. J. C. Evans, PhD. Thesis, University of Wales (1953).

40. H. Rubalcava, PhD. Thesis, California Institute of Technology (1956).

41. D. E. DeGraaf and G. B. B. M. Sutherland, J. Chem. Phys. 26,716-717 (1957).

42. D. E. DeGraaf, Diss. Abs. 18,1462 (1958).

43. R. L. Jones, J. Mol. Spect. 2,581-586 (1958).

44. G. F. D'Alelio and E. E. Reid, J. Am. Chem. Soc. 59,109-111 (1937).

45. E. R. Cox, Ind. and Eng. Chem. 15,592-593 (1923).

46. J. Deschamps, M.-T. Forel, N. Fuson, and M.-L. Josien, Bull. Soc. Chim. France 1959,88-93.

47. M.-T. Forel, N. Fuson, and M.-L. Josien, J. Opt. Soc. Am. 50,1228-1231 (1960).

48. R. L. Jones, private communication to R. M. Badger.

49. R. M. Badger and L. R. Zumwalt, J. Chem. Phys. 6,711-717 (1938).

50. S. L. Gerhard and D. M. Dennison, Phys. Rev. 43,197-204 (1933).

51. D. M. Dennison, Rev. Mod. Phys. 3,280-345 (1931).

52. G. Herzberg, Infrared and Raman Spectra of Polyatomic Molecules, New York: D. VanNostrand Company Inc. (1945) p.437.

53. W. S. Gallaway and E. F. Barker, J. Chem. Phys. 10,88-97 (1942).

54. R. Trambarulo, S. N. Ghosh, C. A. Burrus Jr., and W. Gordy, J. Chem. Phys. 21,851-855 (1953).

55. S. L. Gerhard, Phys. Rev. 42,622-631 (1932).

56. A. Adel and D. M. Dennison, J. Chem. Phys. 14,379-382 (1946).

57. S. H. Bauer and R. M. Badger, J. Chem. Phys. 5,852-855 (1937).

58. H. W. Thompson, J. Chem. Phys. 7,453-455 (1939).

59. V. Z. Williams, J. Chem. Phys. 15,232-243 (1947).

60. A. H. Nielsen and H. H. Nielsen, Phys. Rev. 56,274-275 (1939).

61. E. H. Richardson, PhD. Thesis, University of Toronto (1959).

62. S. Broderson, J. Mol. Spect. 6,511-519 (1961).

63. J. W. Boyd and T. H. Edwards, reported at Columbus Conference on Molecular Structure and Molecular Spectroscopy (1960).

64. S. C. Wang, Phys. Rev. 34,243-252 (1959).

65. H. M. Randall, D. M. Dennison, N. Ginsburg, and L. R. Weber, Phys. Rev. 52,160-174 (1937).

66. R. A. Russell and H. W. Thompson, Spect. Acta. 8,138-141 (1956).

67. L. J. Strong, J. Opt. Soc. Am. 39,320-323 (1949).

68. J. C. Slater and N. H. Frank, Electromagnetism, New York: McGraw Hill Book Company Inc. (1947) p.190.

69. A. A. Michelson, Astrophysics J. 8,37-47 (1898).

70. R. W. Wood, Phil. Mag. (Sixth Series) 20,770-778 (1910).

71. G. K. T. Conn, Proc. Camb. Phil. Soc. 42,240-253 (1947).

72. A. E. Martin, Nature 184,975-976 (1959).

73. T. A. Wiggins and G. D. Saksena, J. Opt. Soc. Am. 48,429-430 (1958).

74. S. G. Rautian, Optics and Spectroscopy (U.S.S.R.) 7,347-348 (1959).

75. G. R. Harrison, J. Opt. Soc. Am. 39,522-528 (1949).

76. S. S. Ballard, K. A. McCarthy, and W. L. Wolfe, Infrared Information and Analysis Center, University of Michigan, Report 2389-11-S (1959) p.41.

77. D. M. Gates, C. C. Shaw, and D. Beumont, J. Opt. Soc. Am. 48,88-89 (1958).

78. Author Unknown, Perkin Elmer Instruction Manual for Model 112 Infrared Spectrometer, Perkin Elmer Corp. Norwalk, Conn. Vol. 1, p.84 (1952).

79. S. Silverman, J. Opt. Soc. Am. 38,989 (1948).

80. V. Twersky, J. Res. Nat. Bu. Stand. 64D,715-730 (1960).

81. K. W. Meissner, J. Opt. Soc. Am. 32,185-210 (1942).

82. R. F. Stamm and J. J. Whalen, J. Opt. Soc. Am. 36,2-12 (1942).

83. W. Friedl and B. Hartenstein, J. Opt. Soc. Am. 45, 398-399 (1955).

84. R. D. Hatcher and J. H. Rohrbaugh, J. Opt. Soc. Am. 46,104-110 (1956); See also J. Opt. Soc. Am. 48,704-711 (1958).

85. H. A. Rowland, Phil Mag. (Fifth Series) 35,397-419 (1893).

86. W. C. Meecham, J. Appl. Phys. 27,361-367 (1956).

87. W. C. Meecham and C. W. Peters, J. Appl. Phys. 28,216-217 (1957).

88. Lord Rayleigh, Proc. Roy. Soc. London A79,399-416 (1907).

89. M. Born and E. Wolf, Principles of Optics, New York: Pergamon Press (1959) p.376.

90. T. M. Apostol, Mathematical Analysis, Reading Mass: Addison-Wesley Pub. Co. Inc. (1957) p.483.

91. Ibid., p.289; Also P. M. Morse and H. Feshback, Methods

of Theoretical Physics, New York: McGraw Hill Book Company Inc. (1953) p.804.

92. J. C. Slater and N. H. Frank, Op. Cit. p.168.

93. M. Born and E. Wolf, Op. Cit. p.378.

94. M. Born and E. Wolf, Op. Cit. p.559.

95. B. A. Lippman, J. Opt. Soc. Am. 43,408 (1953).

96. B. A. Lippman, Nuclear Development Associates Inc. White Plains, New York. Report NDA 18-8.

97. C. W. Peters, P. V. Deibel, W. K. Pursley, and T. F. Zipf, Enginering Research Institute, University of Michigan, Microwave Measurements of the Intensity Distribution of Echelette Diffraction Gratings; Abstract: J. Opt. Soc. Am. 43,816 (1953).

98. T. M. Apostal, Op. Cit. p.306.

99. V. Z. Williams, Rev. Sci. Inst. 19,135-178 (1948).

100. F. P. Dickey and J. M. Hoffman, J. Chem. Phys. 28,1253 (1958).

101. W. H. King Jr., J. Opt. Soc. Am. 43,866-869 (1953).

102. R. C. Nelson and R. Jenkinson, J. Opt. Soc. Am. 43,1181-1183 (1953).

103. W. Kage, R. G. Devaney, J. Opt. Soc. Am. 42,567-571 (1952).

104. C. C. Yang and V. Lagallais, Rev. Sci. Inst. 25,801-807 (1954).

105. T. Cook Jr. and D. C. Smith, Rev. Sci. Inst. 18,173-181 (1947).

106. N. H. E. Ahlers and H. P. Freedman, J. Sci. Inst. 32,61 (1955).

107. H. W. Etzel, J. Opt. Soc. Am. 43,87-90 (1953).

108. D. F. Hornig, G. E. Hyde, and W. A. Adcock, J. Opt. Soc. Am. 40,497-503 (1950).

109. A. Savitzky and R. S. Halford, Rev. Sci. Inst. 21,203-212 (1950).

110. P. Hariharan and M. S. Bhalla, J. Opt. Soc. Am. 47,378-381 (1957).

111. W. R. Wilson, Memorandum Report no. 17, Navy Contract NObs 28373, Dept. of Phys., Northwestern University (1947).

PROPOSITION

It is proposed that, of the automatic diffractometers described in the literature, only the type described by Furnas and Harker[1] is capable of the wide range of possible uses of this instrument.

The diffractometers described in the literature can be grouped into three classes according to the manner in which they examine reciprocal space. In this discussion, the nomenclature recommended by Arndt and Phillips[2] will be used. The first class is based on the same geometry as the rotational film technique. It thus can conveniently examine an entire plane in reciprocal space with a given setting. The second class is designed with a mechanical linkage which causes it to examine a line in reciprocal space. The third class is based on spherical coordinates which make it most convenient to examine single points in reciprocal space.

A diffractometer can examine only one reflection at a time. This limitation makes it highly desirable to develop an automatic diffractometer -- one which would automatically scan through reciprocal space, collecting and recording

data on the reflections observed there. It was the realization that an automatic diffractometer was needed that led to the design of the instruments in the second class, but automatic instruments of each group have been described in the literature.

The means by which each of the three types of instrument investigates reflections serves to classify the functions of the ideal diffractometer. The first class, in the one application to automation described in the literature[3], investigates a net by scanning in a spiral path covering the entire net. The scan is done quite rapidly until a reflection is reached. Then the scan is slowed and the reflection examined to obtain the intensity, after which the speed is again increased. All of reciprocal space in a given plane is covered, and no reflection can be omitted because of inaccurate knowledge of the unit cell. One disadvantage of this type of instrument is that it is necessary to expose the crystal to a great deal of radiation in order to examine it. This radiation can be harmful to crystals of many molecules. Another disadvantage is that with the two-speed scan, which is necessary in order to cover a net

in a reasonable length of time, faint reflections could easily be overlooked.

The second class of instrument scans along a given line in reciprocal space[4,5,6]. This line is adjusted to correspond to those rows in the reciprocal lattice on which the number of reflections is large. It thus can omit large portions of reciprocal space with a significant improvement in the time required to collect data. An accurate knowledge of the reciprocal lattice is presupposed with this type of instrument, since it will examine only those points exactly on the given path. This exact knowledge allows one to be confident that no reflection will be overlooked because of its low intensity. A reflection is scanned, in general, with a speed which is a complicated function of its position along the line. This fact must be taken into consideration when calculating integrated intensities[5].

In the automatic applications which have been described in the literature, the third type of instrument has been programmed to examine a set of reflections whose coordinates are fed into the instrument by some means such as punched paper tape[7,8]. This presupposes again an accurate knowledge

of the reciprocal lattice in order to make the calculations of the input angles. These calculations are typically done on a computer. This requirement of a computer should not be difficult to meet since the type of data collection being done requires a computer for its analysis.

Each of the three types of instruments has its own special capability. The net-scanning instrument can conveniently cover an entire plane of reciprocal space. The line-scanning instrument covers only a single line, but this can be made to correspond to an important line in the reciprocal lattice. Finally the point-examining instrument examines only specific points in reciprocal space.

It is the purpose here to propose that the third type of instrument can be conveniently made to do all three functions as well as to correct small errors in the location of reflections. By the use of a simple analogue computer, the instrument could be made to scan either an entire net or a line. The output of the analogue computer would be fed into the orienter by servo motors. For the case of the net, the computer would be designed to compute either chi or 2θ as a function of the other. Phi would be continu-

ously varied and one or the other of the two other angles varied slowly. The computer would supply the third angle. The mechanism required for the computer is simply a right triangle linkage. The hypotenuse represents the value of 2θ; the base represents the radial distance in the net; and the included angle represents the value of psi. For the case of the path through reciprocal space, it is pointed out that any of the linkages described in the literature could be directly made into analogue computers which would generate input angles for the instrument.

Finally, it is pointed out that the shutter device described by Furnas[9] could usefully be adapted to cause the instrument to correct itself. This device consists of four shutters covering the end of a collimator placed in the diffracted beam. One set of two shutters can be made to cover either the top or bottom half of the beam, while the other set can be made to cover either the right or left half of the beam. If a reflection is centered in the collimator, the effect on intensity of either of the two shutters in a set will be the same. If the reflection is not centered, there will be a difference between the intensi-

ties when the two shutters are alternately closed. If the crystal has been accurately centered to begin with, this difference can be interpreted in terms of the change necessary in psi or omega to center the reflection. This interpretation could be made to take place automatically, thus allowing the instrument to correct small errors in input angles.

PRK:mv

REFERENCES

1. T. C. Furnas Jr. and D. Harker
Rev. Sci Inst. 26, 449-453 (1955)

2. U. W. Arndt and D. C. Phillips
Acta Cryst. 11, 509-510 (1958)

3. W. L. Bond
Acta Cryst.8, 741-746 (1955)

4. A. McL. Mathieson
Acta Cryst. 11, 433-436 (1958)

5. J. Ladell and K. Lowitzsch
Acta Cryst.13, 205-213 (1960)

6. U. W. Arndt and D. C. Phillips
Acta Cryst. 14, 807-818 (1961)

7. E. Prince and S. C. Abrahams
Rev. Sci. Inst. 30, 581-585 (1959)

8. F. Langden and B. C. Frazer
Rev. Sci. Inst.30, 997-1003 (1959)

9. T. C. Furnas Jr.
Instructions for the Single Crystal Orienter
General Electric Company, Milwaukee, Wis.

PROPOSITION

An improvement is proposed for Ito's method of indexing reflections from X-ray powder techniques. This improvement is particularly useful in the application of digital computers to the indexing problem.

Two programs for the computer indexing of X-ray powder data have appeared in the literature[1,2]. These programs employ methods such as Hesse's[3], which are devoted to the higher crystal symmetries, and thus are not useful for all crystals. The single method of indexing a set of powder data for monoclinic and triclinic crystals is the method of Ito[4].

Ito assumed the unit cell of the reciprocal lattice to be determined to be triclinic. He recognized that each x-ray reflection corresponds to a vector in the reciprocal lattice of the crystal producing the pattern. In the case of the powder technique, only the length of each vector is known. He selected three low-order reflections as corresponding to the lengths of the three sides of a unit cell. Having thus determined the lengths of the three unit vectors, he found their interaxial angles by searching the observed

reflections for reflections fulfilling certain equations which could then be solved for the interaxial angles.

Instead of characterizing each reflection by its "d value", or the spacing between the planes producing the Bragg reflection, it is convenient to characterize it by the "Q value", or $1/d^2$. If the six reciprocal cell parameters are defined as

$$Q_a = 1/a^2 = a^{*2}$$

$$Q_b = 1/b^2 = b^{*2}$$

$$Q_c = 1/c^2 = c^{*2}$$

$$Q_a = 2b^*c^*\cos\alpha^*$$

$$Q_\beta = 2a^*c^*\cos\beta^*$$

$$Q_\gamma = 2a^*b^*\cos\gamma^*$$

then the Q value of a reflection is

$$Q_{hk\ell} = h^2Q_a + k^2Q_b + \ell^2Q_c + k\ell Q_\alpha + h\ell Q_\beta + hkQ_\gamma.$$

One of the relations sought in applying Ito's method can now be written as

$$Q_{h00} + Q_{k00} = (Q_{hk0} + Q_{h\bar{k}0})/2. \qquad (1)$$

If such a relation is found among the observed data, Q_γ is

$$Q_\gamma = (Q_{hk0} - Q_{h\bar{k}0})/2.$$

If sufficient relations are found, the unit cell is determined. In general such a unit cell will not show the symmetry of the lattice in question, but by suitable methods, it can be reduced to a cell showing this characteristic symmetry.

Ito's method can be easily applied to a digital computer. A digital computer is able to do a large amount of arithmetic in a short time, so is well adapted to searching for data fulfilling a given equation or set of equations. Two difficulties, however, exist. If an observed reflection is selected as corresponding to the unit vector for a lattice, the chances are not good that the lattice defined by that unit vector will be primitive. The reduction methods referred to above depend on obtaining a primative unit cell. Also, if a primative lattice is not found, all of the observed reflections will not be indexed by the provisional lattice. Second, the reflections selected for unit vectors are the low-order reflections, and thus the least accurate ones. It is important that the lengths of the unit vectors be quite accurate, or relations such as equation 1 will not be found.

It seems likely that in a computer program devoted to the problem of indexing powder data for an arbitrary crystal, methods such as Hesse's will be used first to attempt to index the data in a crystal system of higher symmetry. Only after the failure of these methods, would Ito's method be applied. The reason for this is that Ito's method neglects the symmetry of the crystal, and thus loses a great deal of useful information.

It is proposed here that, upon the failure of attempts to index the data in the cubic, tetragonal, hexagonal, or orthorhombic systems, the set of all differences between the observed Q values be computed. If N reflections are observed for a given crystal, the set of differences can be regarded as an NxN square matrix. Each term of this matrix is to be divided by the set of integers $(h^2 - h'^2)$ such that $h + h'$ is a constant. For example, the set for $h + h' = 10$ is 20, 40, 60, 80, and 100 for $0 \leq h,h' \leq 10$. If a set has n members and there are N reflections, there will result n NxN matrixes of dividends for each set. These nN^2 values are searched for members equal to each other within the limit of experimental error. Each equali-

ty found is assumed to correspond to a relation such as equation 2. Equation 2 is solved for the apparent value of Q_a, and this is stored. This procedure is repeated for other sets of integers $(h^2 - h'^2)$ such that $h + h'$ equals other numbers. For the range $0 \leq h,h' \leq 10$, there are 16 such sets. The accumulated list of possible Q_a values is then examined and the three most-numerous values are selected as unit vector lengths for use in searching for relations such as equation (1).

In summary, it is proposed that, in a computer program devoted to the indexing of powder data, the difference matrix described above be examined in order to obtain a better set of unit vector lengths for the application of Ito's method of indexing a triclinic lattice.

PRK:mv

REFERENCES

1. I. R. Tannenbaum, B. V. Lempke, and D. Kramer
Atomics International Report NAA-SR-4710 (1960)

2. R. Lesker
listed in ACA Mark I Computer Program Listing
accession No. 55 (1960)

3. R. Hesse
Acta Cryst. 1, 200-207 (1948)

4. L. V. Azaroff and M. V. Buerger
The Powder Method in X-Ray Crystallography
New York: McGraw Hill Book Company, Inc. (1958) Ch.10.

PROPOSITION

A paper by Newman, Brice, and Wright describes differential thermal analysis data on the system Ga-Te. A different interpretation is proposed.

The DTA data in the region 30-50°/o Te of Newman, Brice, and Wright are interpreted in terms of the incongruently melting compound Ga_3Te_2 with peritectic point at 33.5°/o Te and 753°C. This interpretation is supported by the observation of four Debye-Scherer lines in the powder pattern of a sample of the constitution 40°/o Te which was quenched from the melt. No lines were observed for a similar sample of the composition 33.3°/o Te.

A number of comments can be made about this paper. For example, the model of the structure of GaTe which is pictured does not have the correct stoichiometry as can be seen from counting the atoms in the model. The meaning of the PT and Px diagrams can be questioned. In particular, however, it is recognized that the confidence in the DTA data should be regarded as low. However, even on the basis of this data, another interpretation is more reasonable.

It is proposed that the data are more consistent with a congruently melting compound Ga_2Te. The melting point is 762°C, and the eutectic point for Ga_2Te + GaTe near 33.5°/o Te and at 753°C. This compound is obviously stable only at high temperature, decomposing to Ga+GaTe at room temperature. To be consistent with the data the decomposition temperature must be within experimental error of 746°C.

The data supporting this proposition, as opposed to the interpretation given in the paper consist of the following:

1. There is a third arrest in the DTA results for the composition 45°/o Te. This is inconsistent with the incongruently melting compound Ga_3Te_2.

2. The data in the region around 33°/o Te clearly indicate a peak in the freezing curve corresponding to a congruent melting point with temperature 762°C.

3. The data at slightly greater Te percentages indicate a total of three distinct arrests, rather than the two that are reported. These three arrests correspond to the freezing curve, whose temperature is variable, the eutectic temperature 753°C, and the decomposition temperature 746°C.

It is proposed that the additional arrest point was overlooked in the original data where only two arrests are reported.

It is proposed that the observation of four powder diffraction lines in the sample of 40^{o}/o Te which was quenched is by no means proof that the compound which gave the lines has 40^{o}/o Te concentration. This is particularly true in view of the statement that the lines of GaTe were also in evidence. An equally good interpretation of this data is that the four lines are due to Ga_2Te, and that, in the sample of this composition, no Ga_2Te was left after quenching.

In summary, it is proposed that, on the basis of probably poor data, a different interpretation is possible. This second interpretation makes further work on the Ga-Te system necessary.

PRK:mv

REFERENCES

1. P. C. Newman, V. L. Brice and H. C. Wright
Phillips Research Reports 16, 41-50 (1961)

PROPOSITION

It is proposed that the anomalous transmission of X-rays in a perfect crystal would be useful in elucidating the nature of Restrahl absorption in the infrared.

Hardy and Smith[1] have shown that the two-phonon infrared spectrum of a crystal can be useful in determining the dispersion surface for the various lattice vibration modes. By studying the spectrum of diamond, they were able to obtain a semi-quantitative picture of the dispersion surface, both of acoustical and optical modes. They did experience certain difficulties in making an unambiguous assignment of certain absorption bands which they observed.

The absorption bands which Hardy and Smith studied represented the interaction of an infrared photon with two phonons. The selection rules for such interactions are such that they are allowed, but of low intensity. After an accurate assignment is made, a consideration of the sums and differences between different energies allows one to plot the dispersion surface. The difficulty is in making the assignments.

Qualitatively, the anomalous transmission of X-rays in a perfect crystal can be regarded as taking place because the nodes of the electromagnetic wave occur at the atomic planes for the anomalously transmitted component, and it is only at the atomic planes that absorption takes place. The exact theory does not change this picture, except to predict some absorption taking place elsewhere.

It is proposed here that the disturbance of the position of an atom by a lattice vibration would decrease the intensity of anomalously transmitted X-radiation in a cooled perfect crystal. With a knowledge of the polarization and direction of transmission of the infrared absorption which gave rise to the lattice vibration, one could identify the mode, or modes involved.

For example, a transverse mode could be distinguished from a longitudinal mode in the [100] direction by adjusting the crystal for Bragg reflection from the (100) planes and infrared absorption in the [100] direction. A decrease in intensity of the anomalously-transmitted component of the X-radiation would indicate the presence of a longitudinal mode, while a transverse mode would have little or no effect.

The first step in the application of this proposal would be to derive an adequate theory for the interaction of X-radiation with infrared radiation in a perfect crystal. Such a theory would have to take into account the multiple scattering of X-radiation in the crystal in order to predict anomalous transmission. An adequate theory would also have to treat the infrared radiation field as a traveling wave in the crystal, since only in this way could an accurate picture be obtained of scattering due to the lattice vibrations. One result of such a theory would be a clear idea of the difference in effect on the anomalous transmission between acoustical modes and optical modes. This is by no means clear with present theories.

While the theory which would predict the effect proposed here does not exist, certain experimental evidence can be proposed to support it. It is pointed out that anomalous transmission has been observed in silicon with a Debye temperature of $658^{\circ}K$ and in Germanium with a temperature of $366^{\circ}K$. The lattice vibrations are certainly well-excited in these crystals at room temperature. Thus there is an anomalously transmitted component in the presence of lattice vibrations.

Batterman[2] has observed the change in intensity of this component with changing temperature, so it can be concluded that the effect of lattice vibrations on the X-ray intensity does exist.

In summary, it is proposed that the effect of a lattice vibration on the anomalously transmitted component of X-radiation in a perfect crystal be used to study the nature of the lattice vibration. This effect is not adequately discussed by existing theories, and a new theory would have to be advanced in order to discuss the results of the experiments proposed here.

PRK:mv

REFERENCES

1. V. R. Hardy and S. D. Smith
Phil. Mag. 6, 1163-1172 (1961)

2. B. W. Batterman, unpublished.

PROPOSITION

An explanation is proposed for a discrepancy noted in a paper by Penning and Polder[1].

In a recent paper, Penning and Polder attempt to extend the dynamic theory of x-ray scattering to deformed crystals. This extension is made by assuming that, the deformation being small, the electromagnetic field within the crystal can be broken up into regions such that, in a single region, a modified dynamic theory holds. This modified theory assumes the same intensity dependence on the absorption coefficient of the crystal as for an undeformed crystal, but assumes a slowly varying reflection vector, and thus a slowly varying wave vector, in the crystal. Implicit in this assumption is the assumption that energy is not scattered into modes into which it would not be scattered in a perfect crystal.

The theory predicts qualitatively the results of experiments done on both mechanically and thermally deformed crystals. In particular, it predicts a curved path for the transmitted and the reflected beams in the crystal. It does

not, however, predict accurately the intensities of the two emerging beams. The experimental beam is much less intense than calculated.

The difficulty here is that a kinematic scattering theory is really being used. The power of the dynamic scattering theory is that it takes into account multiple scattering. This multiple scattering is explicitly eliminated in the Penning-Polder theory by the assumption that no new modes are excited in the deformed crystal. In eliminating all new modes, one has a single-scattering theory. This single-scattering theory is equivalent to the Kirchoff theory used in the first theoretical treatment of the Echelle grating. This type of theory gives the direction of propagation quite accurately, but is restricted in its validity when applied to intensity calculations.

If the Penning-Polder theory is to have validity in <u>any</u> restricted sense, two things must be done. In deriving the theory for an undeformed crystal, a result of Wagner[2] is quoted expressing the relationship between Poynting's vector in the crystal and the gradient in K space of the

frequency dispersion surface. Wagner specifies that this result is valid in the absence of absorption. Penning and Polder make no such restriction in their use of the expression. Further, these authors must now justify the application of an approximate theory, which neglects multiple scattering, to the problem of a deformed crystal.

The correct solution to the problem is suggested, among other places, in a paper by Slater[3]. In his discussion of the interaction of waves in crystals, Slater gives the solution of Maxwell's equations for a dielectric constant which is periodic in space and in time. The correct solution to the problem of the deformed crystal is the solution to the same equation except that a term is to be added to the dielectric constant which gives the effect of the deformation.

In summary, it is proposed that the theory applied by Penning and Polder is not a dynamic theory and that this is responsible for the lack of agreement between theory and experiment. If this theory is to be applied to the problem at all, it must be shown that the approximation of neglecting

multiple scattering is justified. Finally, it must be shown that the use of Wagner's result is justified.

PRK:mv

REFERENCES

1. P. Penning and D. Polder
Phillips Research Reports 16, 419-440 (1961)

2. E. H. Wagner
Acta Cryst. 12, 345-346 (1959)

3. J. C. Slater
Rev. Mod. Phys. 30, 197-222 (1958)